Sensing the Physical World Using Pervasive Wireless Infrastructure

A Dissertation

Presented to
the Faculty of the School of Engineering and Applied Science
University of Virginia

In Partial Fulfillment
of the Requirements for the Degree

Doctor of Philosophy

by

Elahe Soltanaghaei

September 2019

Sensing the Physical World Using Pervasive Wireless Infrastructure

by

Elahe Soltanaghaei

Submitted to the Department of Computer Science
in partial fulfillment of the requirements for the degree of

Doctor of Philosophy

at the

UNIVERSITY OF VIRGINIA

September 2019

Author . . . .
Department of Computer Science
Sept. 18, 2019

Certified by . . . .
Kamin Whitehouse
Professor of Computer Science
Thesis Supervisor

Accepted by . . . .
Craig H. Benson
Professor of Civil and Environmental Engineering
Dean of School of Engineering and Applied Science

Approval Sheet

The dissertation is submitted in partial fulfillment of the requirements for the degree of Doctor of Philasophy (Computer Science)

Professor Kamin Whitehouse ....

Thesis Advisor
Professor of Computer Science

Professor John A. Stankovic ....

Chairman, Thesis Committee
Professor of Computer Science

Professor Madhur Behl ....

Member, Thesis Committee
Assistant Professor of Computer Science

Professor Robert M. Weikle ....

Member, Thesis Committee
Professor of Electrical and Computer Engineering

Professor Steven Bowers ....

Member, Thesis Committee
Assistant Professor of Electrical and Computer Engineering

Accepted for the School of Engineering and Applied Science:

Professor Craig H. Benson ....

Dean of School of Engineering and Applied Science
Professor of Civil and Environmental Engineering

Sensing the Physical World Using Pervasive Wireless Infrastructure

by

Elahe Soltanaghaei

Abstract

WiFi connectivity is ubiquitous nowadays, specially in the new era of Internet of Things (IoT), where the majority of physical devices, home appliances, and vehicles have some kind of network connectivity. On the other hand, recent developments in wireless technologies have transformed the role of wireless signals from a pure communication medium to an enabling tool for non-intrusive sensing. Radio signals propagate along *multiple* paths and reflect from objects before arriving at a receiver, so they carry information from the environment. In this thesis, we exploit the traditionally challenging multipath propagation and convert it into an opportunity for human sensing, device localization, and object tracking by mapping each wireless reflection to relevant physical and behavioral measurements. Beyond leveraging the pervasive wireless infrastructure, the major breakthrough enabled by this thesis is our innovative approach of *unilateral sensing*, in which a single WiFi device unilaterally senses the physical world without requiring coordination or data sharing with any other devices. This, in turn, converts every WiFi-enabled device into an individual sensor that learns about the environment, leading to a scalable sensing platform.

This dissertation delivers four fundamental contributions. First, it presents a novel localization approach called *Multipath Triangulation*, which combines the geometric properties of wireless multipath signals to triangulate WiFi devices and reflection surfaces. Next, the multipath triangulation is exploited to produce the first decimeter-level unaided localization system that requires only a single WiFi receiver to unilaterally locate any other WiFi devices in the room. Beyond localizing WiFi devices, we further extend multipath triangulation to develop the first WiFi-based object tracking system that can localize the passive wireless reflections from a battery-free tag in the presence of complex multipath propagations. Finally, we demonstrate that multipath reflections provide *peripheral WiFi vision* for sensing the presence of people in a room, even if they are stationary, without requiring them to carry any devices or wear a tag.

To deliver these contributions, we employ the underlying physical properties of wireless multipath propagation and map the frequency, temporal and spatial characteristics of these signals to the physical environment. We implement new systems and algorithms that are compatible with commodity WiFi devices, which are also evaluated in regular indoor environments. A broad range of applications benefits from this sensing information including health and elderly monitoring, home automation and security, or search and rescue missions. We believe that these approach becomes a necessity in the near future as IoT devices become even more ubiquitous and context-aware services such as home well-being monitoring, robot assistants, and autonomous driving turn into daily life routines.

Dedicated to my father for teaching me the joy of learning, to my mother for all the sacrifices she made to give me a better life, and to my husband for his endless love and support throughout this journey.

Acknowledgements

It would not have been possible for me to achieve this life milestone without the support and encouragement of my teachers, colleagues, family, and friends. First and foremost, I am immensely grateful to my advisor, Professor Kamin Whitehouse, for his continuous and endless support, guidance, and patience, for believing in me and motivating me whenever I was low on energy. I can't thank him more for all his great advice, for helping me develop my research skills and teaching me critical thinking, for his dedication to brainstorm ideas with me, and for inspiring me during my research process. Without his support and guidance, my achievements would not have been possible. He will always be my academic role model and I hope I can inspire my students as he has for me.

I am also profoundly grateful to my thesis committee: Professor John Stankovic, Professor Robert Weikle, Professor Madhur Behl, and Professor Steven Bowers. Their insightful feedback and invaluable advice throughout my research have helped me a lot to shape my ideas and direct my research toward working systems. I would also like to thank my internship mentors at Microsoft Research, Dr. Bodhi Priyantha and Dr. Jie Liu, for working closely with me on the object tracking project. I have enjoyed collaborating with many other professors, students, and researchers, particularly Professor Cody Fleming, from whom I learned a great deal.

I would like to thank all my labmates: Erin, Avinash, Dezhi, Mahmoud, and Juhi, for all those fun days, their intellectual and emotional support, and their valuable feedback on numerous iterations of my papers and talks. I also thank all the residents of the UVa Linklab for creating a work environment I wanted to visit every day, and for creating an atmosphere with positive energy, respect, and friendship, which made the office life fun for me.

My life in Charlottesville would not have been so much fun if I had not been surrounded by my incredible friends, Neda, Faraz, Leili, Hooman, Amir, Jubeen, Mahboube, Hossein, Ghazale, and Ahmad, who were celebrating with me every success and cheering me up on my sad days; thank you for making my life in Charlottesville a wonderful and enjoyable experience. To all the happy memories that we had and will have together.

Most importantly, I'd like to thank my parents, for the sacrifices they made to provide me a better education, for everything they taught me through every stage of my life, and for encouraging me constantly from overseas. Finally, a special thank to my husband, Mohamad, for enriching my life, being my source of inspiration and motivation, and for staying next to me in every life milestone. His encouragement and support has made all the difference.

Contents

List of Figures

List of Tables

Chapter 1

Introduction

Nowadays, majority of physical devices such as home appliances, wearables, and vehicles have embedded actuators and network connectivity, which enable them to connect with other devices and exchange data, creating a network of *things*. The promise of IoT has been a future where connected devices work together to automate the world. This means a home that monitors your activities and health status, learns your habits and preferences, and automatically controls lighting, air conditioning, and more. With the increasing number of IoT devices, new smart applications have emerged that rely on knowing the whereabouts of devices, people, and objects. However, deploying large-scale localization systems can be cost prohibitive and creates a massive amount of data exchange and communication overhead. In this research, my goal has been to build new systems for sensing the physical world by merely leveraging the pervasive wireless infrastructure. This leads to a vision of *omnipresent sensing*, where the WiFi in every building acts as an efficient non-intrusive sensing system. This research shows how we can convert every commodity WiFi device into an individual sensor to learn about the environment and enable new services ranging from indoor tracking to human sensing.

The motivation behind this research stems from two trends: WiFi is now pervasive in urban environments, and the number of wireless devices is constantly growing and predicted to approach 1 trillion by 2025. In effect, this network of wireless devices creates radio waves that interact with each other and the environment. Each signal travels in the wireless medium along multiple paths reflecting off of walls, furniture, and human body before arriving at a receiver, so it carries information about the environment. While *multipath propagation* is traditionally known as the core challenge underlying most wireless problems, this thesis tries to transform this challenge into an *opportunity* for sensing. I demonstrate that multipath signals can extend indoor localization to any wireless devices by providing *unaided localization*; and each reflection can play as a sensor by revealing information about different parts of the physical environment, advancing object tracking and human sensing.

One of the key advantages of this sensing approach is that it does not require any dedicated sensing infrastructure, coordination between multiple devices, or any sort of data sharing beyond standard WiFi communication. We call this *Sensor Piggybacking*: using the available communications between devices to *unilaterally* sense the physical world without relying on any coordination, data sharing or synchronization between multiple devices. It can operate opportunistically whenever the wireless nodes happen to communicate, with no additional overheard. In addition, it doesn't have to be the WiFi access points that perform the sensing and localization.

Another advantage of the systems developed in this research is that they are compatible with commodity WiFi devices, their hardware imperfections, and intrinsically noisy wireless channel. We take advantage of recent advances in MIMO communications that transmit and receive signals across multiple antennas. We also use WiFi OFDM signals in the ISM band to collect the fine-grained Channel State Information (CSI) from commodity WiFi chips. CSI is measured from the packet preamble and, so can be measured for eavesdropped packets without establishing two-way communication. However, the key challenge in extracting semantics from these channel measurements is that CSI contains the signal distortions due to both multipath propagation and imperfect signal processing in the hardware such as imprecise sampling frequencies between the WiFi transmitter and receiver, or shift of the central frequencies.

We overcome this challenge by developing a novel channel combination scheme that extracts and disentangles multipath reflections by combining measurements from multiple antennas and multiple frequency sub-channels, and then use each signal as an independent measurement. This thesis demonstrates how these individual reflections can contribute to sensing and localization. This innovative system allows any single WiFi device to (1) independently localize nearby WiFi devices even the access points themselves, (2) track battery-free objects or IoT devices that don't have WiFi transceivers, and (3) act as a sensor to detect the presence, location or activities of the occupants without requiring them to carry or wear any devices.

This revolutionizes the way we conduct sensing by increasing its efficiency and accuracy while drastically reducing its cost. It also enables applications in diverse areas including healthcare, robotics, or virtual reality. For example, the HVAC system could detect the entrance or exit of the occupants and adjust the temperature accordingly to save energy while maintaining the occupants comfort; the available WiFi devices in a home could act as security sensors and monitor the entire house while it is empty, and track occupants' activities while they are home; or the robotic vacuum cleaner could navigate inside the room and find the missing objects by just using the available WiFi. We expect these systems to become a necessity in the near future as IoT devices become even more ubiquitous, and context-aware services such as home well-being monitoring, robot assistants, and autonomous driving turn into daily life routines.

1.1 Wireless Multipath: From Challenge to Opportunity

Multipath propagation is an inevitable phenomenon in wireless communication. Wireless signals emitted by a transmitter reflect and refract from objects in the environment, making multiple copies of the signal. The majority of the signal power is transferred through the direct path or Line of Sight (LoS) signal between the transmitter and receiver. However, the received signal is the superposition of all copies of the signal, which combine at the receiver and either reinforce or cancel each other. Multipath propagation has been a challenge in wireless communication as it causes interference in a variety of ways including distortion of the signal, loss of data, and multipath fading. It is even a more challenging problem in indoor applications as walls, furniture, and machinery act as obstacles or reflectors that redirect parts of the transmitted signal.

Unlike the previous works that try to overcome multipath interference by suppressing multipath effect, or isolating the features of the LoS signal, we harness reflections in the environment and show that each reflection contains information from a part of the physical environment. This research builds upon recent advances in wireless communication such as MIMO and OFDM to extend its role beyond simply a communication medium to that of a sensing tool. We present a new method of disentangling multipath signals and estimating the geometric features of each reflection such as direction or distance. We further empower this capability by harnessing the extracted signals to infer human presence, environment characteristics, object locations, or even other devices' locations. A broad range of applications benefit from this sensing information including health/elderly monitoring, home automation and security, or search and rescue missions.

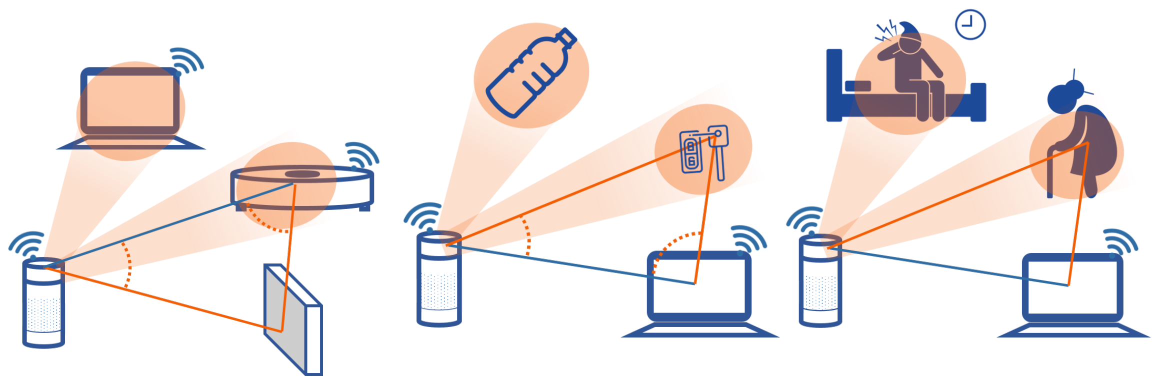

(a) Unaided Device-localization (b) Unaided Object Tracking (c) Peripheral WiFi Vision

Figure 1-1: **Systems Developed.** This dissertation chronicles the evolution of using pervasive wireless infrastructure for sensing, starting with (a) unilaterally localizing WiFi devices, which converts every WiFi-enabled device into a sensor. Then, all these WiFi devices are used to (b) track objects by using a simple battery-free tag and detecting its passive wireless reflections. Eventually, the thesis progresses to a holistic peripheral WiFi vision by providing (c) human sensing without requiring the person to carry a device or wear a tag.

1.2 Research Contributions

In this thesis, the pervasive wireless infrastructure and the multipath propagations are employed to push the limits of indoor localization, object tracking, and human sensing. The systems developed in this research has three key properties that make them particularly powerful: First, they make no assumption on the presence of a dedicated localization or sensing infrastructure. They operate unilaterally on any WiFi-enabled devices without making any assumption about the environment. Second, the systems are built based on the resources and technologies that are available in commodity WiFi devices. Third, all of these systems are implemented in practice and are extensively evaluated in regular indoor environments to demonstrate their feasibility and practicality. Below, the contributions of each of these systems are explained:

1. **Unaided Localization of WiFi Devices:** I present *Multipath Triangulation*, a new localization technique that uses multipath reflections to localize a target device with a single

receiver. In effect, it uses multiple reflections for triangulation similar to the way older systems use multiple devices. The key insight behind multipath triangulation is that the LoS and a reflection path form a *multipath triangle* that localizes the target devices by computing the directions of each path, known as angle of arrival (AoA) and angle of departure (AoD). In addition, to fully constrain the geometry of this triangle, the *relative* Time of Flight (rToF) of two paths, or the length difference of the LoS and reflected path, is computed to define the scale of the triangle. As a result, multipath triangulation overcomes the conventional challenges in range estimation with commodity WiFi and the need for time synchronization between the WiFi transceivers by leveraging the difference in ToF of two paths instead of the absolute ToF.

This led to the design of the first decimeter-level *unaided localization* system [1]. With this approach, any WiFi device can localize other nearby WiFi devices without requiring to perform any coordinated actions or even establishing a two-way communication. For example, a home automation system can localize controllers such as smart thermostats or smart plugs, even if neither the controller nor the home's access point supports a localization protocol. Beside localizing a target device, *Multipath Triangulation* localizes the reflectors with respect to the receiver, which enables new potential solutions for indoor mapping by stitching static localized reflectors, or device-free localization by tracking reflections from the human body without requiring the person to hold or wear a wireless device. In Chapter 3, I elaborate on Multipath Triangulation and present a prototype implementation of this localization system in commodity WiFi devices that we called *MonoLoco*.

2. **Object Tracking using Battery-free WiFi Tags:** While *unaided localization* can achieve accurate tracking of wireless devices, not all the objects have a WiFi transceiver. This dissertation also demonstrates how we can localize any object by simply attaching a tag. Object localization is crucial for many context-aware and automation applications in smart

homes, retail stores, or warehouses. However, no existing object tracking technology offers both simple setup and long-term operation. RFID technology enables low-cost, battery-free tags that can be placed on every object, however, the cost and complexity of covering a space with RFID infrastructure limit its practical adoption. On the other hand, WiFi localization provides simple setup by using the available wireless infrastructure but requires an active WiFi radio on the target of interest. In this research, I present *TagFi* as the first object tracking system that combines the best features of RFID and WiFi localization by using pervasive wireless infrastructure to accurately localize battery-free tags with a single commodity WiFi receiver.

The fundamental challenge in sensing objects is that the wireless reflections from a battery-free tag are considerably weaker than many other multipath signals propagating in the physical environment, so they get overwhelmed by the superposition of all signals in the receiver. To address this challenge, TagFi uses a novel modulation technique to set apart the weak passive reflection of an object among complex multipath signals. Our solution is based on a realization that a *modulated multipath* signal is incoherent with the rest of multipath reflections, which makes it distinguishable regardless of how much this modulated path is attenuated. Chapter 4 presents our design of a WiFi-based tag that employs this realization and demonstrates how TagFi leverages the underlying physical properties of multipath propagation to detect and localize the passive wireless reflection from a battery-free WiFi tag.

3. **Peripheral WiFi Vision for Human Sensing:** beyond localizing devices and objects, this thesis demonstrates that monitoring wireless reflections from objects and the human body enables *peripheral WiFi vision* for human sensing. The ability to automatically control air conditioning, heating, and lighting provide significant monetary and environmental benefits, which can be only realized by efficient and accurate human presence sensing. However, existing occupancy sensors can only detect the motion of people, causing ma-

jor comfort issues when the users are stationary. To address this problem, this research presents PeriFi, an occupancy sensing system that detects human presence, and not just human motion. So, it can sense both moving and stationary occupants by exploiting wireless reflections. Our key insight is to convert each reflection into an individual spatial sensor and track temporal and spatial variations of these wireless paths to increases the sensing area and sensitivity to small movements of a stationary target. Chapter 5 describes our algorithms to classify occupancy states of a room and how to capture the variations of multipath characteristics due to human movements.

1.3 Thesis Outline

The rest of this dissertation is organized as follows:

- Chapter 2 overviews the knowledge background of wireless signals and the underlying technologies that are borrowed in this dissertation from wireless communication. It also discusses the state of the art in WiFi sensing and localization.

- Chapter 3 presents Multipath Triangulation as a novel localization approach and demonstrate its application in device localization with a single commodity WiFi receiver. This chapter revises a previous publication [1]; Elahe Soltanaghaei, Avinash Kalyanaraman, and Kamin Whitehouse. Multipath Triangulation: Decimeter-level WiFi localization and orientation with a single unaided receiver. ACM MobySys 2018.

- Chapter 4 presents a WiFi-based object tracking system that exploits passive wireless reflections from a customized battery-free tag. This chapter, in full, is a reprint of the material for an under-review paper. Elahe Soltanaghaei, Kamin Whitehouse, Bodhi Priyantha, Jie Liu, Gerald DeJean. TagFi: Localizing battery-free objects using a single commodity WiFi device.

- Chapter 5 presents PeriFi, an innovative approach for human sensing by converting wireless distortions caused by body movements to a useful sensing method. This approach proposes the concept of peripheral WiFi vision, which addresses the challenge of detecting the presence of stationary people. This Chapter, in full, revises a previous publication [2]: Elahe Soltanaghaei, Avinash Kalyanaraman, Kamin Whitehouse. Peripheral WiFi Vision: Exploiting multipath reflections for more sensitive human sensing, ACM WPA 2017.

- Chapter 6 concludes the thesis by summarizing the contributions and describing future work.

Chapter 2

Background and Related Work

In spirit, this research advances the well-established problem of indoor sensing and navigation, which has been explored through various means including acoustic signals [3, 4], ultrasound [5, 6], FM [7], infrared [8], RFID [9, 10], Bluetooth [11], cellular [12, 13], Zigbee [14, 15], WiFi [16–18], UWB [19, 20], and more. The advantage of using WiFi signals, however, is that they are already everywhere even in the millions of older buildings that do not have sensing and localization infrastructures in place. One of the earliest WiFi-based indoor tracking systems is RADAR [16] developed at Microsoft. The system utilizes the signal strength captured from multiple WiFi nodes and match it with the radio signatures collected offline from every location in the room. However, the key challenge in inferring position or generally context-based information from WiFi signals is that we live in an ocean of radio signals which bounce off all walls, furniture, and reflection surfaces, so just the movement of a person in the room or displacement of furniture can change the wireless signatures. Traditional solutions to address this challenge follow three research lines of recurrent fingerprinting, suppressing multipath interference, or isolating the features of the LoS path. Unlike these previous works that all try to eliminate the multipath effect, this dissertation demonstrates how each individual multipath reflection can contribute to sensing and localization.

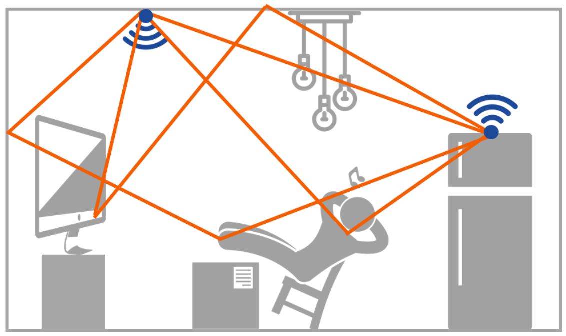

Figure 2-1: **Multipath Propagation.** Wireless Signals propagate along multipath paths in indoor environments creating rich multipath propagation.

This chapter briefly overviews the fundamentals of wireless communication and the underlying wireless technologies that this dissertation is built upon. At last, an overview of the state of the art in WiFi sensing and localization is provided. The related works are then categorized based on the application and the type of techniques used to overcome multipath interference.

2.1 Multipath Propagation

In a wireless link, the electromagnetic signal is emitted from an antenna as a radio wave, which then radiates through the wireless medium or the environment. However, wireless signals do not go on a straight line; they propagate along multiple paths and many copies of the signal arrive at the receiver, as shown in Figure 2-1. The inherent *multi-path* phenomenon of indoor environments is one of the most important channel effects. The superposition of these signals at the receiver results in constructive or destructive interference depending on the phases of the individual signals, thus either giving a good overall signal or mostly canceling each other.

What is worse, the multipath channel characteristics may change over time due to change of channel geometry. Small differences in the delay or phase of multipath signals can make a big difference in the received signal due to the superposition effect. For example, half a wavelength delay of a 2.4GHz reflection will completely null the received signal (assuming that the signal strengths of the two paths are equal). Temporal variations can happen due to the movement of a person inside the room, which changes the length of the wireless path reflected from the body over time, or the person may block some of the existing reflections in the environment. Furthermore, as a result of multipath phenomenon, the received wireless signals significantly vary over *frequency* and *space*, which causes uncertainty in wireless communication. Frequency selective fading is one of the anomalies caused by multipath fading, in which different frequency components of the signal experience uncorrelated fading, causing problems in decoding the symbols. On the other hand, the spatial variation of the wireless signals is the main challenge of mobile wireless nodes because there is a significant probability of deep fading at any given location due to the change of surrounding environment and their corresponding multipath characteristics.

In spite of challenges that multipath propagation causes, an alternative way of looking at this phenomenon is that it provides *diversity*. In a sufficiently rich multipath environment, different copies of the signal are observed across different frequencies and spatial locations. The next section elaborates on two technologies that take advantage of multipath diversity for better communication quality. These two techniques are building the fundamentals of the approaches developed in this dissertation for sensing and localization.

2.2 Overview of MIMO-OFDM Links

MIMO (Multiple Input Multiple Output) and OFDM (Orthogonal Frequency Division Multiplexing) are the two 802.11 schemes that are developed based on spatial and frequency diversity of multipath signals to improve wireless capacity and quality. As shown in Figure 2-2, in OFDM, a frequency bandwidth splits into multiple *subcarriers* each of which

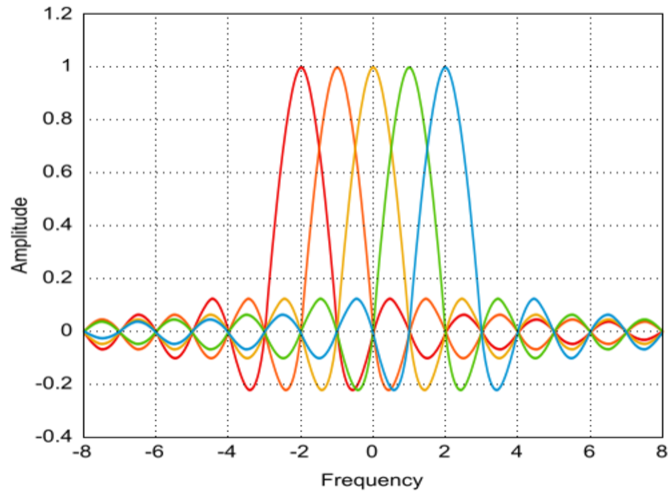

Figure 2-2: **OFDM Scheme.** The subcarriers, in OFDM, are orthogonal to each other.

carries a different modulated bit in parallel. So, it takes advantage of frequency diversity to provide a higher level error-correcting as all subcarriers will not be affected the same way with multipath interference and we never lose all the data due to deep fading of the signal. In addition, each of these subcarriers transfers the bits for a longer time, so it can average out the temporal fades by turning a single fast channel into many slower parallel channels, taking advantage of *time diversity*. As a result, OFDM signals are more resilient to interference and frequency-selective fading. OFDM is widely used as a modulation technique and is available in major communication applications such as WiFi 802.11a/g/n.

MIMO is a wireless technology that takes advantage of *spatial diversity*. The earliest idea of MIMO was proposed in 1970 to configure multiple antennas co-located at one transceiver for improving the link throughput. The key insight is that the antennas separated by at least half a wavelength has independently-faded channels. So, a multi-antenna receiver can combine the received signals from multiple antennas to average out the noise. Similarly, a multi-antenna transmitter can emit multiple signals in a way that the copies arriving at the receiver combine optimally. On the other hand, the spatial diversity caused by multipath propagation leads to splitting the data into multiple independent streams transmitted through

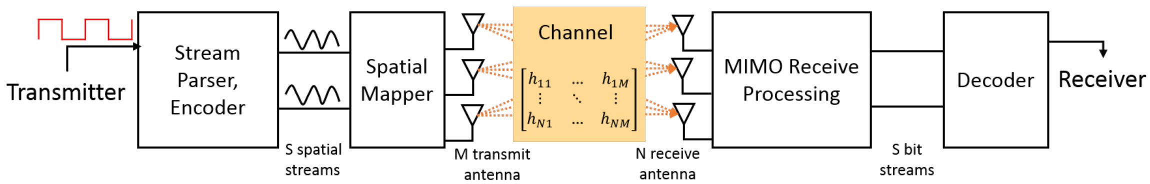

Figure 2-3: **a bloc-view of a MIMO-OFDM link in the context of 802.11n**

different antennas and received by multiple antennas, providing bit rates as high as 450Mbps. This is called *spatial multiplexing* and combined with OFDM, it evolved to MIMO-OFDM technology that is now available in 802.11n.

Figure 2-3 demonstrates the basic model of a MIMO-OFDM link in the context of 802.11n. First, the transmitter generates S spatial streams of symbols for a packet that is OFDM modulated. This codes the bits across frequency and spatially diverse subcarriers. Next, the *spatial mapper* maps the S streams into M transmit antennas. Different spatial mapping algorithms are developed to optimize the decoding process. Then, the signal propagates in the wireless medium that alters the transmitted signals by H. The matrix H known as the Channel State Information (CSI) consists of the phase and amplitude coefficients by which the signal is affected as it travels the wireless medium. It should be noted that the channel H is different for every OFDM subcarrier, although it is demonstrated as a single RF channel in Figure 2-3. Finally, N receive antennas capture the signal and employ one of many MIMO processing algorithms to disentangle the S streams and demodulate the symbols. To do so, the receiver first computes the channel coefficients (H) using the known packet preambles, which is then used to decode the signal. The following section elaborates on this process in details.

2.3 Channel State Information

The central component and the input of the algorithms developed in this thesis is a set of low-level RF channel measurements known as Channel State Information (CSI). For every packet transmitted over the air, the receiver detects the beginning of the packet from the increase of the energy and then estimates the parameters of the wireless channel from the known symbols in the packet preamble to decode the bits. To calculate CSI, the received signal x is expressed in terms of the CSI matrix H and the transmitted signal y as follows.

$$x = Hy + n \tag{2.1}$$

where the various symbols are:

$$\mathbf{y} = \begin{bmatrix} y_1 \\ y_2 \\ \vdots \\ y_N \end{bmatrix} \quad \mathbf{x} = \begin{bmatrix} x_1 \\ x_2 \\ \vdots \\ x_M \end{bmatrix} \quad \mathbf{H} = \begin{bmatrix} h_{11} & h_{12} & \cdots & h_{1M} \\ h_{21} & h_{22} & \cdots & h_{2M} \\ \vdots & \vdots & \ddots & \vdots \\ h_{N1} & h_{N2} & \cdots & h_{NM} \end{bmatrix} \quad \mathbf{n} = \begin{bmatrix} n_1 \\ n_2 \\ \vdots \\ n_M \end{bmatrix}$$

The receiver solves this set of equations for the known preambles (for which both x and y are known) for the CSI matrix H.The CSI includes the channel gain coefficient (both amplitude and phase) for each OFDM subcarrier. For an $N \times M$ MIMO link, the CSI is an $N \times M \times S$ matrix, where each entry represents the channel coefficient from one transmit antenna to a receive antenna for each of S subcarriers. In this dissertation, we leverage the fine-grained CSI measurements to characterize multipath propagation and show how to transform this information into efficient, robust, and accurate sensing and localization systems.

CSI is measured automatically at the receiver in the course of receiving 802.11n packets. We leverage this mechanism and configure the commodity network cards to send the mea-

Figure 2-4: **The Intel Wireless WiFi Link 5300** used for the experiments of this dissertation. This 802.11n device supports three antennas and three spatial streams, and operates on both 2.4GHz and 5GHz frequency bands

sured CSI up to the driver and log this information in the user-space application. For this, we leverage the CSI tool [21] developed for Intel WiFi Wireless Link 5300 network cards (Figure 2-4). These 802.11n MIMO chipsets have three antennas and support MIMO-OFDM and more specifically spatial multiplexing with three data streams. The CSI tool modifies the card's firmware and *iwlwifi* driver for Linux to log the channel metrics for 30 subcarriers in both 20MHz and 40MHz OFDM channels.

2.4 Sensorless Sensing with WiFi Network

The ubiquity of WiFi in every indoor environment and its technological advances have extended the role of WiFi infrastructure from a sole communication medium to a *sensorless sensing platform*. The concept of sensorless sensing refers to the ability of inferring the surrounding environments by merely leveraging a pre-existing infrastructure that is deployed for a different primary usecase. Over the past two decades, there has been increasing interest in using wireless signals and more specifically WiFi to sense the environment and people. The presence of WiFi devices in any indoor environments, the capability of these signals to traverse occlusions, and their sensitivity to any small movement make this sensing modality suitable to be used for detecting the human motions [22, 23], human activities [24–27], and localizing the target in indoor environments where GPS does not work [16, 28–34]. In addition, researchers have inferred more fine-grained information from WiFi signals through applications such as hand gesture recognition [35], keystroke detection [36], object imaging [37] or human identification [38, 39]. In this dissertation, we leverage WiFi signals for localization and sensing with novel capabilities such as unilateral localization of WiFi-enabled devices, or tracking of battery-free objects. We take the unique approach of harnessing wireless reflection instead of eliminating them to deliver these applications, which are discussed in the next section.

2.5 From RSS to CSI

Available in mainstream wireless signal measurements, the Received Signal Strength Indicator (RSSI) has been adopted in vast WiFi-based sensing and localization systems [24, 28, 33, 37, 40]. However, the main problem of RSSI is that it only measures the total amount of power in a link, which does not include the channel properties for different frequency and spatial subchannels that WiFi uses to send independent data. This results in very limited accuracy (e.g. 2-4 m accuracy in localization), especially in complex environments and scenarios. In contrast, CSI is a fine-grained measurement that captures the channel details at the level of frequency-selective fading and independent spatial paths. This makes the PHY layer Channel State Information a promising substitute for MAC layer RSSI. The channel response information on each subcarrier includes both amplitude and phase changes which can be utilized to provide a lot more information than RSSI readings.

One of the common ways of inferring semantic context from WiFi signals is fingerprinting of received signal power or channel information, and adopting a pattern-matching approach. The main idea is to collect signal features for all possible locations in the area of interest and build a fingerprint database. Although this method has been widely used for motion detection [41] and indoor localization [16, 32–34], the achievable performance is limited to a few meters due to complex multipath effect. In addition, these methods rely on a manual training mechanism for every physical environment, thus suffering from cumbersome efforts of characterizing the environment especially if it is dynamic. Some proposals tried to improve the accuracy and practicality by using supervised machine learning models. Although this type of solution is common for occupancy detection [42, 43] and activity recognition [25–27], it does not help localization. In addition, the performance of these methods is still limited to the training dataset, resulting in the need to continuously re-characterize the environment.

To address the limitations of fingerprinting, some proposals focus on RF propagation models [44–46] to estimate the distance between a transmitter and a receiver based on the signal strength reading and known signal attenuation properties. The absolute distance can be estimated by using signal propagation models given that the transmission power at a reference point is known. However, these methods still suffer from poor localization accuracy due to signal fluctuations caused by multipath fading and indoor noise. For example, TIX [47] achieves an accuracy of 5.4 meters by triangulating based on the signal strength models Lim et al. [48] combines the RF propagation method with singular value decomposition to create the map and achieve a median accuracy of 3 meters. Finally, some model-based techniques improve the RF propagation models with bayesian probability to capture the relationship between different nodes [49]. In addition to RSSI and signal strength, later works leverage the channel state information to define finer signatures. However, the majority of research in this domain still focuses on CSI amplitude [25–27, 32].

Another line of research on WiFi sensing analyzes the signal propagation by deriving the intermediate geometric parameters of the signal such as the distance (e.g ToF) or direction (e.g. AoA and AoD) with regard to the reference points. These relative parameters are then converted into location estimates [29–31], trajectory [50], or velocity [51] using geometric algorithms. However, due to fundamental limits in the range resolution of WiFi, these methods either use multiple access points [29–31, 50, 52, 53] or multiple frequency channels [34]. Either approach requires the coordination of multiple WiFi devices, which can be an issue in public spaces that WiFi devices are often in different administrative domains or in environments served by only a single AP including homes and small business. On the other hand, channel switching requires close coordination between the transmitter and receiver, which means that both nodes must be upgraded to run a switching protocol, thus introducing new protocol overhead.

Chapter 3

Unaided Localization of Wireless Devices

In recent years, several new developments have enabled RF localization with tens of centimeters error – a promising and important step towards the vision of accurate and ubiquitous indoor device localization. A common thread that runs through this new generation of techniques is the ability to eliminate the effects of multipath interference by directly measuring geometric features of the line of sight (LoS) signal, such as angle of arrival (AoA) or time of flight (ToF). However, due to fundamental limits in clock synchronization or range resolution, current methods require some form of explicit coordination between nodes. For example, AoA-based methods require coordination across multiple access points (APs) to perform triangulation; and ToF-based methods require establishing two-way communication as well as channel switching between the transmitter and receiver to overcome the challenge of clock synchronization and bandwidth limitation. Coordination between nodes can take many forms but cannot be achieved without introducing complexity, communication overhead, pre-deployed infrastructure, and/or the practical challenges of protocol rollout and adoption.

In this chapter, we present a different approach to WiFi localization: instead of eliminating the effects of multipath reflections, we use them to help localize the transmitter. Every

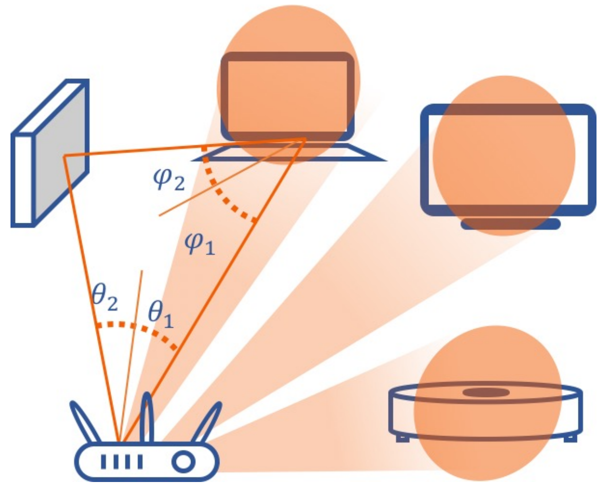

Figure 3-1: **Unaided localization of wireless devices using multipath triangulation**

multipath reflection is considered to be an independent measurement of the target location. As shown in Figure 3-1, we extract features of the multipath signals, including their angle of arrival (AoA), angle of departure (AoD), and relative time of flight (rToF), i.e. their ToF relative to that of the LoS path. These multipath features are combined with the AoA and AoD of the LoS path to form a *multipath triangle* between the target device, the receiver, and the reflector. The key insight behind our approach is that the geometry of this triangle is fully constrained; the AoA and AoD of the two paths define the shape and orientation of the triangle while the rToF uniquely defines its scale. As such, it can be used to triangulate the position of the transmitter relative to the receiver. In effect, this approach uses multipath reflections in the same way that conventional triangulation uses multiple APs. We call this approach *multipath triangulation*.

The main benefit of *multipath triangulation* is that it enables what we call *unaided device localization*: a single receiver can localize a transmitting target without coordinating with any other nodes. It avoids coordination with APs by using multipath reflections to triangulate the target location, and it avoids coordinating with the transmitter by measuring rToF instead of absolute ToF. Unlike ToF, rToF can be measured entirely at the receiver without coordinating with the transmitter because it relies on relative phase values across frequencies, thus not requiring clock synchronization [30]. In contrast, existing systems require the APs to share their locations with mobile nodes [6, 16, 32], to share measurements with each other [30, 31, 52, 53], or to perform coordinated actions with the target node for time synchronization [54, 55] or frequency hopping [29, 40, 56]. Each of these methods incurs some challenges of coordination in terms of complexity, overhead, infrastructure, or adoption.

We leverage this feature of *multipath triangulation* to design *MonoLoco*, the first unaided WiFi localization system with decimeter-level accuracy that requires only a single commodity WiFi receiver and a single channel. As a bonus, it also provides the orientation of the target with degree-level accuracy. MonoLoco uses only Channel State Information (CSI) from a 3-element antenna array to derive AoA, AoD, and ToF of each path. It defines a new model of the wireless channel based on subspace-based super-resolution methods [30, 57, 58] that combines transmitting antennas, receiving antennas and multiple frequency subcarriers into a single large-aperture sensing array. Then, it plugs the derived AoA, AoD, and ToF into a non-linear optimization problem to determine the location and orientation of the target. CSI is already collected by commercial WiFi chipsets without requiring a firmware upgrade, and multi-element arrays are commonly used on APs, laptops, drones, televisions, and many other devices. As such, MonoLoco is *fully-piggybacked* on top of WiFi communication; it does not impose any requirements beyond standard WiFi protocols, including hardware changes, protocol overhead, external clocks, external sensors (such as inertial sensors), or environmental profiling. Thus, MonoLoco can be used opportunistically whenever these nodes happen to communicate, with no additional overhead.

Furthermore, CSI is measured from the packet preamble and, as such, can be measured for eavesdropped packets even without 802.11 association, and even if the packets are encrypted. Thus, MonoLoco allows any WiFi device to localize any other nearby WiFi device even if neither of them is an AP. For example, a home automation system can localize controllers such as smart thermostats or smart plugs (with respect to its own coordinate system), even if neither the controllers nor the home's AP(s) support a localization protocol. In addition, MonoLoco provides orientation estimates with degree-level accuracy, which can enable new context-based applications. For example, when a person asks a smart speaker for a picture or recipe, it can automatically cast the image to a display with a position and orientation that is visible from a given location. Similarly, a robot can navigate to a WiFi power socket while using its estimated orientation to determine the side of the wall from which to approach it.

To evaluate this approach, we implement MonoLoco using Intel 5300 WiFi cards operating at 5GHz with 40 MHz of bandwidth. Each node was equipped with a 3-element linear antenna array with 2.7 cm spacing between antennas. We deployed MonoLoco in four environments with different multipath properties, including an anechoic chamber, a home, two office environments, and two public spaces. Our experiments show that MonoLoco achieves a median localization error of 0.5 *m* and a median orientation error of 6.6 degrees, which are comparable to the best existing systems that require multi-node coordination. Results also show that MonoLoco can approach this accuracy with as few as 7 packets. These results are promising and serve as a proof-of-concept for the *multipath triangulation* approach. We expect these results to improve when used with more advanced resolution algorithms such as Maximum Likelihood methods [59] and non-linear solvers, which are now becoming computable. In addition, Results are also expected to improve when using more number of antennas or larger bandwidth, all of which are possible with today's WiFi chips.

3.1 Background and Related Work

In general, wireless localization schemes either map measurements from wireless signals into geometric parameters such as distance or direction to localize the target with respect to one or multiple reference devices, or prelabel landmarks to directly localize the target in the space.

In this chapter, we focus on the first scenario where two devices are localized with respect to each other. The state-of-the-art device localization systems can be categorized into (1) distance-based (or ToF-based) methods which leverage trilateration or multilateration, and (2) angle-based methods which use triangulation. However, using either of these methods requires some form of explicit coordination between nodes that is explained next.

Time of Flight (ToF) measurement is a widely used technique for device localization, which relies on measurements of travel time of signals between the transmitter and receiver. However, accurate measurement of ToF requires a common clock and strict time synchronization between the transmitter and receiver. To overcome this challenge, traditional ToF-based systems either use multiple synchronized transmitters such as the GPS system [60], or use the "echoing" method [61–65] where the transmitter measures the round trip propagation time. A problem with round-trip ToF-based systems is the response delay at the receiver which highly depends on the receiver electronics and protocol overheads. A recent system called Chronos [40] addresses this problem by leveraging the channel frequency responses and combining these measurements from both transmission directions. In effect, it can accurately estimate ToF by removing the sampling frequency offset caused by lack of time synchronization between two nodes. However, it still suffers from the fundamental limitation of the round-trip techniques, which is the required two-way communication and overhead of message exchanging between any two nodes to localize each other. Cricket [6] is a localization system that overcomes the synchronization problem by using a combination of RF and ultrasonic signals, however, it requires dedicated hardware.

Time Difference of Arrival (TDoA) is another technique to overcome the synchronization problem. It uses relative time measurements between multiple pairs of APs or reference nodes with known locations, instead of absolute time measurements [29, 56, 66, 67]. Each difference of arrival time measurement produces a hyperbolic curve in the location space, so the TDoA from at least three receivers is required to find the intersection and accordingly

	Underlying Method	Decimeter-Level Localization	Orientation	Single Access Point	Unaided	Fully Piggybacked
ToneTrack [29]	Multilateration	✗	✗	✗	✗	✗
PinLoc [32]	Fingerprinting	✗	✗	✗	✗	✓
SpotFi [30]	Triangulation	✓	✗	✗	✗	✓
Chronos [40]	Trilateration	✓	✗	✓	✗	✗
MonoLoco	Multipath Triangulation	✓	✓	✓	✓	✓

Table 3.1: Compared to the state-of-the-art of WiFi localization systems, MonoLoco is the only single access-point solution that provides decimeter-level localization and orientation information and requires no coordination, time synchronization or external networking protocol with the target or with other APs.

the location of the transmitter. Although this technique does not need any time synchronization between the transmitter and receiver, it requires strict time synchronization between the access points.

Another component of ToF (or TDoA)-based localization systems is to convert the time (or distance) measurements into locations using geometric algorithms such as *trilateration* or *multilateration*. These algorithms localize the target by finding the intersection of distance measurements from multiple anchors, which mandates a centralized localization infrastructure with multiple access points or reference nodes to coordinate the localization together. Chronos[40] addresses this issue by performing trilateration between time-synchronized antennas separated by 30cm, however, it still requires coordination between the transmitter and receiver to share their channel measurements for clock synchronization. SAIL [64] is another system that can localize a target with a single access point using round trip ToF measurements. However, it relies on external IMU sensors on the target as well as target movement to perform trilateration.

Besides the synchronization error, the other factors that affect ToF (and TDoA) estimation accuracy are the signal bandwidth and the sampling rate. Time resolution is inversely related to the radio bandwidth, and low sampling rate (in time) reduces the ToF resolution since the signal may arrive between the sampled intervals. Some proposals such as Chronos

[40] and ToneTrack [29] emulate wideband communication by switching between multiple channels and stitching measurements from these channels together to obtain the ToF with high resolution. However, not only these techniques do not overcome the required coordination for time synchronization, they even introduce new coordination between the transmitter and receiver for channel switching. Some other proposals address the bandwidth limitation by using frequency domain super-resolution algorithms [68, 69] and joint estimation of multiple geometric parameters [70].

Angle-based method or triangulation is another group of localization systems that either use beamforming (with directional antenna) to estimate the direction with maximum signal strength, or leverage relative phase measurements in an antenna array to estimate the angle of the LoS path. Although angle-based techniques do not suffer from time synchronization or bandwidth problem, they still require measurements from several (four to six) anchors simultaneously to perform triangulation [30, 31, 50, 52, 53], thus requiring information sharing and coordination of several nodes for accurate localization. In addition, very large antenna arrays (6-8 elements) are usually required [31] to improve the resolution.

Multipath triangulation builds on the state-of-the-art methods and combines the best features of angle-based and ToF-based methods. It avoids coordination between multiple APs by using angular features of multipath reflections such as Angle of Arrival (AoA) and Angle of Departure (AoD), and combining them with those of LoS path. In addition, it overcomes time synchronization problem by leveraging the difference in ToF of two paths instead of the absolute ToF to constrain the localization algorithm. Therefore, it does not require any form of coordination, data sharing, or synchronization. As a result, any two devices can be localized with respect to each other even without establishing a two-way communication. We exploit *multipath triangulation* with WiFi to develop a device-based localization system called *MonoLoco* and show that this technique even works on commodity WiFi devices. MonoLoco is a system that provides decimeter level location and orientation information using just a single unaided WiFi receiver. it defines a novel 3-dimensional super-resolution algorithm that leverages CSI measurements to estimate the geometric features of multipath reflections, and builds upon previous Joint AoA and Delay Estimation (JADE) techniques [30, 70, 71].

Disentangling multipath is a widely studied problem in ToF cameras [72], light imaging [73, 74], or wireless sensing and imaging [2, 71, 75, 76]. A recent system called WiCapture [50] introduces a WiFi-based technique for motion tracking that uses multipath reflections to compensate for the distortions caused by the sampling frequency offset. So, it can estimate the trajectory of the motion (not the absolute position of the target) by using the temporal changes in the phase of the received signal in multiple WiFi access points. Unlike this previous system, *multipath triangulation* directly uses multipath reflections for geometric mapping in place of multiple nodes to perform triangulation.

Besides localizing another device, prior works have also attempted other forms of localization such as device-free localization of a person with FMCW radars [76, 77], UWB impulse radars [78, 79], RFID [80], or WiFi [81, 82], as well as self-localization of a target/robot in the environment with fingerprinting [16, 32–34, 83], ambient signals [84], SLAM-based techniques [85], or dead reckoning [86]. These techniques are complementary to our system where every wireless node can localize other nodes with respect to itself.

Orientation Estimation: The standard way to measure the orientation of a device is via the use of IMUs [87, 88]. However, with IMUs, the gyroscope only provides the derivative of the yaw while the magnetometer can be limited by perturbation in measuring the heading in indoor spaces [89]. As a result, some wireless-based solutions are introduced [90, 91], which use MIMO to estimate AoA and AoD. However, the performance of these methods is limited by coarse-grained multipath resolution. *Multipath triangulation* uses the same principle but applies a 3-dimensional super-resolution algorithm to extract the features of multipath more accurately and identify the direct path from which the orientation is estimated.

3.2 Multipath Triangulation

Conventional features of multipath reflections such as AoA, AoD, and ToF are determined in large part by the location of the reflection surface, which is neither known nor of interest. These multipath features do not contain any information about the relationship of the receiver and the transmitter locations. As such, multipath reflections have generally not been considered useful for localization. This chapter introduces a new geometric algorithm called *multipath triangulation* that combines the geometric features of a multipath reflection with the LoS path to estimate the location and orientation of the target device as well as the location of the reflector. The basic insight behind *multipath triangulation* is that the *relative* ToF (rToF) of two paths, the difference between the length of the reflected path and the direct path, actually does have useful information even while the *absolute* ToF of a multipath reflection does not. The direct path and a reflected path form a triangle with the AP at one vertex, the target at another vertex, and the reflection surface at the third vertex. Two angles of that triangle can be known based on the AoA and AoD of the two paths, and the rToF constrains the relative lengths of the sides of the triangle. Together, these constraints fully determine the triangle and thus the location of the target and the reflector.

More concretely, the following 4-step procedure can determine the location/orientation of the target, as illustrated in Figure 3-2. In step (1), the AoA of the direct path (θ_1) constrains the target location to be on line relative to the orientation of the receiver's antenna array. In step (2), the AoD of the direct path (φ_1) constrains the orientation of the target's antenna array with respect to the receiver's antenna array. This orientation is labeled α. In step (3), the AoA and AoD of the reflected path (θ_2 and φ_2) define a triangle between the target, the receiver, and the reflector, but the size of that triangle is still unconstrained. Here, the key innovation of *multipath triangulation* comes into play. From all possible triangles, only one of them has the corresponding rToF (i.e. the ToF difference of the reflected path and the direct path). Therefore, in step (4), the rToF (ΔT) constrains the size of the triangle such that $b + c - a = \Delta T \times C$, where $b + c$ is the length of the reflected path, a is length of the direct path, and C is the speed of light. This fully determines the triangle, allowing the location of the target (x_1,y_1) and the location of the target (x_2,y_2) to be known.

Conventional triangulation method fully determines the triangle formed by a target and two receivers by using three pieces of information: two AoA estimates from the target to the receivers, and the distance between the reference receivers. This method is based on the clas-

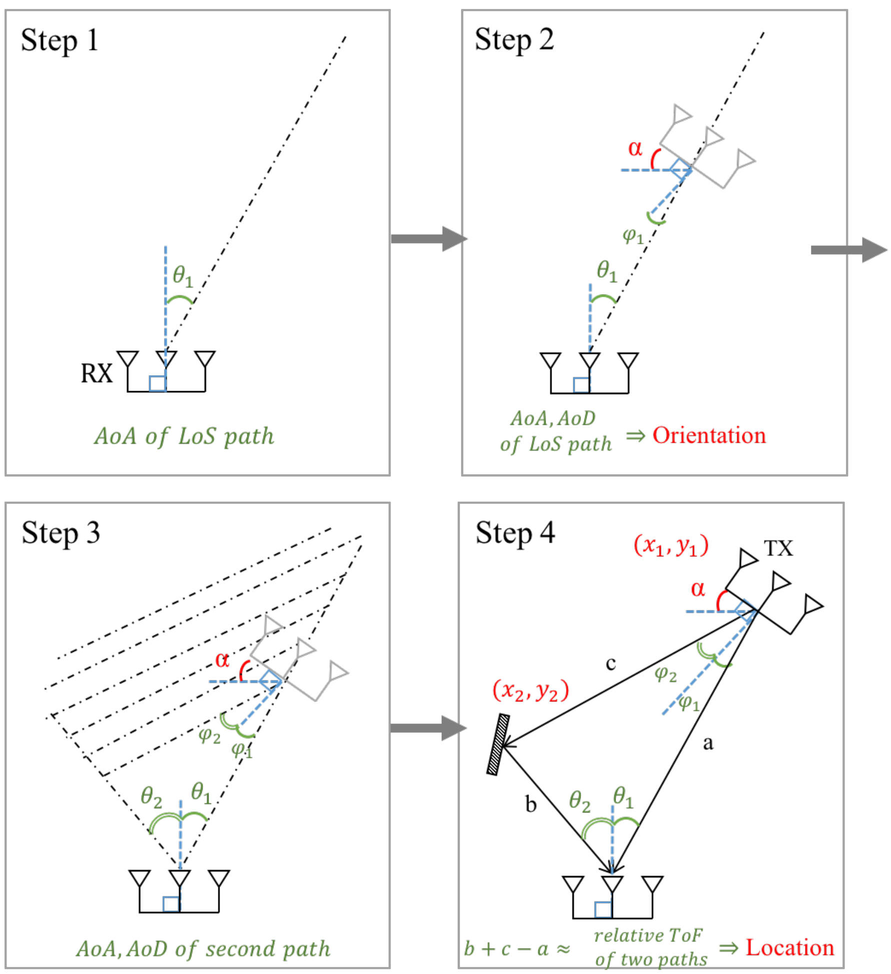

Figure 3-2: **Multipath triangulation** uses the (1) AoA and (2) AoD of the direct path to estimate the target's orientation. Then, in step (3), it uses AoA and AoD of the reflected path to find the relative location of the target with respect to the reflector and the receiver. In step (4), it uses the relative ToF between the two paths to find the target location.

sical angle-side-angle triangle congruence theorem which proves that these three properties are sufficient to fully determine any triangle. *Multipath triangulation* uses a similar process to fully determine the triangle formed by multipath reflections, except that it uses four angle estimates (AoA and AoD of the direct path and a reflected path) and one rToF value.

It should be noted that the principles of *multipath triangulation* are independent of the frequency of the RF signal, antenna array arrangement, or the multipath resolution algorithm. In addition, this new triangulation algorithm can be used for different types of applications where the location or orientation of another device or a reflector is of interest. These applications range from indoor navigation and mapping to health/elderly monitoring. In this chapter, we focus on device-based localization and show that this approach even works on commodity WiFi devices by using MIMO-OFDM technology and only 3 antennas. We use *multipath triangulation* to localize two WiFi devices with respect to each other. This results into *MonoLoco*, the first decimeter-level WiFi localization system that requires no coordination, data sharing or even two-way communication between the transmitter and receiver. In the next section, we explain the details of *MonoLoco* and the implementation of *multipath triangulation* for device-based localization.

3.3 MonoLoco: Unaided Device Localization

Commodity WiFi chips provide the amplitude and phase shifts introduced by the wireless channel in the format of Channel State Information (CSI). MonoLoco exploits *multipath triangulation* algorithm and CSI values from a 3-element antenna array and 30 frequency subcarriers to localize and orient another WiFi device. It uses a new method to resolve the AoA, AoD, and ToF of multiple propagation paths between the transmitter and receiver. The basic intuition is that (a) the AoA creates a predictable phase shift on the different sensing elements of the receiving antenna array, (b) the AoD creates a predictable phase shift from

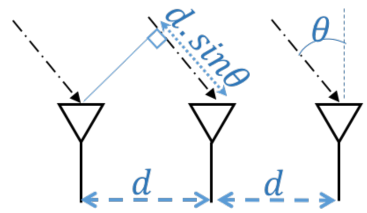

Figure 3-3: **MIMO Antenna Arrays.** The phase shift across the antenna array is a function of the antenna spacing d and the angle of arrival θ of the signal.

each of the transmitting antennas on a given receiving element, and (c) the ToF creates a predictable phase shift across different frequencies. To calculate these values, MonoLoco combines measurements across multiple subcarriers on multiple receiving antennas, from each of the transmitting antennas. In our implementation, we use 3 receiving antennas, 3 transmitting antennas, and 30 subcarriers for a total of 270 sensing elements. In theory, this large aperture could resolve as many as 269 different propagation paths. In practice, however, only a handful of paths can be resolved due to measurement noises. Still, this set of 270 sensing elements contains enough information to estimate the AoA, AoD, and ToF and the large aperture allows for a higher accuracy than state of the art methods. Implementations that use more antenna elements or more frequencies could achieve even higher accuracy.

Given this sensing array, MonoLoco resolves multipath features using a joint estimation technique that we call *3-dimensional super-resolution*. This approach builds on well-established noise subspace methods such as MUSIC [58] and Joint AoA and Delay Estimation (JADE) techniques [30, 70]. We first explain how the standard MUSIC algorithm works, and then present our extensions for joint estimation of AoA, AoD, and ToF.

3.3.1 MUSIC Overview

MUSIC is based on the intuition that when different propagation paths have different AoAs, the paths can be resolved by leveraging the extra phase shift introduced by the paths on the antenna array. As shown in Figure 3-3, this additional phase shift is due to the extra distance that the signal travels to reach the succeeding elements of the antenna array. This added phase shift $\Phi(\theta_l)$ is a function of both the AoA of that path and the distance between antennas, and can be expressed as:

$$\Phi(\theta_l) = e^{-j2\pi f d \sin(\theta_l)/C} \tag{3.1}$$

where θ_l is the AoA of the l^{th} path, d is the distance between the antennas, C is the speed of light, and f is the frequency of the transmitted signal. Consequently, the resulting vector of received signals across the antenna array due to l^{th} path can be written as a linear combination of the signal incident on the first (reference) antenna as:

$$X(t) = [x_1(t), ..., x_M(t)]^T = a(\theta)s(t) + N(t) \tag{3.2}$$

where M is the number of receiving antennas, $s(t)$ is the received signal at the first antenna and $N(t)$ is the noise vector. $a(\theta)$ is called the *steering vector* and expresses the expected phase differences across the antenna array:

$$a(\theta) = [1, \Phi(\theta)^1, ..., \Phi(\theta)^{M-1}]^T \tag{3.3}$$

When there are L incident paths arriving at the antenna array, the signal received at each antenna is the superposition of all paths. Therefore, Equation 3.2 can be written as

$$X(t) = \sum_{i=1}^{L} a(\theta_i)s_i(t) + N(t) \tag{3.4}$$

The MUSIC algorithm analyzes the eigen structure of the correlation matrix by defining $M - L$ eigenvalues as the noise subspace $E_L = [e_1, ..., e_{M-L}]$ and the other L eigenvalues as the signal subspace. Then, it searches for the AoAs whose steering vectors are orthogonal to the noise subspace, which appear as peaks in the following spatial spectrum function:

$$P(\theta) = \frac{1}{a^H(\theta)E_L E_L^H a(\theta)} \tag{3.5}$$

3.3.2 3D Super-resolution of AoA, AoD, and ToF

We extend the standard MUSIC algorithm into a 3 dimensional joint estimation by leveraging the spatial diversity in receiving antenna array to estimate AoA, the spatial diversity in transmitting antenna array to estimate AoD, and frequency diversity across OFDM subcarriers to estimate relative ToF. The signal emitted from a linear transmit array will be received with a phase shift $\Gamma(\varphi)$, which is function of AoD. For l^{th} path with AoD φ_l, the phase shift across transmitting antennas is given by:

$$\Gamma(\varphi_l) = e^{-j2\pi f d' \sin(\varphi_l)/C} \tag{3.6}$$

where d' is the distance between transmitting antennas.

Furthermore, the current WiFi standards such as 802.11 leverage OFDM technology wherein data is transmitted over multiple subcarriers. For equispaced OFDM subcarriers, the l^{th} path with ToF of τ_l introduces a phase shift of

$$\Omega(\tau_l) = e^{-j2\pi f_\delta T_l} \tag{3.7}$$

across two consecutive OFDM subcarriers with f_δ frequency difference. We point out that the phase shifts due to AoA and AoD across subcarriers are negligible due to the small frequency difference across WiFi channels [30].

MonoLoco jointly estimates AoA, AoD, and ToF by defining the sensor array from all subcarriers of all receiving antennas for all streams transmitted from multiple antennas. This information is accessible in commodity WiFi chips with MIMO-OFDM techniques (more specifically MIMO spatial multiplexing). The overall attenuation and phase shift introduced by the channel measured at each subcarrier by each antenna is reported as the *Channel State Information* (CSI) in a $3 \times 3 \times 30$ format - 3 receiving antennas, 3 transmitting antennas, and 30 subcarriers. Therefore, the measured sensor array X is constructed by stacking CSI from all the subcarriers at all antennas, resulting in a single column vector of length $3 \times 3 \times 30$ (= 270). The new steering vector $a(\theta, \varphi, \tau)$ is formed by phase shifts introduced at each of the sensors, and is given by:

$$a'(\theta,\tau) = [\overbrace{1..\Omega_\tau^{K-1}}^{RX_1}, \underbrace{\Phi_\theta, ..., \Omega_\tau^{K-1}\Phi_\theta}_{RX_2}, ..., \overbrace{\Phi_\theta^{M-1}, ..., \Omega_\tau^{K-1}\Phi_\theta^{M-1}}^{RX_M}]^T \tag{3.8}$$

$$a(\theta,\varphi,\tau) = [a'_{\theta,\tau}, \Gamma_\varphi a'_{\theta,\tau}, ..., \Gamma_\varphi^{N-1} a'_{\theta,\tau}]^T \tag{3.9}$$

where $\Omega(\tau)$ is written as Ω_τ, $\Phi(\theta)$ as Φ_θ, and $\Gamma(\varphi)$ is written as Γ_φ. Therefore, the new measurement matrix X is constructed using the above steering vector, and three parameters of AoA, AoD, and ToF that maximize the spatial spectrum function (Equation 3.5) will be estimated. However, this requires finding the peaks in a 4D space $(\theta, \varphi, \tau, P)$. To solve this problem, instead of implementing the standard MUSIC algorithm, we use the improved version called RAP-MUSIC [57], which uses an iterative mechanism to find the paths from signal subspace instead of noise subspace. Therefore, in each iteration, the global maximum is considered as the resolved path.

Another challenging issue is that the ToF estimates do not capture the actual time that the signal travels. The reason is that the WiFi transmitter and receiver are not time-synchronized. Furthermore, the estimated ToFs also include the delays from sampling time offset and packet detection delay [30, 32]. To address this challenge, in the next section, we explain MonoLoco's ToF sanitization approach, which results in accurate estimation of the relative

ToF between different resolved paths.

3.3.3 ToF Sanitization

One of the challenges in estimating ToF with commodity WiFi devices is that the measured channel at the receiver experiences a random phase shift due to sampling time offset (STO) and packet detection delay (PDD) across packets [32]. While the variations due to sampling time offset may seem small, packet detection delays are often an order of magnitude larger than ToF [40]. To address this challenge, MonoLoco applies a ToF sanitization algorithm similar to the ones proposed in PinLoc [32] and SpotFi [30].

STO and PDD have a constant effect across all transmitting (TX) or receiving (RX) antennas since all the radio chains of a WiFi card are time-synchronized. Hence, an additional delay of τ_s adds a phase shift of $-2\pi f_\delta(k-1)\tau_s$ to the phase of the k^{th} subcarrier in each antenna. For each CSI measurement, we remove the offset by removing the linear fit of the unwrapped phase shifts across subcarriers of all $N \times M$ antennas. Suppose $\psi(n,m,k)$ is the unwrapped phase of the CSI at the k^{th} subcarrier of a packet transmitted from the n^{th} TX antenna and received at the m^{th} RX antenna, then we can obtain the optimal linear fit as:

$$\hat{\tau}_s = arg\min_{\beta} \sum_{n,m=1}^{N,M} \sum_{k=1}^{K} (\psi(n,m,k) + 2\pi f_\delta(k-1)\beta + \alpha)^2 \tag{3.10}$$

Intuitively, β is the common slope of the received phase responses for all antennas, and α is the offset. The modified CSI phase is then defined to be:

$$\hat{\psi}(n,m,k) = \psi(n,m,k) - 2\pi f_\delta(k-1)\hat{\tau}_s \tag{3.11}$$

Note that this technique does not estimate the exact value of τ_s for each packet. The slope of unwrapped phases across the subcarriers consists of the delay caused by STO/PDD as well as the phase shift due to ToF of the shortest path. Therefore, subtracting this value leaves only enough information to derive the *relative* ToF (rToF) between multipaths. In other words, the values τ_l derived in Section 3.3.2 are not valid after ToF sanitation, but the rToF value $\Delta T_j = \tau_j - \tau_1$ for path $j > 1$ with respect to the shortest path is still valid.

3.3.4 Localizing the Target

MonoLoco localizes the target by combining the resolved geometric features of multipaths described above: the AoA and AoD of multiple propagation paths, and the rToF between the LoS path and each reflected path. MonoLoco defines the LoS path to be the resolved path with the shortest ToF value. To localize, MonoLoco finds the orientation and location of the target that best explains these observed multipath features, as described below.

Without loss of generality, we explain MonoLoco's multipath geometry in a simple case of two paths; but the method generalizes to more multipath signals in a straightforward manner. Figure 3-4 illustrates an example of the target location and orientation. The path angles are defined to vary between $-\frac{\pi}{2}$ to $\frac{\pi}{2}$ going from the 3rd array element to the 1st, as illustrated. In the example in the figure, the LoS signal is transmitted from the target with AoD φ_1, propagates a distance a and arrives at the receiver with AoA θ_1. The multipath reflection is transmitted from the target with AoD φ_2, propagates a distance $b + c$ and arrives at the receiver with AoA θ_2. These values represent the 5 multipath features resolved by the signal processing algorithms in Section 3.3.2: AoA (θ_1) and AoD (φ_1) of the LoS path, AoA (θ_2) and AoD (φ_2) of the reflected path, and the relative ToF between two paths $\Delta T = \tau_2 - \tau_1$.

Given these values, MonoLoco must estimate 5 new parameters: the target orientation (α), the target location (x_1, y_1), and the reflector location (x_2, y_2). We define the coordinate system with respect to the receiver's antenna array and the orientation of the target α is defined to vary between 0 to 2π moving clockwise. With these definitions, the multipath geometry defines four triangles named $\mathbb{A}-\mathbb{D}$, as shown in Figure 3-4. We use these triangles to define the following 4 equations that relate the observed multipath features to the location and orientation parameters we are trying to estimate:

$$\begin{aligned}
\triangle\mathbb{A}: &\quad \frac{x_1}{y_1} = \tan(\theta_1) \\
\triangle\mathbb{B}: &\quad \frac{x_2}{y_2} = \tan(\theta_2) \\
\triangle\mathbb{C}: &\quad \frac{x_1 - x_2}{y_1 - y_2} = \tan(\alpha - \varphi_2), \text{ where} \\
&\quad \alpha = \varphi_1 + \theta_1 \\
\triangle\mathbb{D}: &\quad b + c - a = \Delta T \times C, \text{ where} \\
&\quad a = \|x_1, y_1\|_2 \\
&\quad b = \|x_2, y_2\|_2 \\
&\quad c = \|(x_1 - x_2), (y_1 - y_2)\|_2
\end{aligned} \tag{3.12}$$

where C is the speed of light. Intuitively, equations derived from triangles $\mathbb{A}$ to $\mathbb{C}$ define the relative location of the target with respect to the receiver and the reflector. The equation derived from triangle $\mathbb{D}$ leverages the relative ToF to define the actual scale of these triangles since there is only one scale that satisfies $b + c - a = \Delta T \times C$. Finally, the orientation of the target is defined to be

$$\alpha = \varphi_1 + \theta_1 \tag{3.13}$$

MonoLoco solves for α directly using the equation above and solves for the location parameters $XY = [\hat{x}_1,\ \hat{y}_1,\ \hat{x}_2,\ \hat{y}_2]$ by solving the following non-linear optimization problem:

$$[\hat{XY}] = \underset{XY}{\operatorname{argmin}}\, S(XY) \tag{3.14}$$

where

$$S(XY) = [\tan(\theta_1) - \frac{x_1}{y_1}]^2 + [\tan(\theta_2) - \frac{x_2}{y_2}]^2$$
$$+ [\tan(\alpha - \varphi_2) - \frac{x_1 - x_2}{y_1 - y_2}]^2 + [(\Delta T \times C) - (b + c - a)]^2$$

To optimize this objective function, we search for the most likely location of the target and reflector by forming a 20 centimeter by 20 centimeter grid, and evaluating $S(XY)$ at each point in the grid. Then, we use constrained nonlinear optimization (the fmincon solver in Matlab) on the three positions with minimum $S(XY)$ in the grid to find the best solution.

Note that the above equations will hold for any arrangement of target-reflector location and orientation, and could be applied to different antenna array arrangements. We will

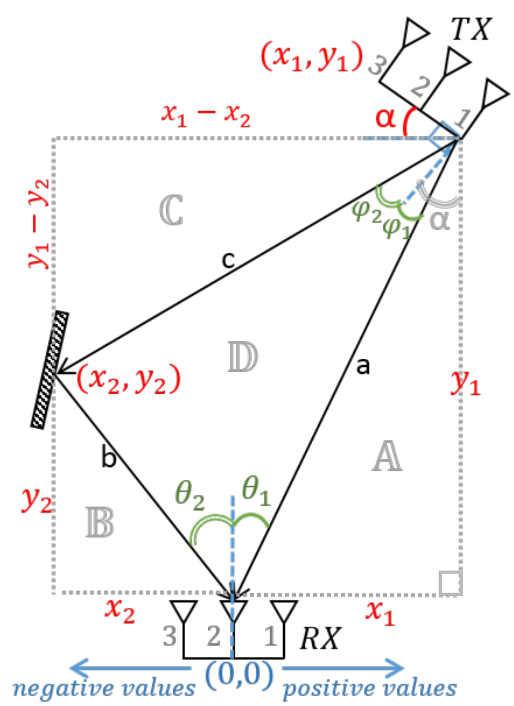

Figure 3-4: **Multipath Geometry.** The direct path and a multipath reflection form a triangle (𝔻) between the AP, the target, and the reflector. This triangle defines a relationship between the target location/orientation and the observed AoA, AoD, and rToF values. That relationship can be encoded in terms of three other triangles (𝔸, 𝔹, and ℂ).

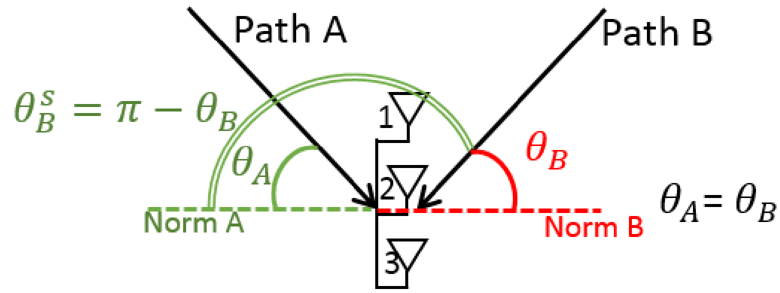

Figure 3-5: **The symmetry of a linear antenna array** creates ambiguity in AoA and AoD measurements. Therefore, MonoLoco solves for the target location that best explains either the resolved angle or its supplementary angle.

discuss symmetry ambiguity of linear arrays in Section 3.3.5 and explain the required modifications to provide 360-degree coverage.

3.3.5 Overcoming Antenna Symmetry

The angle spectrum resolved with a linear antenna array is 180 degrees, so it cannot determine from which side of the array the signal is arriving. Figure 3-5 illustrates an example of this ambiguity in which incident paths A and B arrive from different sides of the array but the observed AoA for the two paths are equal ($\theta_A = \theta_B$). The reason for the angle ambiguity is that a linear array has reflectional symmetry along the direction of the array, and so signals from both sides produce equivalent phase shifts across a linear antenna array.

In many applications such as robotics and virtual reality where WiFi devices can be anywhere in the surrounding environment, a circular or non-linear array is used to break this symmetry by adding a sensing element in a second dimension, thereby increasing the angle resolution to a full 360 degrees. However, most commercial APs still use linear antenna arrays and so, we evaluate MonoLoco using linear antenna arrays. This is a worst-case analysis and future products that can be built with circular arrays can achieve higher accuracy.

Given this symmetry, any AoA (or AoD) value θ could actually be one of two possible values: θ or $\pi - \theta$. To address this challenge, MonoLoco applies the localization algorithm using both the resolved angle and its supplementary angle. Therefore, it runs 8 optimization processes in parallel to examine the symmetry ambiguity for the AoA and AoD of the reflected path and AoD of the direct path (e.i. 3 slots with 2 possible values for each result in 8 combinations or 8 symmetry scenarios). Then, from 8 estimated locations, MonoLoco chooses the one with minimum cost value of the objective function in the corresponding estimated location. The intuition behind this algorithm is that only one of these 8 conditions is geometrically feasible, which appears with minimum cost value. It should be noted that this approach is not a solution for identifying the symmetry scenario, but just a mechanism to estimate the location and orientation of the target regardless of the symmetry ambiguity. We expect to have errors in estimating the correct symmetry scenario in the case of large errors in multipath resolution, but eventually, we expect that the final estimated location is the best solution since it has the minimum cost value.

3.3.6 Improving Localization using Multiple Packets

Every packet that is received creates a new observation of the 5 resolved multipath features described above. If more than one packet is received, these observations can be combined to create an over-constrained system of non-linear equations in order to further improve localization. There are many ways to solve this non-linear system and in this section we describe a 3-step data cleaning process. This process is motivated by our observation that noise in some packets can cause super-resolution to resolve spurious paths, while other packets resolve correct paths. The three steps are described below.

Step 1: We estimate the location/orientation parameters for each packet independently, using the methods described before. Any packet with spurious paths will generally result in geometrically infeasible conditions, which will manifest as high values of the objective function $S(XY)$. Therefore, MonoLoco uses a very low threshold value to discard any packets with objective values substantially higher than zero. Note that any packet with geometrically feasible multipath features will have an objective value that is close to zero, so this step does not eliminate all packets with errors.

Step 2: Previously, we assumed the path with the shortest ToF is the direct path. However, in the presence of spurious resolved paths, this assumption may not be held. To this end, Multipath features from the remaining packets are used to determine the true LoS path. MonoLoco applies the K-means clustering algorithm on all paths from remaining packets. The number of clusters is set to 5, based on the typical number of dominant paths in an indoor environment [31, 53]. Then, we extend the SpotFi's direct path likelihood function [30], where the likelihood of l^{th} path being the direct path is calculated as

$$P_l = exp(\omega_C \bar{C}_l - \omega_\theta \bar{\sigma}_{\theta_l} - \omega_\varphi \bar{\sigma}_{\varphi_l} - \omega_\tau \bar{\sigma}_{\tau_l} - \omega_s \bar{\tau}_l) \tag{3.15}$$

where $\bar{C}_l$ is the number of points in the cluster of l^{th} path, $\bar{\tau}_l$ is the average ToF of the cluster, and $\bar{\sigma}_{\theta_l}$, $\bar{\sigma}_{\varphi_l}$, and $\bar{\sigma}_{\tau_l}$ are the population variances of the estimated AoAs, AoDs, and ToFs for the corresponding cluster, respectively. The ω weighting factors are constant values to account for different scales of the corresponding terms [30]. The intuition behind this approach is that the parameters of the direct path have small variations over time compared to the estimated reflected paths. Therefore, the size and variance of each cluster are strong indicators of the LoS path.

After the true LoS path is identified, MonoLoco filters any remaining packets that have a resolved path that is shorter than the LoS path. In other words, it recalculates the rToF between the reflected path and the LoS path and filters out the packets where the identified direct path does not have the shortest ToF:

$$\exists\, \tau_i^{ref} \mid (\tau_i^{los} - \tau_i^{ref}) < 0 \tag{3.16}$$

where τ_i^{los} and τ_i^{ref} are the ToF of the direct path and the reflected path in i^{th} packet, respectively.

Step 3: The set of remaining packets is called ($P_{filtered}$), each of which has its own location/orientation estimate. MonoLoco chooses the packet that has the lowest objective value. This could be expressed as

$$[\hat{XY}, \hat{\alpha}] = \arg\min_{XY_i} S(XY_i), \quad i \in P_{filtered} \tag{3.17}$$

Intuitively, MonoLoco chooses the packet for which the 5 resolved multipath features are most consistent with each other, presumably because this packet was subject to the least noise. We did not do a comprehensive exploration of the selection algorithm and present this one only as a proof of concept. We believe that other approaches to solve full non-linear system defined by $P_{filtered}$ may indeed produce better results.

3.4 Evaluation

3.4.1 Experimental Setup

We evaluate our system using Intel NUCs D54250WYK[1] equipped with off-the-shelf Intel 5300 WiFi cards which support three antennas. We employed Linux CSI tool [92] to obtain the PHY layer CSI information for each packet. The experiments are conducted in the 5 GHz WiFi spectrum using 40 MHz bandwidth. We built 9 nodes and used one node as the access

[1]https://ark.intel.com/products/76977/Intel-NUC-Kit-D54250WYK

point (AP) and 8 nodes as target devices in multiple locations (as illustrated in Figure 3-6). We use the method introduced in WiCapture [50, 93] for calibration and operated all nodes in monitor mode. Each node was equipped with three 3dBi omni-directional antennas[2] in a uniform linear array. The distance between any two antennas is equal to 2.7 cm (half a wavelength). The nodes were placed atop 110cm speaker stands during the experiments to represent a practical height.

All experiments were conducted as follows. First, all nodes (both AP and target nodes) are set in monitor mode on channel 118 with 40 MHz bandwidth in the 5GHz band. Then, for every target location shown in the testbeds, 500 packets were transmitted with a 5 ms interval using the spatial multiplexing protocol in 802.11n. Measurements were collected in both directions – from the target to the AP and from the AP to the target – both of which were analyzed independently as separate experiments to estimate the location of one device with respect to the other one. The main results are calculated using 20 packets and the impact of the number of packets on localization is discussed in Section 3.5.3.

We first validate the localization model in an anechoic chamber as shown in Figure 3-7(a). This enabled experiments with known propagation paths. The number of reflections was varied between 1 to 5 and different orientations and positions were measured, resulting in 30 different target positions in total, as shown in Figure 3-6(a). Then, to evaluate the performance of MonoLoco in more realistic conditions, we deployed in a home with two occupants, in two offices environments and a large public arena with the presence of 1-5 occupants. Locations of WiFi APs and 51 target locations are depicted in Figures 3-6(b)-(d) with the snapshots of the deployment environments in 3-7(b)-(d). These experiments resulted in 102 different experimental scenarios, including both directions (from AP to target and target to AP). In cases where more than one AP is deployed to span the area, the closest AP to the target location was used for localization. The majority of node distances are

[2] https://www.data-alliance.net/antenna-5-1-5-8ghz-3dbi-omni-directional-dipole-w-rp-sma-male-connector/

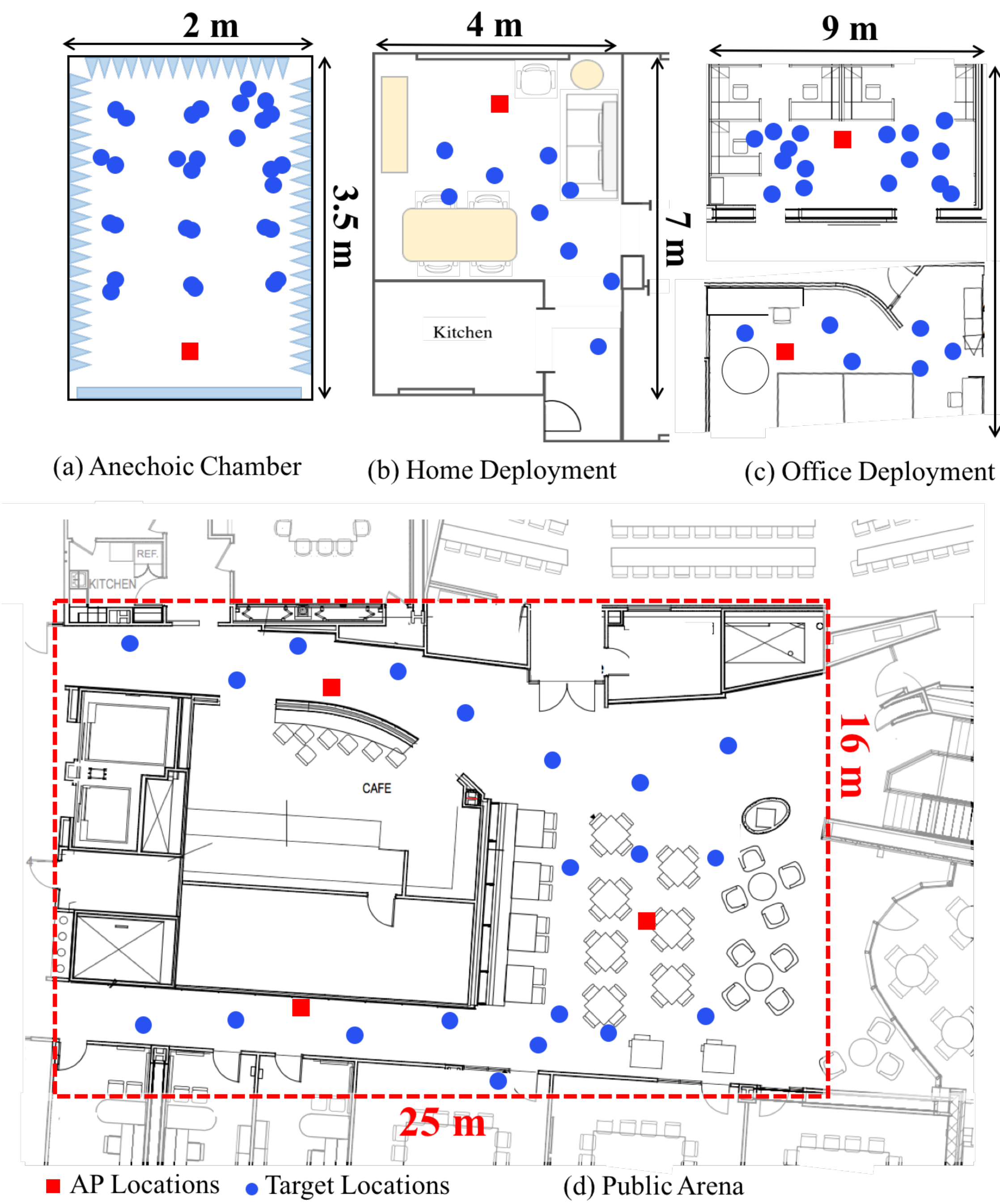

Figure 3-6: **Experimental Setup.** Experiments were run in four environments with varying size and multipath complexity. The closest AP to each target was used for localization.

between $1m$ to $4m$ due to the size of the spaces available, but 26% of total experiments evaluate distances larger than $4m$ especially in the corridor and public arena. This is similar to the experimental setup of the related works [31, 40] with 25-35% of localization tests having $4m$ to $15m$ distances. Ground truth location and orientation were measured using a combination of laser range finder, a construction protractor, floor and ceiling tiles, and architectural drawings of the building.

We compare the performance of the proposed 3D super-resolution algorithm with the 2D method proposed in Spotfi [30]. However, the closest available localization system to MonoLoco is Chronos [40] that demonstrates accurate WiFi localization with a single AP,

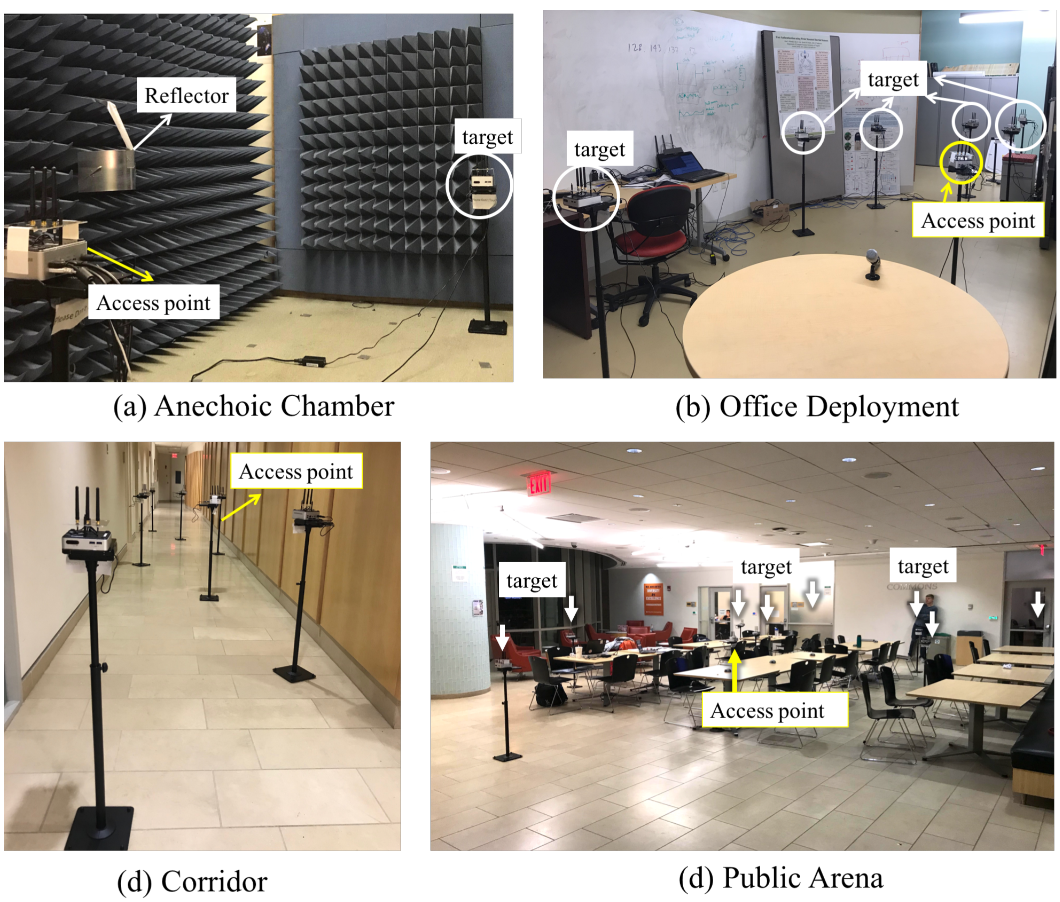

(a) Anechoic Chamber (b) Office Deployment

(d) Corridor (d) Public Arena

Figure 3-7: **Snapshot of Experimental Setups.** The four experiments tested different distances, angles, and multipath environments.

but it relies on external coordination between the transmitter and receiver for sharing channel measurements in each side of transmission as well as frequency hopping. In contrast, MonoLoco assumes no coordination or data sharing between the two nodes. In addition, Chronos requires a large spacing in the AP's antenna array (12-30cm) and so it would be severely handicapped if run on the hardware designed for MonoLoco. So a head-to-head comparison would not be meaningful and only a qualitative comparison is provided.

3.4.2 Model Validation in Anechoic Chamber

Before testing in a realistic environment, we validated the proposed localization model in a controlled environment such as an anechoic chamber with known propagation paths. This experiment establishes an experimental upper bound on accuracy by limiting multipath reflections. We first established the lack of multipath reflections in the anechoic chamber by verifying that no packets are received since the spatial multiplexing technique in 802.11n requires multipath propagation to make multi-stream transmissions. Any reflections in the chamber were not strong enough to enable transmission. Then, we placed 1-5 curved metal sheets at different locations in the chamber to generate controlled multipath geometries. These geometries included the ambiguity caused by antenna symmetry described in Section 3.3.5. The metal sheets were curved to create a scattering effect, increasing the chance that the reflections reach the receiver. We used packet reception rate to verify the incidence of at least one reflection path.

From Figure 3-8, we observe that the proposed localization method achieves a median localization error of $25cm$ and median orienting error of 3.5 degrees in anechoic chamber. There are likely two main sources of this error. First, ground truth: since the coordinate system is defined relative to the AP antenna orientation, ground truth errors can produce error in target location. Second, multipath resolution: the resolution capability of MUSIC

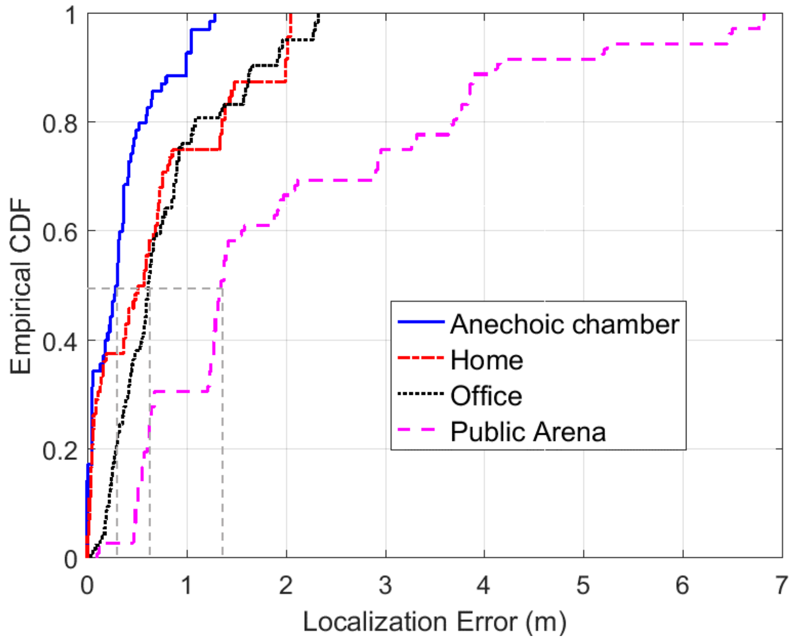

Figure 3-8: **Localization Accuracy.** The cumulative distribution of location error shows that MonoLoco's median error varies between 0.2m to 1.3m across environments with different multipath complexity.

is limited by the angular separation of multipath components, and the physical geometry of the linear antenna arrays causes lower resolution of estimated angles as they approach their extremes ($-pi/2$ and $pi/2$) [31].

3.4.3 Location Accuracy

Next, we evaluate MonoLoco in realistic indoor environments with complex multipath propagation. We deploy multiple WiFi nodes equipped with WiFi cards in three sets of environment with different levels of complexity: (1) a home deployment, which is a cluttered environment with a lot of furniture nearby the nodes; (2) two office environments, which includes deployment in two offices on two sides of a corridor. During the experiment there were 1 to 5 occupants inside the offices sitting at the desks, and (3) two public areas, including a large open space and two corridors. The open space area contained many tables and chairs at about the same height as the WiFi nodes, which resulted in a complex multipath environment and NLoS scenarios. Both areas enabled larger distances between the AP and the targets, compared to the home and office deployment. The open area allowed reflection paths that were much longer than the LoS signal while the corridors were narrow and limited the separation of propagated paths from the LoS signal.

As seen from Figure 3-8, the median localization error of MonoLoco is $0.54m$ and $0.64m$ in home and office deployments, respectively. Under stressful conditions in the public arena deployment, the median localization error approaches $1.3m$ which is proportional to the distance of the links. The higher error rate in this area is due to rich multipath propagation and lower resolution of multipath estimates. In addition, the public arena deployment contains NLoS conditions due to obstacles in the LoS path such as furniture and glass walls. We point out that the reception of direct path is essential for MonoLoco's localization algorithm, but the results show that it is robust to partial LoS blockage. These results show that MonoLoco's accuracy is comparable to state-of-the-art indoor localization systems that use multiple APs [30, 31, 52], or frequency hopping for ToF measurements [40, 64].

3.4.4 Orientation Accuracy

Besides localization, MonoLoco provides the orientation information. In the experiments performed in four environments shown in Figure 3-6, random orientations are chosen for each target location ranging between 0 to 2π. As seen in Figure 3-9, MonoLoco achieves a median orientation error of 3.5 degrees in anechoic chamber, 4.2 degrees in home, 5.5 degrees in office deployments, and 10 degrees in public arena deployment. The main reason for MonoLoco's high performance in estimation of the orientation is that orientation is mainly derived from AoA and AoD of the direct path, which is the dominant component in the received signal, and therefore less prone to multipath resolution error.

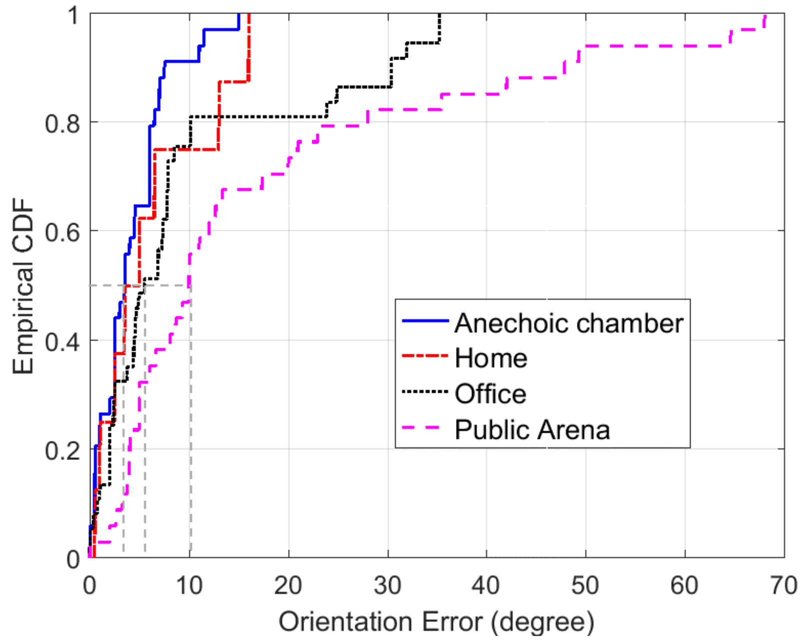

Figure 3-9: **Orientation Accuracy.** The cumulative distribution of orientation error shows that the median error varies between 3.5 to 10 degrees across environments with different multipath complexity.

MonoLoco achieves high accuracy in estimating location and orientation for two main reasons. First, MonoLoco's multipath super-resolution algorithm resolves multipath components more accurately by using a 3D joint estimation. Second, MonoLoco jointly computes the location and orientation by minimizing the geometric errors along multiple paths. Therefore, identifying the orientation allows to compensate the errors in localization estimation.

3.5 Sensitivity Analysis

3.5.1 AoA-AoD Estimation Accuracy

The goal here is to show that MonoLoco's 3D super-resolution algorithm provides a more accurate AoA and AoD estimation than state of the art. However, we don't have the ground truth parameters of the reflection paths in the realistic environments. Therefore, in Figure 3-

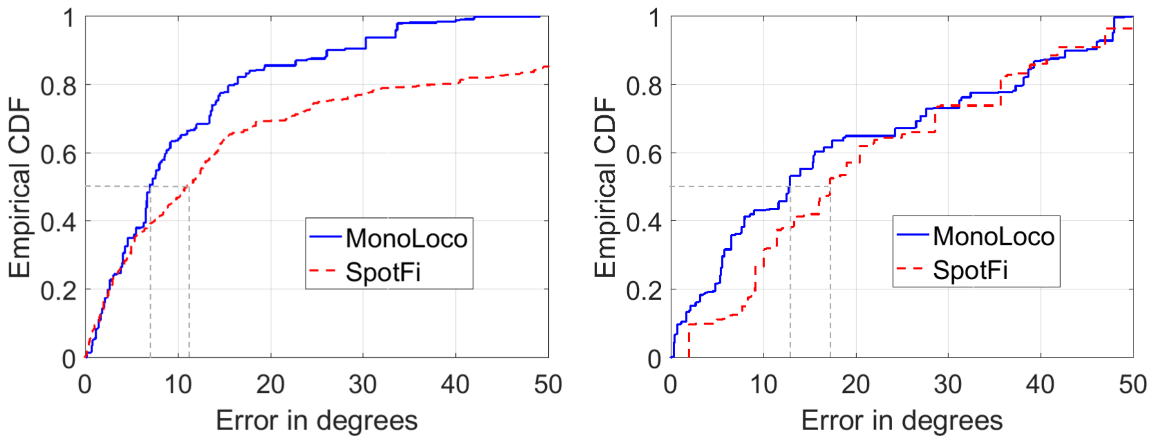

(a) AoA Estimation error (b) AoD estimation error

Figure 3-10: **MonoLoco's 3D super-resolution algorithm** improves both (a) AoA and (b) AoD estimation in comparison with SpotFi's 2D approach [30].

10, we show the accuracy of the AoA and AoD estimations only for the direct path. After running the super-resolution algorithm, we choose the resolved AoA and AoD values that are closest to the LoS path and calculate their difference from the ground truth values. We compare this error with the 2D AoA-ToF estimation method proposed in SpotFi [30]. To measure AoD with SpotFi, it is applied on transmitting antenna array incident on the first receiving antenna.

Figure 3-10(a) plots the CDFs for AoA estimation error for all links in all experiments. MonoLoco achieves median AoA accuracy of 4.02 degrees better than that achieved by SpotFi. In AoD estimation, shown in Figure 3-10(b), MonoLoco achieves an improvement of 4.53 degrees in the direct path error. The reason for the higher performance of MonoLoco compared to SpotFi is that a larger sensor array consisting of 3 transmitting antenna, 3 receiving antenna, and 30 subcarriers ($3\times3\times30 = 270$) is used, which provides larger aperture to separate multipath components. In addition, in AoD estimation, both methods converge to similar error rates in 80^{th} percentile of the error. This is more a limitation of the linear antenna array; any method will produce higher error when the incident angle of the signal approaches the angle of the array.

3.5.2 Impact of Distance

Next, we evaluate the impact of the distance between two transceivers on location and orientation accuracy. Figure 3-11 plots the distance between each target location and the AP against localization and orientation error in the 4 deployments. In Figure 3-11(a), we observe that the average localization error increases with the increase of the distance between two nodes. This is primarily due to the reduced signal-to-noise ratio at greater distances, which results in lower accuracy in multipath resolution (especially for reflected paths). In addition, the majority of target locations with long distances belong to the public arena deployment which is a cluttered environment with narrow corridors and complex multipath propagation.

It should be noted that the population of the experimental locations is not uniform across different distances with a lower density around large distances ($> 5m$). This imbalance is taken into account in calculation of 90%-percentile confidence intervals, which appeared as an increasing pattern across distances. On the other hand, the localization accuracy is provided for each environment separately in Figure 3-8 since the distribution of link distances are not uniform in all experimental environments. In Anechoic chamber where link distances are between $0.85m$ to $2.7m$, the median localization error is $25cm$. In home and office environment with link distances between $1.1m$ to $5.5m$, the location error is $0.54m$ to $0.64m$. Finally, in the public arena with link sizes between $1.5m$ to $12.7m$, the median accuracy is $1.3m$. Therefore, we can conclude that the accuracy is proportional to the distance of the nodes.

Figure 3-11(b) shows the orientation accuracy against the distance between each target location and the AP. Although it is expected that the average orientation error increases with an increase in distance, our observations show the distance is not the main factor in the accuracy of orientation estimates. The reason is that orientation is mainly calculated from

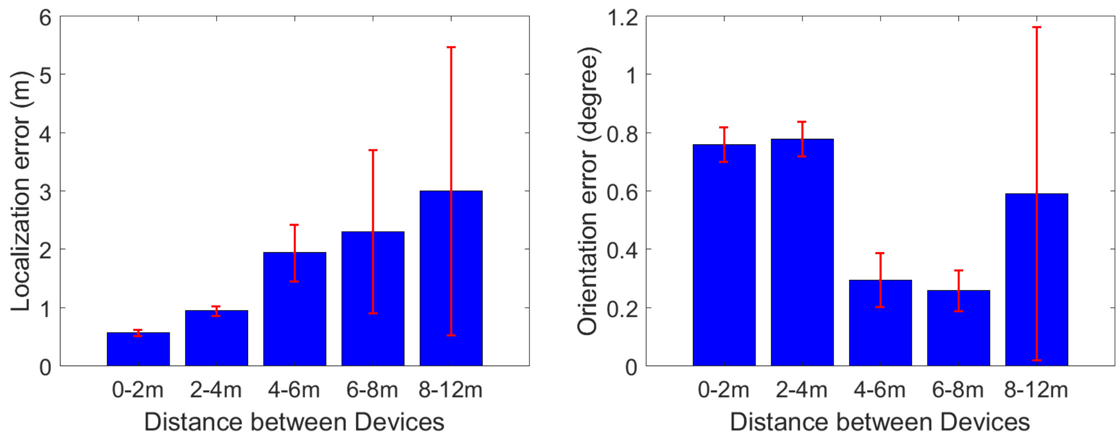

(a) (b)

Figure 3-11: **Distance vs. Accuracy.** The average (a) localization, and (b) orientation errors increase as the distance between the target location and the AP increases.

the AoA and AoD of the direct path which carries the dominant signal power, thus less prone to the additional noises from further distances. Theoretically, the accuracy of the resolved angles is the main factor affecting the orientation estimation. The resolution of subspace methods such as MUSIC degrades as the incident angles approach the edges of the spectrum (e.g. $-\pi$ and π in linear antenna arrays). Therefore, for a linear antenna arrangement, the accuracy of the orientation estimation would be lower if the target's antenna array is either perpendicular or in-line to the AP's array.

3.5.3 Impact of Number of Packets

Section 3.3.6 describes how MonoLoco combines data from multiple packets, if available. Figure 3-12 shows how this approach affects localization accuracy as the number of packets used for localization is changed from 7 packets to 50 packets. Each line represents the cumulative distribution of the combined error in all four environments for a given number of packets. Even with 7 packets, MonoLoco achieves a median localization accuracy of $0.84m$ using all deployments including the public arena, compared to $0.5m$ obtained using

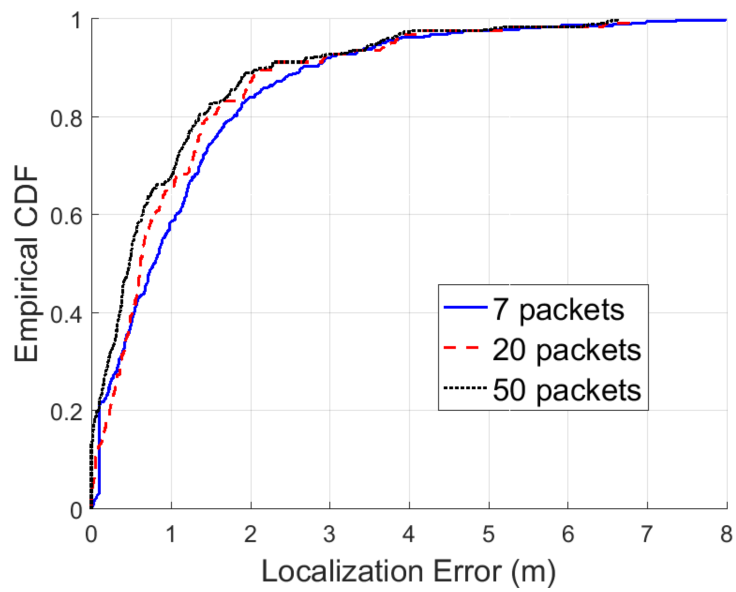

Figure 3-12: **Number of Packets vs. Accuracy.** The cumulative distribution of localization error for 7, 20, and 50 packets shows that MonoLoco works well with small number of packets. All target locations in 4 deployments are aggregated in this graph.

50 packets. With only 1 packet, it was able to achieve $0.7m$ error in the home and offices and approximately $2m$ error in the public arena. These results indicate that MonoLoco is able to achieve location estimates with reasonable accuracy with only the first few packets, and gets diminishing returns as more packets are received. Although some nodes will want the highest accuracy possible, this speed can be beneficial in cases when the target can only send a small number of packets or needs a location estimate quickly.

3.6 Discussion

One limitation of *multipath triangulation* is that it relies on the existence of a propagation path going directly from transmitter to receiver. The evaluation demonstrates that it works well even in NLoS scenarios where the direct path is not the strongest signal, but in the case of complete blockage it will actually produce the wrong location estimate. Currently, all other decimeter-level WiFi localization systems also have this limitation, and localizing targets with no LoS path is still an open problem. A second limitation of *multipath triangulation* is that it requires a 3-element antenna array on both the transmitter and receiver, similar to Chronos [40]. As such, it cannot localize/orient small devices such as smart phones or smart watches that typically have only one antenna. However, many WiFi devices including laptops, APs, robots, and smart appliances do have 3-element antenna arrays, which are becoming more common with MIMO technology. MonoLoco can be used by a single autonomous robot to localize multiple APs, which could in-turn be used to localize single-antenna devices using protocols such as SpotFi [30]. Moreover, the presence of the 3-element array on the target is what enables orientation inference. Finally, *multipath triangulation* relies on first order reflections and assumes that the second order reflections are too weak to be resolved. In indoor environments, it is rare to receive a second order reflection, but if so, we can filter out these reflections in the post-processing step and use another pair of paths.

The main contributions of this chapter are the new *multipath triangulation* techniques, and the 3D super-resolution algorithm to estimate the geometric features of multiple paths. These techniques are not limited to WiFi, and can be used in many ways besides single-device WiFi localization. MonoLoco is just a proof-of-concept for the wide range of applications where these techniques can produce substantial gains such as in indoor mapping, object imaging, or device-free localization. In future work, we plan to explore how MonoLoco could interact with WiCapture [50], which uses multipath reflections to provide accurate motion tracking. WiCapture can only get relative motion and not absolute position, so these two systems are complementary and could be combined. Additionally, the current version of MonoLoco uses a subspace super-resolution algorithm to resolve multipath features with a linear antenna array. However, the fundamental methods are independent of the multipath resolution technique and the antenna configuration. Therefore, we will explore how MonoLoco's performance could be improved by advances in multipath resolution such as the recent works in Maximal Likelihood Estimation techniques [59], larger antenna arrays, or circular antenna arrays.

3.7 Conclusion

This chapter presents *multipath triangulation*, a new localization technique that leverages multipath reflections to estimate the location of a target and a reflector with respect to the receiver. We use *multipath triangulation* to develop MonoLoco, the first localization system that provides decimeter-level localization and orientation information without any information sharing or coordination across multiple nodes. A single WiFi node or access point can localize any other WiFi transmitter that it hears. The protocol is fully piggybacked on top of the WiFi protocol. We expect *multipath triangulation* and its use of multpath reflections for localization to lead a universal paradigm shift in IoT where the WiFi in every home and office can act as an efficient non-intrusive yet omnipresent sensing system which does not require new sensor hardware installation. We believe that *multipath triangulation* is more widely applicable to protocols other than WiFi and for problems other than target localization, including device tracking, indoor mapping, object imaging, and device free tracking, which are among our future works.

Chapter 4

Tracking Battery-free Objects with Commodity WiFi

Object location and tracking is an essential part of the smart, automated systems that are envisioned for the home, office, and retail spaces of the future. People want to locate a bag or jacket at home, a tool in a workshop, or an exhibit at a museum. However, no existing object tracking technology offers both simple setup and simple long-term operation. With RFID technology, one can track an object simply by attaching a low-cost, battery-free tag, but only after a complex setup involving one or more RFID readers, anchor tags, and/or mobile readers [94–96]. On the other hand, WiFi localization systems offer simple initial setup by taking advantage of the pervasive wireless infrastructure, but can only localize WiFi radios that are difficult to keep powered on over the long term [1, 97]. In order for the vision of pervasive computing to be fully realized, new object tracking solutions must be developed that support low-cost, battery-free tags without requiring new infrastructure deployment.

This chapter presents a new localization system that we call *TagFi*: the first technique to enable a user to localize a passive object with decimeter-level accuracy simply by using commodity WiFi devices – with no need for initial setup. To do this, TagFi combines the best features of RFID and WiFi localization: 1) low cost, battery-free tags by using backscatter technology, and 2) turnkey setup by leveraging existing WiFi devices to eliminate the need for new infrastructure. TagFi works with unmodified WiFi and no hardware, firmware, or protocol changes are required. It only uses Channel State Information (CSI), which is collected by commercial WiFi chipsets. In addition, CSI is measured from the WiFi packet preamble and can, therefore, be used to localize a tag just by eavesdropping on WiFi packets. This converts any WiFi-enabled device into an individual sensor to locate "things", whether a battery-free object or a low-power IoT device that does not have a WiFi transceiver.

The basic idea of TagFi is to create a tag that reflects a WiFi signal, and then to triangulate the position of the tag by measuring the angle of arrival (AoA) and angle of departure (AoD) of this reflection. However, the main challenge is that these passive reflections are considerably weaker than the Line-of-Sight (LoS) path between the WiFi transceivers. Moreover, wireless signals propagate along multiple paths reflecting off of walls and furniture, so the received signal is the superposition of all these paths, making the detection of the tag reflection even more challenging.

To overcome this problem, we build TagFi based on a realization that a *modulated mul-*

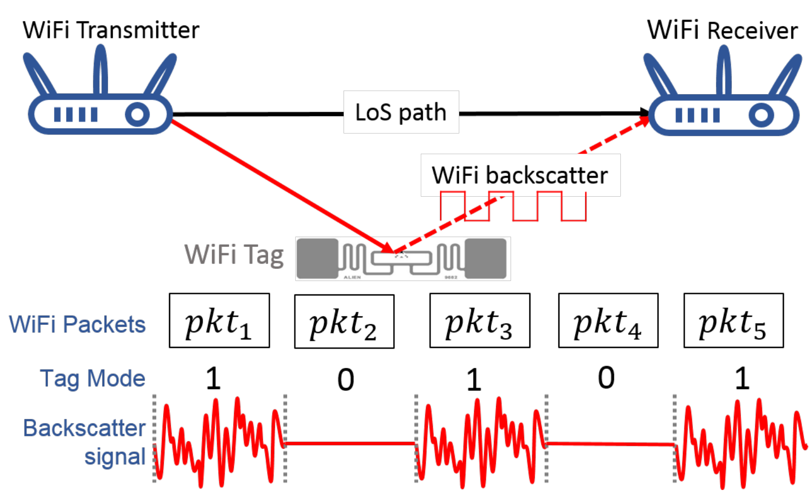

Figure 4-1: **High level design.** WiFi packets are backscattered from the WiFi tag carrying a modulation pattern.

tipath signal is incoherent with the rest of multipath reflections. This incoherency enables super-resolution algorithms to identify the weak passive reflection of an object among complex multipath propagations. We borrow the technique of *backscatter modulation* from conventional RFID to build a battery-free tag that modulates the WiFi signals across packets by switching its internal impedance between reflective and non-reflective modes. As shown in Figure 4-1, when the tag's switch is off (Tag Mode=0), it acts as an open terminal and the received WiFi packet is completely absorbed by the tag, resulting in no reflection from the tag to the receiver (and creating the possibility of harvesting energy). However, when the switch is on (Tag Mode=1), it acts as a shorted terminal, which creates an impedance mismatch and a total reflection of the WiFi packet from the tag. In this manner, the tag is capable of modulating the backscattered WiFi signal.

TagFi leverages this unique property of the tag reflection to extract the geometric features of the backscatter signal. It combines CSI measurements from multiple packets carrying the modulated backscatter signal, as well as measurements from multiple transmitting antennas, receiving antennas, and multiple frequency subcarriers to estimate angle-of-arrival (AoA), angle-of-departure (AoD) and time-of-flight (ToF). We leverage the incoherency of the modulated backscatter signal and develop a new super-resolution algorithm to extract the angle and time features for the tag reflection. This effectively enables localizing the tag by forming a *multipath triangle* between the WiFi transmitter, the tag, and the WiFi receiver.

We implement TagFi using Intel 5300 WiFi chips as the WiFi transmitter and receiver, operating at 5GHz with 40MHz bandwidth. Each transceiver is equipped with a 3-element linear antenna array. We also made a prototype of the WiFi tag using an off-the-shelf RF switch, whose ports are connected to a regular WiFi antenna, a 50Ω and a short circuit cap. We deploy TagFi in an office building and evaluate its performance in multiple scenarios. Our empirical results show that TagFi achieves a median localization accuracy of $0.2m$, which is comparable with the best existing WiFi localization systems, all of which require a WiFi transceiver on the object and coordination between multiple APs.

Contributions: TagFi introduces multiple key innovations:

- TagFi exploits a novel technique of modulating the backscatter signal across multiple packets to overcome complex multipath interferences, which enables object tracking with commodity WiFi even in the presence of strong LoS path between the WiFi transceivers.
- The simple structure of TagFi's tag enables a new paradigm of sensing and tracking battery-free objects with any WiFi-enabled device.
- TagFi introduces the first WiFi-based object tracking system that provides decimeter-level localization accuracy by only using CSI measurements in a single commodity WiFi receiver. It does not require any type of modification in WiFi transceivers, external hardware or even time synchronization between the WiFi transmitter and receiver.

4.1 Background and Related Work

TagFi is related to previous works in three areas: localization of commercial RFID tags, device localization of WiFi radios, and backscatter communication. Combining the bests of all these systems, TagFi introduces the first object localization system with a single commodity WiFi receiver, enabling a new paradigm of sensing and tracking battery-free objects with commodity WiFi. It avoids expensive and extensive deployment overheads by leveraging the pervasive wireless infrastructures. In addition, it overcomes multipath interferences by customizing a WiFi-based tag that modulates the backscatter signal. Finally, the tag passively backscatters the WiFi packet, therefore, it does not require an active WiFi transceiver on the target and can operate by harvesting energy from WiFi signals. In what follows, we discuss how TagFi relates to related works.

RFID-based Localization. Tracking of battery-free objects with RFID has received considerable attention for many decades. In these systems, a battery-free tag backscatters the excitation signal transmitted by an RFID reader and encodes its own information on the reflected signal. The phase and amplitude of the backscattered signal is then used for localizing the tag by either calculating the received signal strength (RSS) [9, 98–100], the time of flight based on phase measurements [95, 101–104], or the angle of arrival (AoA) using multiple antennas [105–109]. However, to deal with multipath interferences, they require to either use a dense deployment of reference tags in the area of interest [94], leverage a moving reader's antenna to create a synthetic aperture radar [95], or perform frequency hopping across all RFID channels [96] to emulate a wider bandwidth. Additionally, all these RFID-based approaches require dedicated infrastructure and expensive RFID readers. In contrast, TagFi leverages the available pervasive WiFi infrastructure and enables object tracking with every single WiFi device. We borrow the RFID modulation technique that is designed for RFID reader-tag communications and transform it into a technique for identifying the weak WiFi backscatter signal in the presence of complex multipath propagations.

WiFi-based Localization. Active radios such as WiFi has been extensively used for localizing devices, which require a WiFi transceiver mounted on the target. The transmitted signal is then collected by one or multiple WiFi receivers to compute the location of the target. The first generation of WiFi-based localization systems look at the received signal strength and use fingerprinting to determine the location of the target [16, 44, 46, 110, 111]. However, these methods require an extensive effort to characterize the environment. Recent techniques eliminate the effect of multipath interferences by directly measuring the geometric features of the line of sight (LoS) path between the target and the WiFi receiver(s). AoA-based methods [1, 31, 52, 53, 112–114] use an array of antennas to compute the direction of the LoS signal, while ToF-based methods [63–65, 110, 115, 116] use signal measurements from multiple frequency channels to estimate the distance between the transmitter and receiver. Since all of these systems require an active WiFi transceiver on the target, they are not suitable for tracking of battery-free objects. In contrast, TagFi utilizes the passive wireless reflection from an object by using a battery-free tag attached to the target.

WiTag [117] is the closest related work to our system, which leverages the reflections of a passive low-power tag and localizes the tag with commodity WiFi radios. However, to deal with multipath interference, the tag shifts the incident signal to an adjacent frequency channel that is not overlapped with the original frequency band. However, frequency shifting causes several issues that limit the performance and practicality of this solution. First, shifting the signal frequency requires a high-frequency oscillator which consumes more power, therefore the tag cannot operate by harvesting energy. Second, explicit coordination between the two WiFi transceivers is required to agree on the secondary frequency channel, therefore, the localization protocol cannot be piggybacked on top of the available communications, increasing the networking overhead and interference with the data communications. In contrast, TagFi does not require any frequency shifting or power-hungry operation inside the tag, so it can operate on battery-free tags.

WiFi Backscatter Communication. The concept of utilizing the passive WiFi reflection is originally proposed for connecting battery-free objects to the Internet. WiFi Backscatter [118], BackFi [119], and Passive WiFi [120] are the examples of these systems that use specialized readers for decoding WiFi backscattering signals. However, all of these systems either require modification on the WiFi device or specialized hardware to cancel multipath interference. A recent category of backscatter communication systems utilize commodity WiFi devices, but they deal with multipath interferences by shifting the frequency of the backscatter signal to a non-overlapping channel [121] or changes the phase of the signal [122, 123]. In all of these cases, the tag's switch should operate at 20 MHz or higher frequencies to modulate the backscatter signal, which significantly increases the power consumption of the tag [124]. In contrast, TagFi does not require any specialized WiFi transceiver, extra WiFi helper, or frequency shifting in the tag, so it can gracefully operate using commodity WiFi radios and battery-free tags. Although TagFi mainly focuses on object tracking, we believe it can be extended to a WiFi backscatter communication system.

Finally, recent works [125, 126] have demonstrated the ability to harvest power from WiFi transmissions. [127] shows the feasibility of harvesting 0.5 – 1 mW of power from beamformed WiFi transmissions and [128] harvests power from existing WiFi chipsets while preserving network performance. TagFi builds upon this capability and designs a new WiFi-based tag with a functionality as simple as switching the impedance of an antenna, which can fairly operate with WiFi energy harvesting.

4.2 System Design

TagFi is a WiFi-based tracking system for battery-free objects. It enables a tag to be localized with existing WiFi devices without requiring any modification on the WiFi device or external coordination with other nodes. As shown in Figure 4-1, a WiFi device such as a laptop or cellphone receives the packets from an access point or any other WiFi device. At the same time, the tag modulates the WiFi packets and backscatters them, which is also received at the WiFi receiver. TagFi measures the CSI values of the received packets and identifies the tag reflection from complex multipath signals by exploiting the modulation of the backscatter signals across multiple packets. Figure 4-2 shows an overview of TagFi, which works in three steps:

- **Backscattering modulated WiFi signals:** Multipath interference is the main challenge of detecting the weak backscattered signal of the tag. TagFi addresses this challenge by modulating the tag reflection at the packet level. Section 4.2.1 explains how this approach effectively enables extracting the tag reflection from the rest of the multipaths.

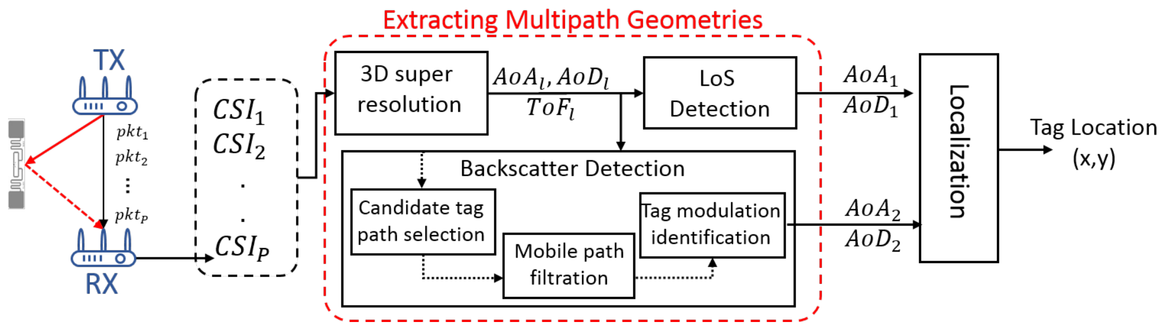

Figure 4-2: **System Overview of TagFi**

- **Extracting multipath geometries:** The backscatter signal, along with other multipath signals, is then received by a WiFi receiver to extract the CSI information. TagFi leverages the phase difference across multiple antennas on the WiFi transmitter and receiver to estimate the angular geometries of the tag reflection and the LoS path. Section 4.2.2 explains how TagFi differentiates the backscatter signal from a mobile path and extracts its modulation pattern.

- **Localizing the tag:** TagFi defines a triangle between the WiFi receiver, the tag and the WiFi transmitter. It constrains the geometry of this triangle by obtaining the AoA and AoD information of the tag's backsattered path as well as the LoS path, thus localizing the object.

In the following sections, we elaborate on each of these steps and then present the performance of the proposed method in a regular office building. Finally, the chapter concludes with a few applications of this system followed by discussions on system limitations and future works.

4.2.1 Backscattering Modulated WiFi Signals

To detect and localize a battery-free tag with WiFi, the tag backscatters the incident signal from a WiFi transmitter and the WiFi receiver measures the received signal from an antenna

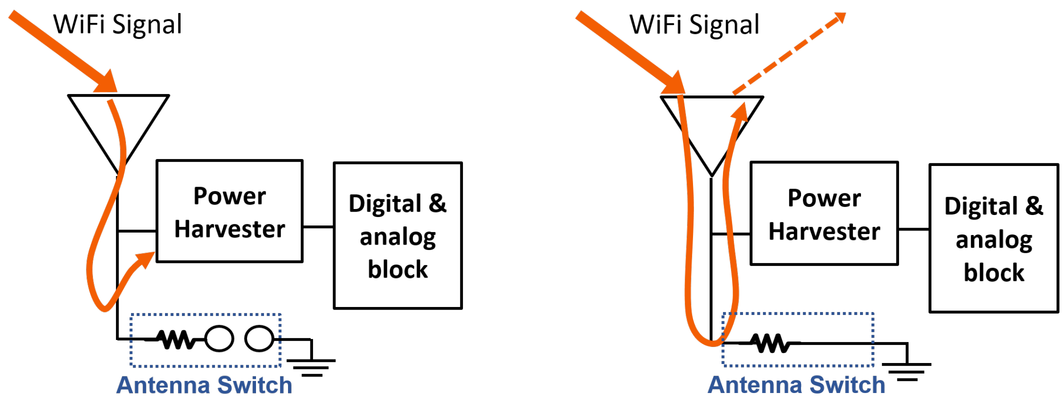

(a) Switch Off (b) Switch On

Figure 4-3: **Backscatter Modulation.** TagFi modulates the backscatter signal by either reflecting or adsorbing the WiFi packets, which is used to break the coherence of the backscatter signal with other multipath reflections.

array to estimate the signal's angular geometries. However, the presence of multipath signals specially the strong LoS path coming directly from the WiFi transmitter dominates the received signal, which makes it very challenging to extract the tag reflection.

To address this problem, TagFi leverages a realization that a modulated signal is incoherent with the rest of multipath signals, which makes it distinguishable regardless of how much this modulated path is attenuated. We harness this property and design a new tag that is tuned to the WiFi frequency range and modulates the WiFi packets by switching the tag's internal impedance between *reflective* and *non-reflective* modes. As shown in Figure 4-3a, when the tag's switch is off, it acts as an open terminal and the received signal flows into the circuit for energy harvesting. However, when the switch is on, it acts as a short terminal, which results in impedance mismatch and total reflection of the received power (Figure 4-3b). So, per WiFi packet, the tag is either in reflective or non-reflective mode, thus modulating the backscattered signal across multiple packets. It essentially reflects or absorbs the WiFi packet received by the tag to modulate the WiFi channel between the tag and the receiver, which will be next used to effectively separate the weak backscatter signal from strong multipath interferences.

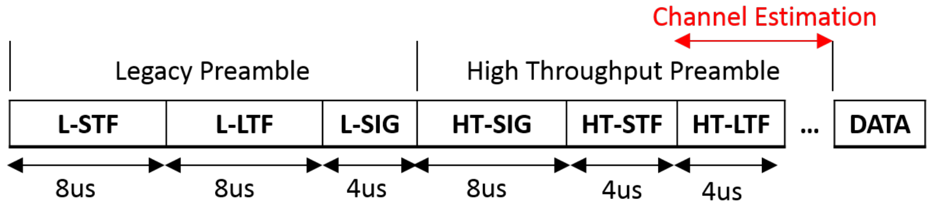

Figure 4-4: **802.11n high throughput (HT) packet structure.** The long raining symbols (HT-LTFs) are used for MIMO channel estimation.

While TagFi's tag is modulating the WiFi packets, the WiFi receiver measures the Channel State Information (CSI) for each WiFi packet, which includes the amplitude and phase shifts introduced by superposition of all multipath signals including te tag backscatter signal. However, the WiFi receiver should capture a valid WiFi signal backscattered from the tag to be able to localize the tag. Therefore, the tag needs to properly reflect the preamble of the WiFi packets used for CSI measurements. According to IEEE 802.11n high throughput (HT) packet structure [129], the preambles of each MIMO-OFDM packet contains long symbols (called HT-LTF in Figure 4-4), which are used for MIMO channel estimation. The number of HT-LTF symbols depends on the number of transmitted spatial streams. In the case of spatial multiplexing with 3 transmitting antennas, the duration of the training symbols is between 40 to 50 microseconds. Therefore, the minimum period that the tag maintains its impedance has to be larger than the duration of HT-LTF training symbols.

It should be noted that since TagFi performs modulation in the packet level, it works seamlessly with any packet transmission rate or even if the packets are not being sent at fixed intervals. In other words, the tag decides to change the modulation based on the arrival of a new packet and detects the starting point of a packet using a low power envelop detector used in the conventional WiFi backscattering systems.

4.2.2 Extracting Multipath Geometries

TagFi exploits CSI values to estimate (1) the direction at which the signal is arriving at the tag (known as AoD), (2) the direction at which the backscattered signal is arriving from the tag to the WiFi receiver (known as AoA), and (3) the relative Time of Flight (ToF) of the tag's reflection with respect to the LoS path. When the tag is in the reflective mode, it is technically a shorted antenna that reflects back any received signal, thus behaving like a static reflector. So, the tag's reflection can be considered as one of the multipath signals. However, this passive reflection will disappear when the tag switches to the non-reflective mode. In the following sections, we first explain how CSI at the receiver can be modeled in terms of the AoA, AoD, and ToF of the received multipath signals and how backscatter modulation helps to estimate these parameters for the tag reflection.

4.2.2.1 Multipath Resolution.

The WiFi receiver is equipped with an antenna array, so each multipath signal introduces a phase shift across the receiving antennas, which is due to extra distance that it should travel to reach every antenna. As shown in Figure 4-5, this phase shift is a function of the path's AoA:

$$\Phi(\theta_l) = e^{-j2\pi f d \sin(\theta_l)/c} \tag{4.1}$$

where θ_l is the AoA of the l^{th} path, d is the distance between the antennas, f is the frequency of the transmitted signal, and c is the speed of light. Therefore, the resulting vector of the received signals due to the l^{th} path can be written as $\vec{a}(\theta_l)\Gamma_l$, where Γ_l is the complex attenuation along the path at the first antenna and $\vec{a}(\theta_l)$ is the corresponding steering vector defined as

$$\vec{a}(\theta_l) = [1, \Phi(\theta)^1, ..., \Phi(\theta)^{M-1}]^T \tag{4.2}$$

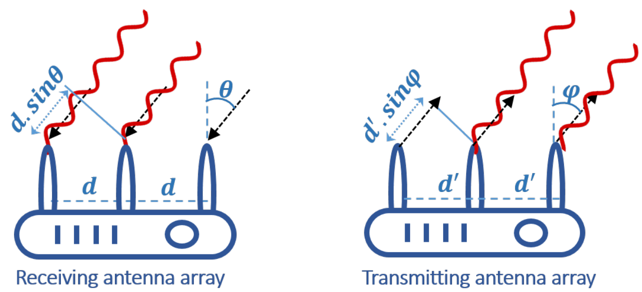

Figure 4-5: **MIMO Antenna Array.** Each wireless path has to travel an extra distance to reach (or leave) different elements of an antenna array, which causes a phase shift that is a function of the antenna spacing and the direction of the signal (AoA or AoD).

where M is the number of receiving antennas. In the presence of L paths, the overall signal will be written as the superposition of the signal received from all the paths:

$$\vec{\chi} = \sum_{i=1}^{L} \vec{a}(\theta_i)\Gamma_i \tag{4.3}$$

This is the standard form for applying the well-known super-resolution MUSIC algorithm [58] to compute AoA of multipath signals including the tag reflection. However, the main challenge is that the tag's backscattered signal is multiple times weaker than the signal that comes directly from the WiFi transmitter or even other multipath reflections. So, the tag reflection will not be among the top 6-8 reflections [97] that are detectable by typical super-resolution techniques. TagFi overcomes this challenge by leveraging the modulation of the backscatter signal. The key intuition is that a modulated path is incoherent with the rest of multipath signals, which means there is no constant phase and amplitude relationship between them.

TagFi's mathematical trick to extract the weak reflection of a tag in a rich multipath environment is best demonstrated through an example in Figure 4-6. Without loss of generality, let us consider two packets and assume there are only the LoS and the backscatter paths between the WiFi transceivers. During the first WiFi packet transmission, the tag is in the

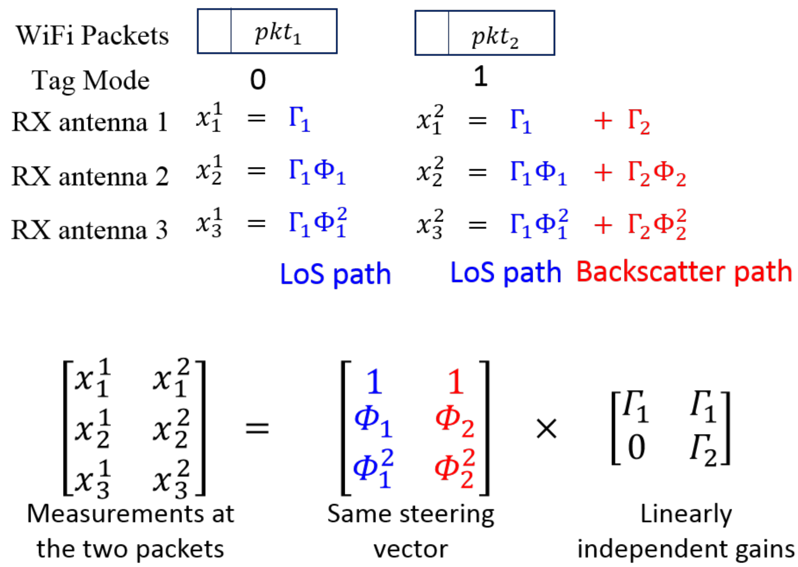

Figure 4-6: **Impact of Backscatter Modulation.** WiFi packets received with different tag modes can be written as a linear combination of the same steering vectors but independent gain vectors.

non-reflective mode, thus absorbing the signal and there will be no path between the tag and the WiFi nodes. So, the phase shift across the receiving antennas is caused by only the AoA of the LoS path. During the second packet transmission, the tag switches to the reflective mode, which results in a phase shift caused by AoAs of both the LoS and the backscatter paths. Figure 4-6 shows that the CSI measurements of these two packets can be written as a linear combination of the same steering vectors derived from the AoAs of both paths, but linearly independent complex gains. So, the CSI of different packets, that includes the modulated backscatter signal, are incoherent with each other.

We leverage this realization and combine the signal measurements from multiple WiFi packets to increase the rank of the modulated backscatter path and realize the detection of the tag's weak backscatter signal. So, a new measurement matrix $\mathbb{X}$ can be constructed, which concatenates the CSI values from multiple packets:

$$\mathbb{X} = [\vec{H}_1 \; \vec{H}_2 \; ... \; \vec{H}_P] \tag{4.4}$$

where $\vec{H}_p$ is the CSI measurement of the p^{th} packet. We further generalize this formulation by combining the signal measurements from multiple transmitting antennas and multiple frequency subcarriers since the same non-linearity will be hold for their corresponding phase shifts. The signals emitted from different sensing elements of the transmit antenna travel different distances, which appears as a phase shift of $\psi(\varphi_l)$, and is a function of AoD:

$$\psi(\varphi_l) = e^{-j2\pi f d' \sin(\varphi_l)/c} \tag{4.5}$$

where φ_l is the AoD of the l^{th} path, and d' is the distance between transmitting antennas. Furthermore, the current WiFi standards such as 802.11n leverage OFDM technology wherein data is transmitted over multiple subcarriers. For the signal received along l^{th} path, the phase shift across two subcarriers is given by

$$\Omega(\tau_l) = e^{-j2\pi f_\delta \tau_l} \tag{4.6}$$

where f_δ is the frequency difference of two consecutive OFDM subcarriers and τ_l is the ToF along l^{th} path. Therefore, the overall signal obtained at the m^{th} receiving antenna from the n^{th} transmitting antenna at the k^{th} subcarrier can be written as follows and is reported as CSI values:

$$x_{m,n,k} = \sum_{i=1}^{L} \Gamma_i (e^{-j2\pi(m-1)d\sin(\theta_i)/\lambda} \times e^{-j2\pi(n-1)d'\sin(\varphi_i)/\lambda} \times e^{-j2\pi(k-1)f_\delta \tau_i}) \tag{4.7}$$

We redefine the vector $\vec{H}_p$ and use the new $\mathbb{X}$ to extract the geometric parameters of multipath signals.

$$\vec{H}_p = [\overbrace{\vec{X}_{1,1}, ..., \vec{X}_{M,1}}^{TX\ antenna\ 1}, \underbrace{\vec{X}_{1,2}, ..., \vec{X}_{M,2}}_{TX\ antenna\ 2}, ..., \overbrace{\vec{X}_{1,N}, ..., \vec{X}_{M,N}}^{TX\ antenna\ N})]^T \tag{4.8}$$

$$\vec{X}_{m,n} = [x_{m,n,1} \ \ ... \ \ x_{m,n,k}] \tag{4.9}$$

Equation 4.7 is in a standard form to apply joint AoA-AoD-ToF 3D super-resolution algorithms such as the one proposed in [1]. The basic idea of the 3D super-resolution algorithm is eigen decomposition of the correlation matrix $R_{\mathbf{X}}$, where $R_{\mathbf{X}} = \mathbb{E}[\mathbf{X}\mathbf{X}^H]$ is a square matrix of size $S = (M \times N \times K)$ for M receiving antennas, N transmitting antennas, and K subcarriers. The eigenvectors corresponding to the smallest $(S - L)$ eigenvalues construct the noise subspace $E_N = [\vec{e}_1, ..., \vec{e}_{S-L}]$. Since the signal and noise subspaces are orthogonal, the parameters of the paths appear as sharp peaks in the following spatial spectrum function:

$$P(\theta, \varphi, \tau) = \frac{\vec{a}(\theta, \varphi, \tau)\ \vec{a}^H(\theta, \varphi, \tau)}{\vec{a}^H(\theta, \varphi, \tau)\ \vec{E}_N\ \vec{E}_N^H\ \vec{a}(\theta, \varphi, \tau)} \tag{4.10}$$

where $\vec{a}(\theta, \varphi, \tau)$ is the paths corresponding steering vector determined as:

$$\vec{a}(\theta, \varphi, \tau) = [\vec{a'}\ ,\ \vec{a'}\ \psi_\varphi\ , ...\ ,\ \vec{a'}\ \psi_\varphi^{N-1}]^T \tag{4.11}$$

$$\vec{a'}(\theta, \tau) = [\overbrace{1..\Omega_\tau^{K-1}}^{RX_1}, \underbrace{\Phi_\theta, ..., \Omega_\tau^{K-1}\Phi_\theta}_{RX_2}, ..., \overbrace{\Phi_\theta^{M-1}, ..., \Omega_\tau^{K-1}\Phi_\theta^{M-1}}^{RX_M}] \tag{4.12}$$

where $a'(\theta, \varphi)$ is written as a'. The incoherency of the modulated backscatter signal with other multipaths results in a sharp peak at $P(\theta_b, \varphi_b, \tau_b)$, where b corresponds to the tag backscatter signal. After resolving the parameters of multipath signals, TagFi's next step is to identify which path represents (1) the LoS signal between the WiFi transmitter and receiver, (2) the tag backscatter signal. By identifying these two paths, TagFi then combines the angular features of them to constrain a triangle between the WiFi transmitter, receiver, and the tag, thus localizing the tag.

LoS Detection. TagFi defines the LoS path to be the path with the shortest ToF value since it does not go under any reflection before reaching the receiver. It is worth noting that commodity WiFi radios can only estimate the relative ToF between multipath signals [1] due to the sampling frequency offset (SFO) and sampling time offset (STO) caused by lack of time synchronization between the two nodes. However, the relative ToF is sufficient to find the shortest path which is determined to be the LoS path.

4.2.2.2 Selecting Candidate Tag Reflections

To identify which resolved path represents the parameters of the backscatter signal, TagFi first employs the unique feature of the tag reflection which is its modulation. As mentioned before, the backscatter signal is the only multipath that is modulated across WiFi packets and it is only detectable if multiple packets are concatenated in the super-resolution algorithm. So, TagFi identifies the potential backscatter paths by comparing the output of the super-resolution algorithm on the ensemble of packets and on every single packet. Let us assume a sequence of P modulated packets are received and the geometric parameters of $\{\theta_l, \varphi_l\}$ are estimated for L paths using the ensemble of the packets. TagFi then finds this parameter set for each individual packet by applying the super-resolution algorithm on single $\vec{H}_p$, which results in a set of resolved paths as

$$\bigcup_{p \in P} \bigcup_{l \in L^{(p)}} \{\theta'_l, \varphi'_l\} \tag{4.13}$$

TagFi finds the unique elements of this parameter set by clustering the resolved paths and selecting the cluster centroids $\zeta = \{\theta'_c, \varphi'_c\},\ \zeta \in \mathbb{C}$, as the path representatives. Then, the candidate backscatter signals are extracted as:

$$\{\ \{\theta_l, \varphi_l\} \mid l \in L \ and\ \{\theta_l, \varphi_l\} \pm \varepsilon \notin \mathbb{C}\ \} \tag{4.14}$$

ε is the threshold used to account for the noise in measurements and the estimation variances and is set to 3° in our current implementation. It should be noted that there is usually more than one multipath signal incident at the tag as the transmitted signal reflects off of objects before arriving at the tag. Similarly, the signal backscattered by the tag bounces off of objects and reaches the receiver along multiple paths. However, the second-order reflections are significantly attenuated and won't be among the 6-8 dominant paths resolved by 3D super-resolution algorithm. So, TagFi assumes that the candidate backscatter paths are first-order reflections.

4.2.2.3 Mobile Path Filtration

In practice, it is necessary for an object tracking system to work robustly in a dynamic environment with people moving around. However, the main challenge is that the movement of a person introduces Doppler frequency on the reflected signal from the body, which changes the length of the path over time. This makes the mobile path incoherent with the static paths as well as the backscatter signal, so it will be mistakenly selected as a candidate backscatter signal. Another challenge in identifying the backscatter signal is that the super-resolution algorithm may resolve spurious paths due to noises in signal measurements, which may be confused with the backscatter signal. TagFi handles these challenges by employing v sequences of P modulated packets and a clustering technique on their corresponding candidate tag reflections. The intuition is that the AoA and AoD of the backscatter signal have smaller variations over time compared to falsely resolved or mobile paths. On the other hand, the AoA and AoD estimates from the same paths but different sequences will be clustered together. So, the diameter of each cluster will define the angular variations of each path across packet sequences. TagFi applies a K-means clustering algorithm on the candidate backscatter paths extracted for v sequence of P packets and calculates the following likelihood function per cluster:

$$P_l = exp(\omega_C \bar{C}_l - \omega_\theta \bar{\sigma}_{\theta_l} - \omega_\varphi \bar{\sigma}_{\varphi_l}) \tag{4.15}$$

where $\bar{C}_l$ is the number of points in the cluster of l^{th} path, and $\bar{\sigma}_{\theta_l}$ and $\bar{\sigma}_{\varphi_l}$ are the population variances of the estimated AoAs and AoDs, respectively. The ω weighting factors are constant values to scale the corresponding terms [1]. The cluster with the highest likelihood will be eventually determined as the backscatter path.

4.2.2.4 Extracting Tag Modulation Scheme

Finally, TagFi extracts the modulation scheme of the tag, which represents the identification of the object. Now that we have the AoA and AoD of the tag reflection, the expected phase shifts due to tag's reflection across the transmitting and receiving antenna arrays can be computed, thus the corresponding steering vector $\vec{a}(\theta_b, \varphi_b)$. The tag's modulation scheme will be determined by computing the correlation of the tag's steering vector with the CSI of every modulated packet in a sequence. Specifically, we expect this correlation to be higher when the tag is reflecting the WiFi signal since the corresponding steering vector is contained within the signal subspace and will be orthogonal to the noise subspace. As such, we define a thresholding mechanism on the following correlation function

$$Corr_p = \frac{\left\|\vec{a}(\theta_b, \varphi_b)\right\|}{\left\|\vec{a}(\theta_b, \varphi_b) \times \vec{E_n^p}\right\|} \quad , p = [1, 2, ..., P] \tag{4.16}$$

where $\vec{E_n^p}$ is the noise subspace computed from the CSI of the p^{th} packet. If $Corr_p$ is greater than $Tres_c$, the modulation mode is determined as 1 (or reflective) for that packet and 0 (or non-reflective) otherwise. We define threshold $Tres_c$ to be $\mu \pm \sigma$, where μ and σ are the mean and standard deviation of $Corr_p$ across the P packets.

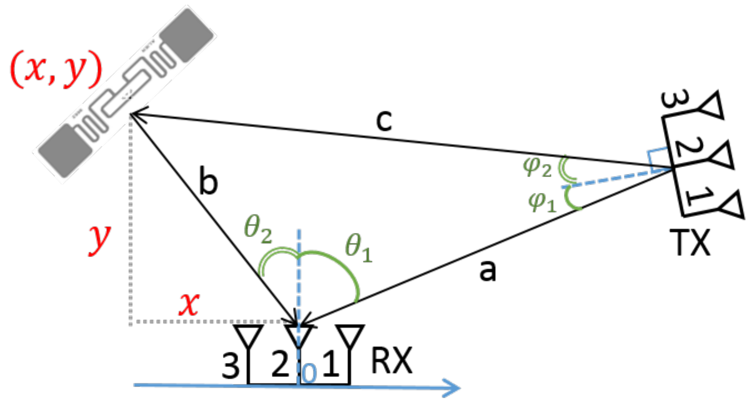

Figure 4-7: **Object Localization Algorithm.** TagFi localizes a tag by creating a multipath triangle between the WiFi transmitter, WiFi receiver, and the tag. The triangle is constrained based on AoDs (φ_1, φ_2), AoAs (θ_1, θ_2), and the distance between the two WiFi transceivers (a).

4.2.3 Localizing the Target Tag

TagFi localizes the tag with the derived AoA and AoD of the backscatter path along with the ones for the LoS path between the WiFi transmitter and receiver. As shown in Figure 4-7, the LoS signal transmits with the AoD of φ_1, propagates a distance a, and arrives at the receiver with the AoA of θ_1. Similarly, the backscatter path from the tag has left the WiFi transmitter with the AoD of φ_2 and arrives at the WiFi receiver with AoA of θ_2. The AoAs and AoDs are calculated from the CSI measurements using 3D multipath resolution algorithm [1]. Given these values, we denote the location of the tag as (x, y), which can be derived from the intersection of the semi-ellipse determined by the range and the semi-line determined by AoAs:

$$\begin{cases} b = \frac{a \sin(\varphi_1 - \varphi_2)}{\sin(\pi - (\varphi_1 + \varphi_2 + \theta_1 + \theta_2)} \\ x = b \sin \theta_2 \\ y = b \cos \theta_2 \end{cases} \tag{4.17}$$

Since the WiFi transceivers are fixed and their locations are available, we assume that the link distance a can be directly calculated. However, it should be noted that the super-resolution algorithm, presented in section 4.2.2.1, also calculates the relative ToFs for all paths. So, if the link distance is not available in practice, TagFi can still localize the tag using Multipath Triangulation [1] which relies on relative ToF of the LoS path and the backscatter signal. In addition, in the case of having multiple WiFi transmitters in the monitoring area, we can further improve the localization performance by solving the following optimization problem:

$$argmin \sum_{i=1}^{Q} (x_i - \hat{x})^2 + (y_i - \hat{y})^2 \tag{4.18}$$

where Q is the number of WiFi transmitters. It should be noted that this is only for further improvements in case more than one transmitter is available. TagFi properly works with a single pair of WiFi transceivers.

4.3 Evaluation

4.3.1 Implementation

We implement TagFi using a pair of Intel NUCs equipped with Intel 5300 NIC and three 7 dBi omni-directional antennas[1], which form a uniform linear array. We install Linux 802.11n CSI tool [21] in the transceivers to collect CSI measurements from 3-element antenna arrays in each of the WiFi transmitter and receiver, and 30 frequency subcarriers. Devices are set to work in monitor mode using channel 128 at 5.63 GHz frequency with a 40 MHz bandwidth. The transmission rate of packets is set to 3000 Hz. We use the antenna calibration method introduced in WiCapture [50, 93] to compensate for the local oscillator offsets of radio chains. It should be noted that TagFi does not require any extra coordination or a specific type of packet, so it can piggyback localization on top of any communicated WiFi

[1]https://www.data-alliance.net/antenna-dual-band-2-4ghz-5ghz-7dbi-omnidirectional-outdoor-indoor-rp-sma/

(a) Tag prototype

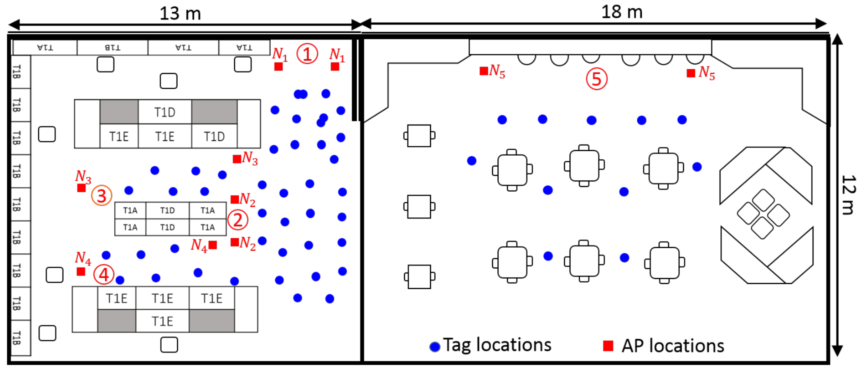

(b) Experimental Setup

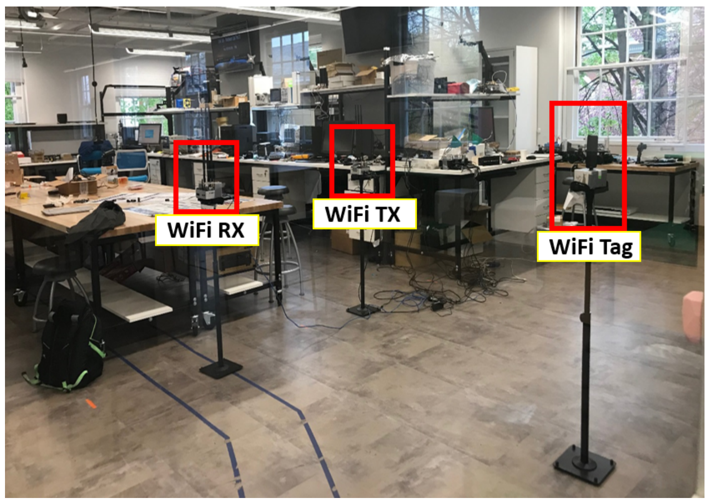

(c) Snapshot of the tested cluttered environment

Figure 4-8: **TagFi's Experimental Setup.** (a) A prototype of TagFi's tag is built using an off-the-shelf RF switch connected to a WiFi antenna, and (b) is tested for different distances and angles in (c) a cluttered multipath rich environment.

packets.

We built a prototype of the WiFi tag, shown in Figure 4-8a, using a IDT-F2977EVBI[2] switch that is connected to a 5 GHz WiFi antenna, a 50Ω and a short circuit cap to emulate "reflective/non-reflective" states. It should be noted that the tag is not equipped with any WiFi transceiver since it just requires to passively backscatter the available WiFi signals.

[2]https://www.idt.com/document/dst/f2977-datasheet-rev-o

4.3.2 Experimental Setup

We deploy our system in a regular office building that spans an area of $12 \times 30m$, as illustrated in Figure 4-8b, in the presence of 1-5 occupants and a lot of furniture and electrical equipment with rich multipath propagation. We place the transmitter-receiver pair in 5 different locations, shown in Figure 4-8b, and place the tag in random locations for a total of 51 test spots. In addition, for any tested location in figure 4-8b, we collect CSI measurements in both directions and estimate the location of the tag for both communication directions, which results in a total of 102 different experimental scenarios. In each experiment, 1000 packets are transmitted with a $3ms$ time interval and the tag's modulation mode changes per packet, obtaining a uniform "..0101.." modulation scheme. The main results are calculated based on the sequences of 10 modulated packets and the impact of the number of packets on localization is discussed in Section 4.4.3.

Note that we do not compare with state-of-the-art WiFi-based object tracking systems like WiTag [117] and BLoc [130] because they rely on frequency shifting and therefore require a customized tag to eliminate multipath interference and separate the backscattered signal. In addition, we do not compare with RFID-based localization systems like [104] since they require the installation of specialized RFID readers. Therefore, a head-to-head comparison would not be meaningful and only a qualitative comparison is provided.

4.3.3 Benchmark Verification

We first verify the key innovation of TagFi, which is utilizing the backscatter modulation for eliminating the coherence of the backscatter signal with other multipath reflections. We place a pair of WiFi transceivers in an empty environment at proximity of 1 meter to each other, shown in Figure 4-9a. The tag is equipped with a 10 dBi directional antenna[3], to enforce a stronger reflection for better visualization, and is placed between the transmitter and receiver in a position that creates a backscatter path with AoA and AoD of 0° for verification. First, we switch the tag into "reflective" mode, so a backscattered path is expected from the transmitter to the tag to the receiver. However, we can see in Figure 4-9c that only one cluster of AoA-AoDs is obtained, which is due to the strong LoS path between the transmitter and receiver. The tag's reflection is not detected in this case since it is multiple times weaker than the LoS path, thus being swamped by the multipath interferences.

Next, the tag starts modulating the backscatter signal by continuously switching the modulation mode between reflective and non-reflective. We can see in Figure 4-9d that two clusters of AoA-AoDs are derived in this case: one belongs to the LoS path and the other belongs to the backscatter path. The AoA and AoD of the new derived path are clustered at 0°, matching the angles of the tag. This confirms the mathematical formulations presented in Section 4.2.2.1 and the expected rank increase in the system of equations due to the backscatter modulation. Finally, Figure 4-9b demonstrates that this approach effectively detects the tag reflection even though there is no obvious change in the raw CSI values as the tag switches the modulation mode. This confirms the importance of this realization and the significant improvement over the state-of-the-art WiFi backscattering techniques [118] that rely on the changes of the raw CSI amplitude to extract the modulated information in ranges as short as 0.5 *meter*.

4.3.4 Tag Localization Accuracy

We evaluate TagFi localization accuracy by deploying the system in two spaces of $12 \times 13m$ and $12 \times 18m$ with rich multipath propagation that replicates the scenarios used for evaluation

[3] Alfa APA-M25 dual band 2.4GHz/5GHz 10dBi high gain directional indoor panel antenna with RP-SMA connector

of state-of-the-art systems like [130]. It should be noted that the experiments of this chapter are conducted in the presence of moving people, which confirms the robustness of TagFi in dynamic environments. We first place the tag at each of the tested locations shown in Figure 4-8b. we also vary the location of the TX-RX link throughout the evaluation area between locations 1-5. For each tag location shown in blue, we choose the closest TX-RX link to the tag for localization. Since the detection range of the tag is constrained by the power of the backscattered signal, we discard instances where the tag does not respond and will analyze the tag detection rate later in Section 4.3.5.

Figure 4-10 shows the CDF of TagFi's localization error along each of the X and Y di-

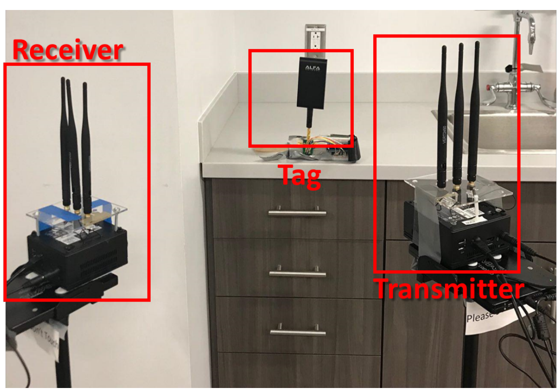

(a) Experimental setup

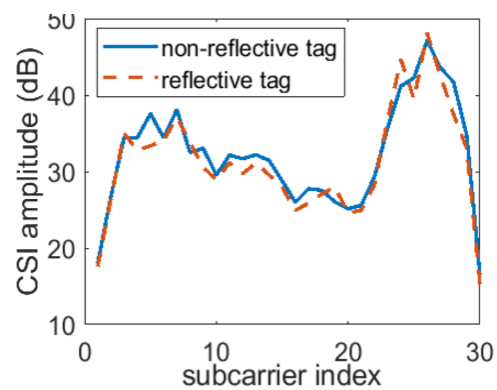

(b) CSI of the two modulation modes

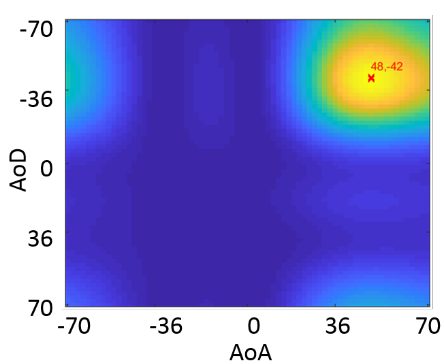

(c) Tag is continuously on

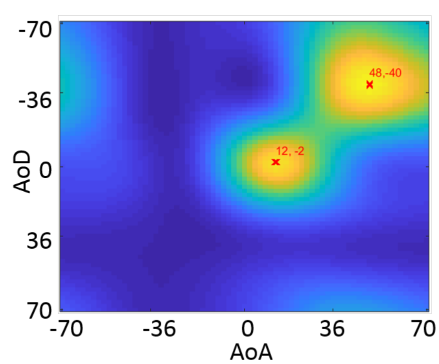

(d) Tag is modulating

Figure 4-9: **Benchmark experiments.** The tag reflection with AoA and AoD of 0° is only detectable when the tag starts modulating the WiFi packets by switching between reflective/non-reflective modes. This is despite the fact that no obvious variation can be observed in the raw CSI values as the tag modulation changes.

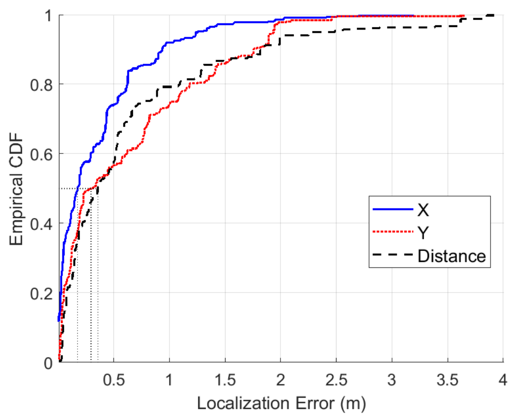

Figure 4-10: **TagFi's Localization Accuracy.** TagFi can achieve median error of 17 and 29 cm along X and Y dimensions.

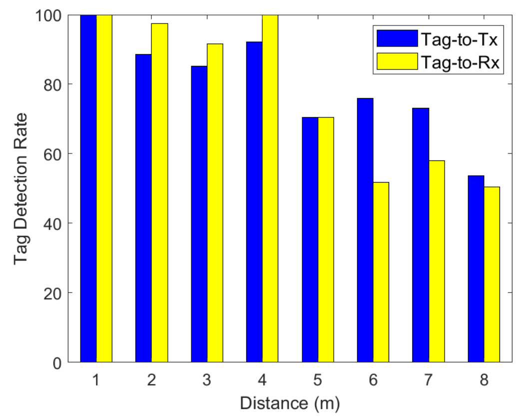

Figure 4-11: **TagFi's Detection Rate.** The detection rate decreases from 100% in 1m to 50% in 8m distance from the links.

mensions. TagFi can achieve a median error of 17cm and 29cm, as well as 80th percentile errors of 62cm and 1.2cm across x and y coordinates, respectively. These results are comparable to state-of-the-art WiFi-based tag localization systems that use multiple APs and battery-powered tags [117, 130]. The primary reason behind the high performance of TagFi is its ability to separate the backscatter signal from multipath interferences. Generally, the tag localization accuracy depends on several factors including the profile of multipath propagation, the distance from WiFi link, and the presence of obstacles. For example, Figure 4-10 shows that TagFi's localization accuracy is lower along Y dimension than X dimension. The reason is that the tested locations are further away from the WiFi link in the Y axis. Therefore, a small error in AoA and AoD estimations causes a larger error in Y-axis localization. Nevertheless, TagFi still achieves an overall Euclidean distance error of 35cm and the 80th percentile of 1cm as shown in Figure 4-10.

4.3.5 Tag Detection Rate

To test the working range of TagFi, we first fix the tag-to-TX distance at 0.7m, while varying the tag-to-RX distance, and vice versa. Figure 4-11 shows the tag detection rate with respect to its distance from the WiFi transmitter and receiver. As the tag moves away from the WiFi transmitter, the detection rate decreases from 100% in 1*m* to 53% in 8*m* distance. Similarly, as the tag moves away from the WiFi receiver, the tag detection rate decreases from 100% to 50% in 1*m* and 8*m* distances, respectively. Theoretically, the power loss of a radio signal is proportional to the inverse square of the distance, so as the length of the backscattered signal increases, it undergoes more attenuation and a smaller fraction of the signal arrives at the receiver along the backscatter path.

We can also see that the detectability of the tag is more sensitive to the tag's proximity from the WiFi receiver, so we can ensure high detection performance by maintaining a clean direct path between the tag and the WiFi receiver. This requirement can be fairly satisfied in regular office buildings, considering that there are usually multiple WiFi devices locating in different rooms. In addition, TagFi only requires a single WiFi receiver to locate the object with no additional coordination with any other devices. So to locate an object in practice, the smart building controller will inquiry all WiFi devices, they independently eavesdrop the transmitted packets and apply TagFi. So, we can expect that the WiFi device in the vicinity of the object to accurately locate it.

4.4 Sensitivity Analysis

4.4.1 Impact of TX-RX Location

Next, we evaluate the effects of the WiFi link location on detecting the tag's backscatter signal. In each location, we place the WiFi transmitter and receiver such that they are 0.7 to 6*m* away from each other. The WiFi link locations are shown as 1-5 in Figure 4-8b. For each tag location shown in blue, we choose the closest TX-RX link to the tag for localization. Figure 4-12 plots the tag detection rate as a function of different TX-RX locations. We can see that

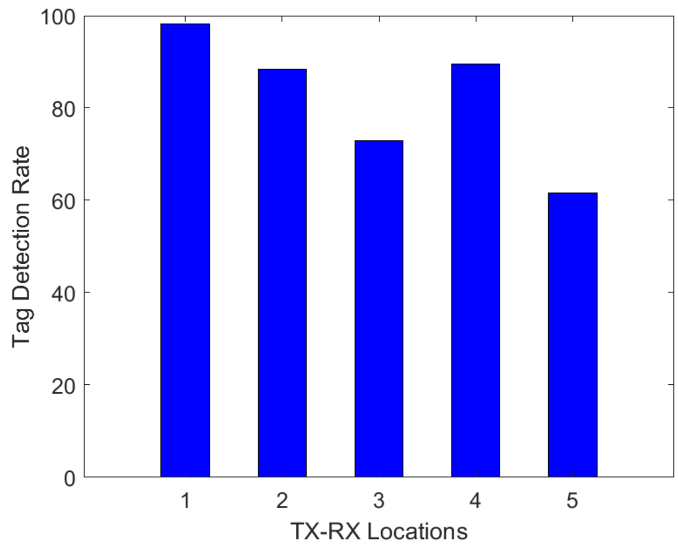

Figure 4-12: **TagFi Performance vs. Distance** The tag detection rate varies based on the location of the WiFi link and is expected to be lower for a highly multipath rich environment.

the probability of detecting the tag is changing from 98% in location 1 to 60% for location 5. The main factors affecting these variations are a combination of destructive/constructive interference and the distance of the tag from the WiFi link. For example, in locations 3 and 4, the tag is located between cluttered tables and multiple electronic and metallic items, creating rich multipath propagation, which results in lower detection rate. In addition, in location 5, the tag is located in longer ranges from the WiFi transmitter and receiver, for which the strong LoS path between the WiFi transmitter and receiver swamps the backscatter signal, making the tag detection more challenging.

4.4.2 AoA-AoD Estimation Accuracy

We measure the accuracy of AoA and AoD estimations using the absolute difference between the ground truth and estimated values for both the backscatter path and the LoS path between WiFi transceivers. Figure 4-13a shows the CDF of the AoA estimation errors. TagFi can achieve median errors of 7° and 5° and 80^{th} percentile of 10° and 13° for the

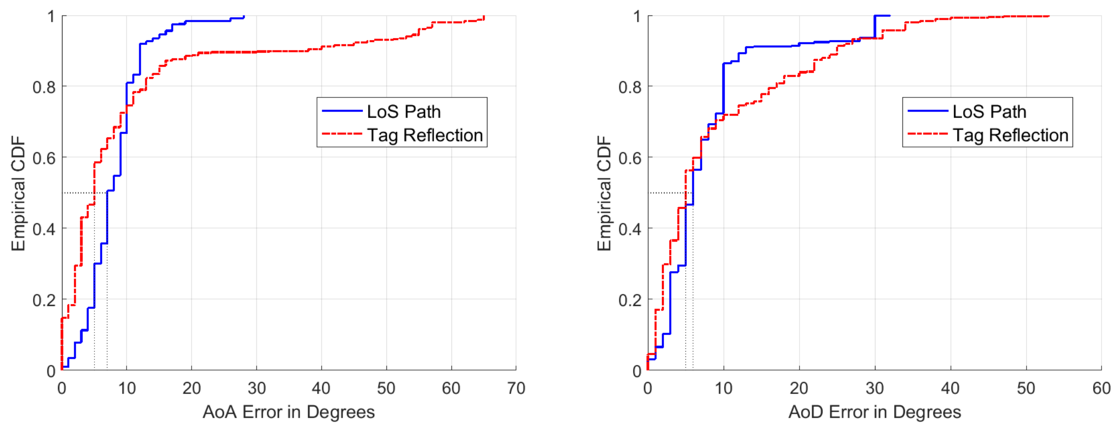

(a) (b)

Figure 4-13: **TagFi Performance in Angle Estimation.** The high performance of TagFi in tag localization is the result of the high-resolution estimations of the AoAs and AoDs for both the LoS and the backscatter paths.

LoS and backscatter paths, respectively. In addition, Figure 4-13b shows the performance of AoD estimations, for which TagFi achieves median accuracy of 6° and 5° for the LoS and backscatter paths, respectively. The 80^{th} percentile accuracy of AoD estimations degrades to 10° and 18°. These results are comparable to WiTag's performance [117], which also reports a median accuracy of 7° to 14° in AoA estimation. The key point is that TagFi achieves similar accuracy without requiring to shift the frequency of backscatter signal or a high-power circuitry in the tag.

As can be seen in Figure 4-13, the LoS estimates in both the AoA and AoD CDFs have shorter tales compared to the ones for the backscatter path. Since a higher signal power propagates along the LoS path, the angular estimates are more accurate for this path. Another factor affecting the performance of super-resolution algorithms is the direction of the incident signals. In other words, a higher estimation error is expected as the incident angle of the signal approaches the angle of the array. For example, when the direction of the backscatter signal is close to 90°, it is hard to identify the direction since similar phase differences will be introduced across the antennas for both $90° - \varepsilon$ and $-90° + \varepsilon$ for $0° \leq \varepsilon \leq 30°$. In our current

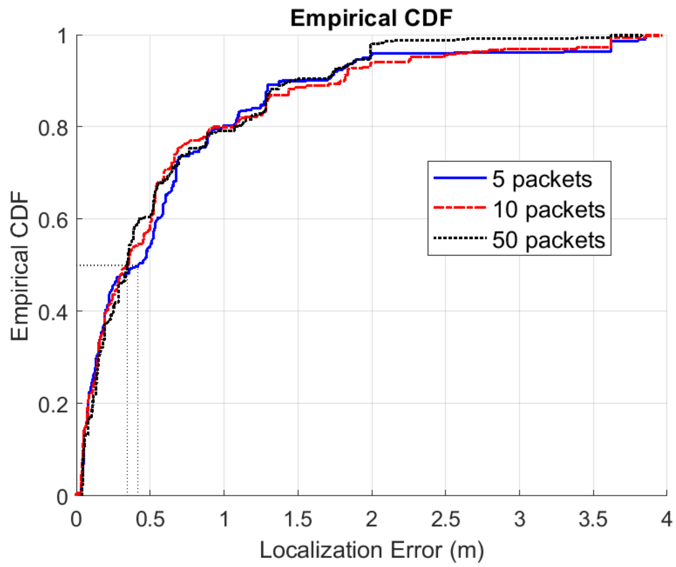

Figure 4-14: **Number of Packets vs. TagFi's Accuracy.** TagFi is capable of localizing the tag with small number of packets.

experiments, the majority of the tag positions (78%) create a backscattered signal at AoAs or AoDs larger than 40°, which results in a higher super-resolution error for the backscatter signal. This is though more a limitation of the linear antenna arrays and can be addressed by using circular antenna arrays.

4.4.3 Impact of Number of Modulated Packets

TagFi primarily relies on the modulation of the tag reflection to identify this weak backscatter signal from complex multipath propagations. So, receiving WiFi packets with different modulation modes is critical for achieving high accuracy in tag localization. We would like to evaluate the impact of the number of modulated packets in localization accuracy. Figure 4-14 measures the Euclidean distance of the estimated locations and the ground truths for all tested tag locations, as the number of packets changes from 5 to 50 packets. We can see that even with 5 packets, TagFi achieves a median localization accuracy of 20cm. These results indicate that TagFi can achieve high performance with only few packets. It is

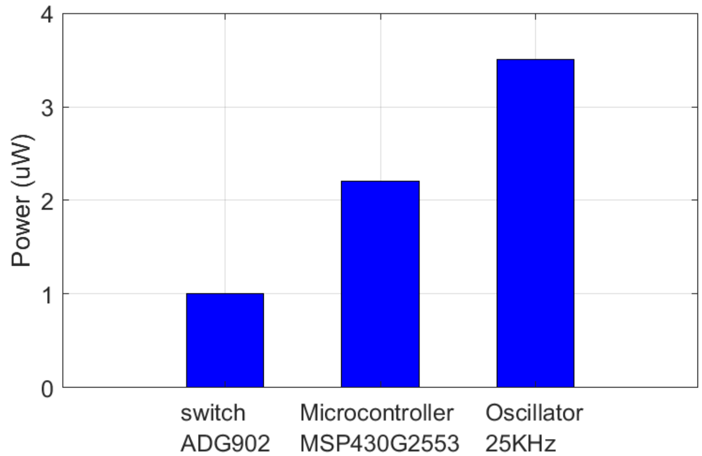

Figure 4-15: **TagFi's tag power consumption** is low enough to operate with WiFi energy harvesting.

worth noting that the minimum number of required packets is a function of the modulation patterns. For example, in the performed experiments, there is only one active tag using uniform "...01010.." modulation, where 0 means the tag is in non-reflective mode during one packet transmission and switches to the reflective mode for the next packet, indicated as 1. Therefore, TagFi technically requires only 2 consecutive packets to remove the coherence of backscatter signal. However, utilizing more packets can improve the localization performance by filtering out the noise in measurements. It should be noted that the performance of TagFi is independent of the modulation pattern or the order of "reflective/non-reflective" modes across packets as the super-resolution algorithm has no notion of packet order.

4.5 Discussions

4.5.1 Tag Power Consumption

One of the remaining questions here is the power consumption of TagFi's tag. The current prototype of the tag uses off-the-shelf components, which are not designed for battery-free or low power use-cases. As a result, we come up with an equivalent realization of TagFi based on the energy harvesting circuitry in the literature and leave the tag fabrication for future work. Figure 4-15 shows a high-level breakdown of the power-hungry components of the tag. Considering the simple functionality that we expect from the tag, the major source of power consumption is the clock generation block or the oscillator, which has a power consumption proportional to the clock frequency. For example, prior work such as WiTag [117], that needs to shift the backscatter signal to another frequency channel, requires an oscillator that operates in 20 Mhz, which consumes more than $1mW$ of power. However, TagFi does not require to shift the frequency of the signal, so even a $25KHz$ clock is sufficient, which consumes a few microwatts of power. Moreover, recent research on WiFi energy harvesting [127, 128] shows the possibility of harvesting between 30 to 400 microwatts from WiFi transmissions, which is more than enough for TagFi design.

4.5.2 Effect of Backscattering on WiFi Networks

TagFi performs localization without requiring any explicit coordination between the tag and WiFi transceivers or WiFi devices themselves. Moreover, since the backscatter modulation changes per packet, TagFi works seamlessly with any packet transmission rate or even if the packets are not being sent at fixed intervals. Therefore, it can be fully piggybacked on top of the available WiFi communications without imposing any requirements beyond standard WiFi protocols.

In addition, the presence of an active tag in the environment does not affect the quality of ongoing WiFi communications since the tag reflections are considerably weaker than the typical indoor multipaths. As shown in Figure 4-9b, the modulation of the backscatter signal has minimal impact on the raw CSI values so it does not interfere with existing WiFi traffic. Our analyses show that 99.3% of the packets transmitted in the conducted experiments has been received properly during the tag modulation. In other words, an active tag can be considered as a passive reflector in the environment similar to any other object or furniture in the room.

4.5.3 Co-existence of Multiple Tags

One of the important improvements of TagFi over conventional RFID or WiFi-based localization systems is its potential capability of localizing multiple tags simultaneously. The key intuition is that the backscatter signals of different modulations not only are incoherent with the other multipath signals, but also they are incoherent with each other. So, the active tags only require to have unique modulation schemes so that TagFi can separate their reflections from each other.

To better explain this capability, let's say there are two active tags with the modulations of 010101 and 001001 across 6 packets, where "1" means the tag is in the reflective mode and "0" indicates the non-reflective mode. Without loss of generality, let us assume there are only the LoS path and the backscatter signals between the WiFi transmitter and receiver. The two tags create different superpositions of signals across the first three packets, for which the received signals across the antenna array will be written as

WiFi Packets	pkt_1	pkt_2	pkt_3
Tag1 Mode	0	1	0
Tag2 Mode	0	0	1
RX_1	$x_1^1 = \Gamma_1$	$x_1^2 = \Gamma_1 + \Gamma_2$	$x_1^2 = \Gamma_1 + \Gamma_3$
RX_2	$x_2^1 = \Gamma_1\Phi_1$	$x_2^2 = \Gamma_1\Phi_1 + \Gamma_2\Phi_2$	$x_2^2 = \Gamma_1\Phi_1 + \Gamma_3\Phi_3$
RX_3	$x_3^1 = \Gamma_1\Phi_1^2$	$x_3^2 = \Gamma_1\Phi_1^2 + \Gamma_2\Phi_2^2$	$x_3^2 = \Gamma_1\Phi_1^2 + \Gamma_3\Phi_3^2$
	LoS path	tag1 path	Tag2 path

The measurements at these three packets can be written as a linear combination of the

AoAs of the two backscatter paths and the LoS path, while the vectors of complex gains are linearly independent of each other. Therefore, the three measurements are incoherent with each other:

$$[\vec{\chi}^1 \quad \vec{\chi}^2 \quad \vec{\chi}^3] = \begin{bmatrix} 1 & 1 & 1 \\ \Phi_1 & \Phi_2 & \Phi_3 \\ \Phi_1^2 & \Phi_2^2 & \Phi_3^2 \end{bmatrix} \times \begin{bmatrix} \Gamma_1 & \Gamma_1 & \Gamma_1 \\ 0 & \Gamma_2 & \Gamma_2 \\ 0 & 0 & \Gamma_3 \end{bmatrix} \tag{4.19}$$

As such, to separate R modulating tags from each other, TagFi requires to receive $R+1$ WiFi packets with unique combinations of active tags. In addition, the modulation of multiple active tags can be synchronized by sending a preamble from the WiFi transmitter and having a low power envelope detector in the tags to decide when to start modulating. Designing a coordination and query protocol for the multi-tag scenarios is part of our future work.

4.5.4 Applications

TagFi's capability in object localization leads a new paradigm of using commodity WiFi devices for sensing and tracking battery-free objects or IoT devices that do not even have WiFi transceivers. This enables a rich set of context-based applications and is going to have a significant impact on the smart home, smart health and IoT domains. Some of these applications are presented as follows.

Scalable IoT Infrastructure: With the increasing number of IoT devices such as sensors and actuators, new smart applications have emerged that rely on knowing the location of devices, people, and objects. However, relying on dedicated localization infrastructures creates massive amount of data exchange and communication overhead and is not a scalable solution. TagFi takes a step toward the vision of *omnipresent sensing* by converting every commodity WiFi device into an individual sensor to locate ”things” whether a battery-free object or a low-power IoT device that does not have a WiFi transceiver. TagFi leverages the available wireless infrastructure to piggyback localization on top of the ongoing communications without relying on any explicit coordination, data sharing, or imposing any extra overhead on the wireless medium.

Smart Health: well-being and elderly monitoring is another set of applications that significantly benefit from a robust object tracking system. For example, in a vision of ”homes as caregivers” for in-aging people, the home’s smart controller exploits all the available WiFi devices in different rooms to monitor the activities of the person and her interactions with the objects in the environment, for example, if she takes her medication properly. TagFi’s capability in tracking battery-free objects, along with device-free localization techniques such as Widar2.0 [131] for human tracking, would realize this vision by automatically providing the whereabouts of people and objects on every single WiFi receiver.

Backscatter Communication: Although the main focus of this chapter is object tracking, TagFi does show high potential in other use-cases such as backscatter communication. Data and bits can also be transferred through the modulation of the tag, thus creating a communication means with battery-free objects. Section 4.2.2.4 describes how TagFi identifies the modulation pattern by exploiting the correlation of the identified backscatter path with every single packet. The same technique can be used to decode the bits. We expect a high correlation with packets transmitted during tag’s “reflective” mode, thus representing bit “1”; and low correlation with packets that are transmitted when the tag is off, representing bit “0”. Extending TagFi as a backscatter communication system and optimizing it for bit-rate is part of our future work.

4.5.5 Discussion

To localize an object, TagFi requires a direct path from the WiFi transmitter to the tag to the WiFi receiver. So, the performance of TagFi degrades in the case of complete tag blockage. Currently, all other object tracking systems also have this limitation and localizing tags with no direct reflection is still an open problem. In addition, TagFi's detection range is still limited to ranges below 6-8 meters as the current tag prototype uses off-the-shelf components, which causes low radar cross-section and significant power loss in the tag circuitry. As part of our future work, we plan to fabricate the tag on PCB board that is optimized for minimum signal attenuation, and design an antenna with high radar cross-section. Nevertheless, considering the fact that TagFi can perform localization with a single WiFi receiver, we can assume that the smart building controller compensates for the short range by inquiring all the WiFi devices to independently search for the object of interest and we can expect that at least the closest WiFi device to the object will detect and accurately localize it.

In addition, in the current implementation of TagFi, we assume that both WiFi transceivers are stationary while the environment can be dynamic. The movement of WiFi transceivers will affect all multipath signals, thus degrading the incoherence of the modulated backscatter signal with other paths. In our future work, we plan to extend TagFi for mobile WiFi devices by incorporating the on-device IMUs to compensate for the mobility. It should be noted that the evaluations of this chapter are performed in a dynamic environment which confirms TagFi's robustness to the presence of moving people and objects in the environment.

4.6 Conclusion

This chapter presents *TagFi*, a novel WiFi-based object tracking system that leverages the passive wireless reflection from a battery-free tag. The key innovation of TagFi is its unique mechanism to extract the weak tag reflection from complex multipath propagations in indoor environments. TagFi shows that modulating the backscatter path across WiFi packets eliminates the coherence of this signal with other multipath signals, enabling super-resolution algorithms to estimate the parameters of the backscatter signal. TagFi is the first tracking system that localizes battery-free tags by using a single WiFi device without requiring any hardware modification, or coordination and information sharing between multiple devices. As a result, a single WiFi device can piggyback the localization task on top of any ongoing communication.

TagFi leads a new paradigm in IoT world by enabling unilateral sensing and tracking of ”things” with commodity WiFi and can be widely applied to novel context-based applications in smart building, smart health, and robotics. We believe TagFi can be extended to other use-cases such as WiFi backscatter communications, opening new research problems on WiFi energy harvesting, multi-tag coordination, and long-range communication.

Chapter 5

Human Sensing Using Wireless Reflections

Human presence sensing has significant potential to provide monetary and environmental benefits by saving energy. Motion sensing is often used for lighting control and, although current systems often turn off the lights when occupants are not in motion, these errors can easily be fixed by moving or waving at the motion sensor. However, they would cause major comfort issues with heating and cooling control due to the thermal inertia and resulting time lag. The ability to automatically control air conditioning has been available for over hundred years, but the potential energy saving have not been fully realized due to lack of a sensing system that can detect human presence, and not just human motion.

Recent advances in wireless techniques such as MIMO-OFDM have extended its use beyond simply a communication medium to that of a device-free human sensing tool. The previous works that have explored the possibility of inferring occupancy from WiFi signals [41–43, 132] focus on detecting motion of the target and measure the temporal variations of WiFi signals caused by target movements as an indicator of occupancy. However, they suffer from high false negative rates since they cannot differentiate an unoccupied room from a non-moving person. Rich multipath distortions in indoor environments is one of the main challenges of these systems, causing the signal disturbance produced by people to be swamped in the noise distortion subspace due to destructive interferences. This limitation is particularly problematic for long sedentary activities such as movie watching or sleeping.

To address this problem, we propose a new technique called *Peripheral WiFi Vision (PeriFi)*: using multipath signals to increase the sensing area and sensitivity levels of WiFi sensing. The basic approach is to resolve multipath reflections and leverage each path as an individual sensor, rather than treating it as just a distortion. The intuition is that analyzing each path independently allows more sensitive detection of disturbances caused on weak Non-Line-Of-Sight (NLOS) signals which would otherwise be swamped by the strong Line-Of-Sight (LOS) signal when looking only at the aggregated received signal. This allows the approach to be more sensitive to small movements of a stationary target. In addition, people affect the multipath reflections even when they are perfectly still, while other approaches require the person to be moving.

Instead of any special wireless hardware, we leverage on the ubiquity of commodity WiFi devices. The presence of several WiFi-enabled devices or plug-in modules deployed in every room of a home creates a wireless mesh, which can serve as a sensor network and provide rich information about the environment. To sense the person's presence, PeriFi firstly characterizes the multipath environment of an empty room by using a novel subspace methods that we call *Multipath Smoothing*. Then, it looks for changes in that multipath environment such as (1) multipath variations in a time window caused by a moving person, or (2) multipath attenuation and reflections caused by a stationary (sitting or standing) person. To capture these changes, PeriFi employs supervised classification models with one-time training.

To implement PeriFi, we leverage the PHY layer Channel State Information (CSI) provided by commercial WiFi cards, which offer fine-grained channel responses at the granularity of OFDM subcarriers. We evaluate PeriFi in 6 individual physical configurations with 11 different occupancy states resulting in 66 individual conditions and 96 minutes worth of data. Our extensive analysis and experiments show that the relative phase information and multipath characteristics play a key role in determining the occupancy specifically if the target is stationary or completely still. Also, results indicate that PeriFi can detect occupancy with 96.7% accuracy, compared to the conventional solution with 56.1% and 76% accuracies.

5.1 Related Work

Device-free passive detection with WiFi signals have drawn much attention in the past years. Recent works focus on fine-grained PHY layer CSI as a promising substitute for MAC layer RSSI. We can categorize these works into three main approaches: fingerprint-based, threshold-based, and respiration-based. Unlike PeriFi which analyzes the multipath signals individually, all of these approaches look at the aggregate CSI values, which makes them less sensitive to fine movements without relying on scenario-specific calibration.

The fingerprint-based approaches [41] measure the similarity of CSI fingerprint of an occupied room with the reference unoccupied condition. The intuition behind this technique is that the disturbance of CSI values created by human motions reduce the similarity between occupied and unoccupied fingerprints. However, similar to any fingerprinting approach, they require a large database of all occupied scenarios in different locations, which is practically impossible due to random movement behavior of occupants. The threshold-based algorithms [42, 43, 132] define an individual metric as a threshold line to differentiate occupied and unoccupied conditions based on the temporal correlation of CSI values [42, 43], or the correlation of CSI values over multiple frequencies [132]. Although these algorithms are fairly accurate in detecting human motion, they are incapable of detecting stationary or still occupants since the fine or even absence of the target movements causes no measurable temporal or frequential variation of WiFi signals.

Apart from the above works, DeMan [43] proposed respiration rate as a metric to detect stationary target by justifying a sinusoidal model and looking for desired breathing frequency component in the signal. Although the performance of this method is promising in extremely controlled scenarios, small body movements or the working distance range limit the performance and make it impractical for occupancy detection. Besides these WiFi-based occupancy detection method which use commodity devices, there some high resolution breath detection [133], and device-free localization systems [77], which require specialized bulky hardware and radar techniques such as FMCW, thus cannot be implemented by commercial products. We build PeriFi upon noise-subspace methods [30, 134] to capture multipath reflections. Although these methods focus on better estimation of the LOS signal by discarding the NLOS signals, PeriFi leverages all multipath components and use each as a spatial sensor to infer occupancy.

We design PeriFi upon previous works and add some features to capture Doppler Shift caused by a moving person, and attenuation and reflections caused by a stationary or still person. For this purpose, we build our model on noise-subspace methods [30, 134] proposed for device-base or device free localization to capture multipath reflections. The difference between our approach and these localization solutions is that they assume the presence of the target in the environment and accordingly the existence of a reflection from human body. However, without this assumption in occupancy detection, we require further considerations to distinguish empty from occupied states, which will be elaborated in the next section.

5.2 Peripheral WiFi Vision

Complex indoor environments cause wireless signals to propagate along multiple paths, reflecting off of walls, furniture and human body (shown in Figure 5-1). The received signal

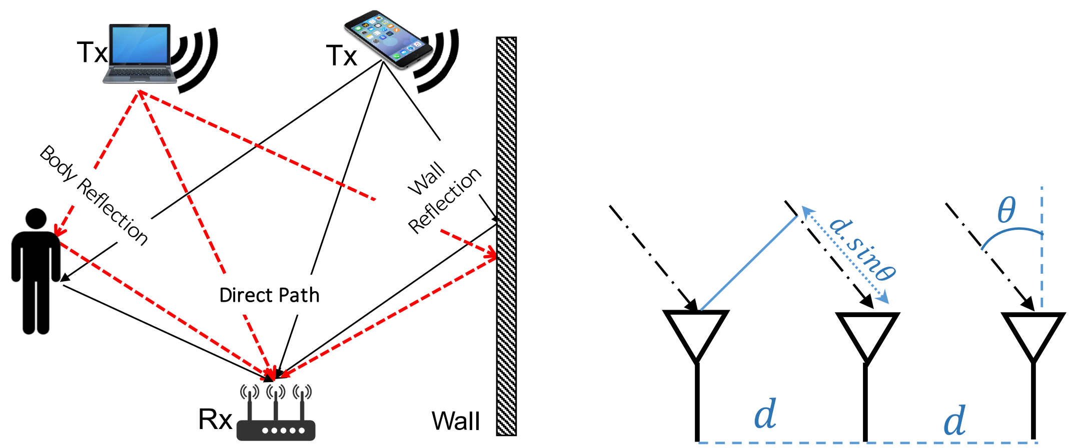

Figure 5-1: **Multipath Propagation.** An illustration of (left) multipath propagation in the presence of a target, and (right) additional phase shift of the incident signal in the second antenna.

is the combination of all these paths, thus suffering from multipath interference. In the occurrence of destructive inferences, the human body disturbance may be canceled out in the aggregated signal. In addition, the properties of the received signal are dominated by objects in the Fresnel zone of the LoS path, resulting in a linear sensing region despite the omnidirectional nature of the antennas. So, in the presence of an occupant in the NLoS area, the resulting disturbances are weak and can be swamped by the LOS signal when looking at the aggregate value.

To address this challenge, we leverage multipath reflections and analyze them independently to provide peripheral WiFi vision. Each of these paths reveals information about a different part of the physical environment and acts as an additional sensor. This increases sensitivity by allowing LoS and NLoS paths to be analyzed independently, thus can differentiate between empty room and an occupied room with a stationary or completely still target. We further improve the sensitivity of this approach by leveraging the presence of several WiFi-enabled devices in a building. PeriFi takes advantage of these spatially diverse WiFi components such as personal computers, smart TV, or thermostats to create a wireless mesh that covers the home and can view different aspects of a target simultaneously.

PeriFi leverages the PHY layer Channel State Information (CSI) provided by commercial WiFi cards. CSI provides a small version of fine-grained channel frequency response at the granularity of OFDM subcarriers. While previous studies [41, 42] show that CSI suffers from arbitrary phase offsets due to Packet Detection Delay (PDD) and Sampling Time Offset (STO), we show that the effect of these noises can be eliminated by converting raw CSI values into multipath components. The intuition behind this idea is that our novel multipath resolution method leverages multiple subcarriers of a WiFi channel to eliminate phase offsets caused by STO and PDD, and uses multiple transmitting antennas to separate coherent multipath signals, thus providing more accurate estimation of the stationary environment. The details of our data preprocessing method are explained in Section 5.2.1.

Similar to threshold-based algorithms, PeriFi requires a prior multipath characteristics of the environment with no human presence. However, unlike fingerprint-based approaches, it doesn't need scenario-specific calibrations for all possible occupancy states. So, in the first step, PeriFi characterizes the multipath components of an empty room for each Tx-Rx link and converts each path into multiple features over both time and space such as the power, Angle of Arrival (AoA), and relative Time of Flights between paths (rToF). Then, in a sliding window fashion, PeriFi monitors and scans these paths multiple times per second and uses a classifier to detect the presence of people. The details of multipath resolution algorithm and extracted features are explained in Sections 5.2.2 and 5.2.3, respectively.

5.2.1 Data Preprocessing

Leveraging OFDM and MIMO technologies in the current WiFi standards such as 802.11n, the commercial WiFi cards can provide the overall attenuation and phase shifts of the transmitted signal introduced by the channel. This information is represented in the form of CSI in the granularity of 30 subcarriers for 3 antennas,

$$CSI\ Matrix = \begin{bmatrix} csi_{1,1} & csi_{1,2} & \dots & csi_{1,30} \\ csi_{2,1} & csi_{2,2} & \dots & csi_{2,30} \\ csi_{3,1} & csi_{3,2} & \dots & csi_{3,30} \end{bmatrix}$$

where $csi_{m,n}$ is the CSI of m^{th} antenna and n^{th} subcarrier, which includes the received signal from all paths.

Each CSI value depicts the amplitude and phase responses of the channel. Although CSI phase values are more sensitive to small changes in the environment, they are prone to arbitrary errors caused by PDD and STO. To address this issue, we leverage the constant behavior of STO across antennas and the linearity of this offset across subcarriers. On the other hand, our observations from extensive experiments [135] show that the CSI phase is significantly noisy in the frequencies with destructive interference. So, we sanitize the phase values by using a similar technique as in [30], but for a portion of subcarriers with no deep fading.

5.2.2 Resolving Multipath Propagation

In wireless communications, signals from a transmitter arrive at the receiver in multiple paths after reflecting off the objects in the physical environment. Each of these paths have their own specifications which could be characterized by the Angle-of-Arrival (AoA), Angle-of-Departure (AoD), path delay or Time-of-Flight (ToF), and fading. Many techniques have been proposed for estimating AoA in a MIMO array such as super-resolution subspace methods [58]. However, they assume that the received reflections are from different targets, thus uncorrelated with each other; while the wireless multipath reflections in indoor environments are emitted from a single source, thus phase-synchronized and highly correlated.

To address this issue, some signal processing methods such as spatial smoothing [31, 136] and forward-backward averaging [137] are proposed to decorrelate the multipath signals. However, they decrease the array aperture and the degree of freedom, resulting in lower accuracy and fewer number of resolved paths. Recent works try to overcome these limitations by developing joint estimation in both ToF and AoA dimensions [30, 70], but they still suffer from reduced effective aperture.

In this research, we propose a new smoothing algorithm called *MIMO Smoothing*, which leverages the recent advances in wireless techniques such as *MIMO-OFDM* to improve the accuracy of multipath estimation. MIMO arrays employ multiple transmitting antennas for emitting multiple data streams, and multiple receiving antennas for separating these signals. This results in spatial diversity both in transmitting and receiving antenna arrays. In addition,

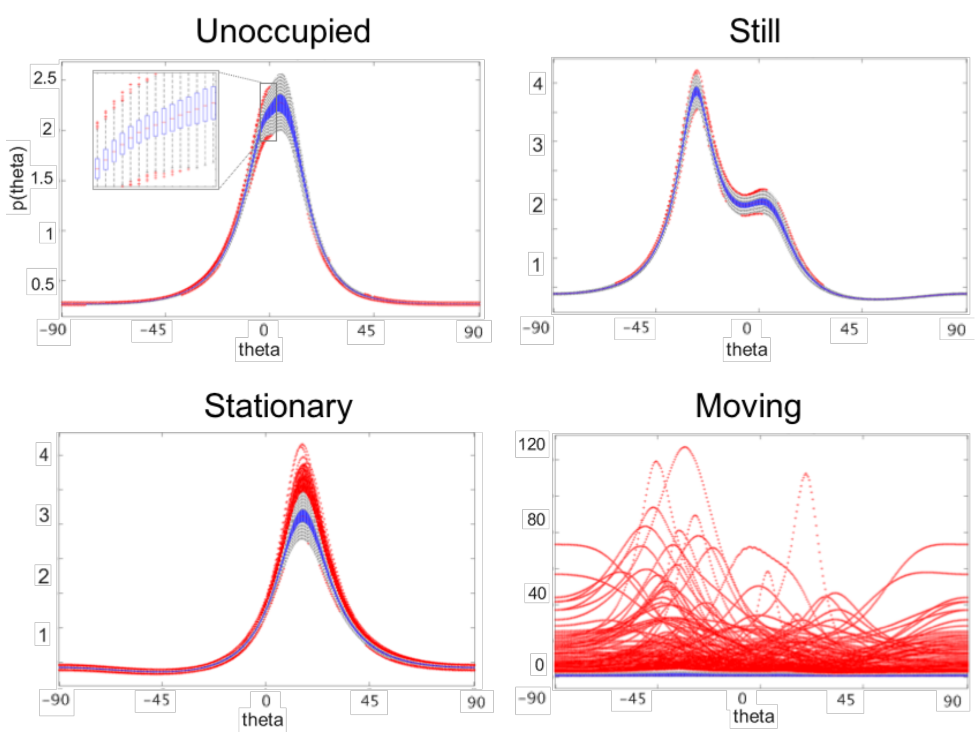

Figure 5-2: **Human Body Movements on Wireless Signals.** PeriFi detects different occupancy scenarios based on changes in multipath characteristics of empty room as well as stability of AoA spectrum in each angle.

OFDM as a modulation format has been widely used in wireless communication for encoding data streams on multiple carrier frequencies, which provides frequential diversity due to multipath selective fading. MIMO smoothing combines the frequential and spatial diversity to accurately separate coherent signals, without decreasing the effective aperture.

The basic idea in MIMO smoothing is that the signals transmitted from any of the transmitting antennas will be incident in any of the receiving antennas, provided they are in far field. However, each propagation path has to travel an additional distance if transmitted from the second antenna, introducing a constant phase shift on the received signal. Therefore, the propagation paths received from multiple transmitting antennas have similar steering vectors, while the superimposed received signals across receiving antennas are linearly independent. This is due to different phase shifts associated with multipath components from the transmitting antennas to the receiving antennas. As a result, the transmitting antennas could be successfully used to separate the received signals and vice versa, which are explained in details in the next section.

5.2.2.1 MIMO Smoothing

The super-resolution sub-space methods such as MUSIC [58] resolve multipath components by relying on extra phase shifts across sensor arrays due to additional travel distance (shown in Figure 5-1). The introduced phase shift of k^{th} path with AoA of θ_k at m^{th} antenna is denoted as a function of AoA:

$$\phi(\theta) = e^{-j2\pi f d \sin(\theta)/c} \tag{5.1}$$

where d is the distance between antennas, c is the speed of light, and f is the frequency of the transmitted signal. The MUSIC algorithm uses this information and creates a measurement matrix X based on the received signal across antennas as:

$$X(t) = [x_1(t), ..., x_M(t)]^T = a(\theta)s(t) + N(t) \tag{5.2}$$

where M is the number of antennas, $s(t)$ is the received signal vector at the first antenna and $N(t)$ is the noise vector. $a(\theta)$ is called the steering vector and expresses the phase differences at the antenna array:

$$a(\theta) = [1, \phi(\theta), ..., \phi(\theta)^{M-1}]^T \tag{5.3}$$

The MUSIC algorithm calculates the eigenvectors of XX^H, and divides them into noise and signal subspace. Then, it searches for the AoAs whose steering vectors are orthogonal to the noise subspace. This method assumes that the incoming signals are from different sources and are uncorrelated with each other. However, the multipath signals are phased-synchronized, thus resulting in a reduction in the rank of the covariance matrix and superposition of coherent signals in the output of MUSIC. Therefore, a preprocessing scheme such as spatial smoothing [136] is required to convert the covariance matrix into a full rank matrix[31, 136]. In spatial smoothing, the receive antenna array is divided into a number of smaller overlapping sub-arrays as shown in Figure 5-3. Then, the covariance matrices of all sub-arrays are averaged. However, this smoothing method reduces the aperture of the sensor array from M to $M - r + 1$, where $r = L + 1$ is the size of sub-arrays and L is the number of coherent paths.

To address this problem, we leverage the presence of multiple transmit and receive antennas in MIMO systems. The idea is that the incoming signals from different transmitting antennas can define the virtual subarrays required in spatial smoothing. The intuition behind this idea is that the signals emitted from a linear transmit array will be received with a phase

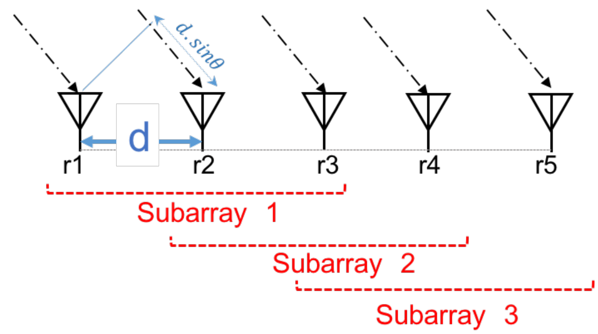

Figure 5-3: **Spatial Smoothing.** The Conventional spacial smoothing approach reduces the array aperture length and degree of freedom

shift $\Gamma(\varphi)$, which is a function of AoD

$$\Gamma(\varphi_l) = e^{-j2\pi f d \sin(\varphi_l)/c} \tag{5.4}$$

where φ_l is the AoD of the lth path. Since each received signal from different transmitting antennas has its own AoD, the virtual subarrays are linearly independent, thus increasing the rank of the covariance matrix. A MIMO radar with M receiving and N transmitting antennas can resolve $L = min(M, N)$ coherent paths using MIMO smoothing, while the effective aperture of the sensor array remains M. For more clarity, let's consider an example, where $L = 2$, $M = 3$, and $N = 2$. As shown in Figure 5-4, $x_{i,j}$ shows the received signal at antenna i from transmitting antenna j. The measurements of the two virtual transmit subarrays can be written as a linear combination of the same steering vectors, but with linearly independent complex gains due to AoD phase shift. Therefore, we can successfully apply MUSIC on the averaged covariance matrix of multiple transmitting antennas, while increasing the rank of the covariance matrix.

We further improve the multipath resolution, by combining MIMO smoothing with joint estimation of multipath characteristics. The current WiFi standards such as 802.11 leverage MIMO-OFDM technology, in which data streams are transmitted over multiple antennas and multiple subcarriers. Therefore, instead of just estimating AoA of each propagation path, we

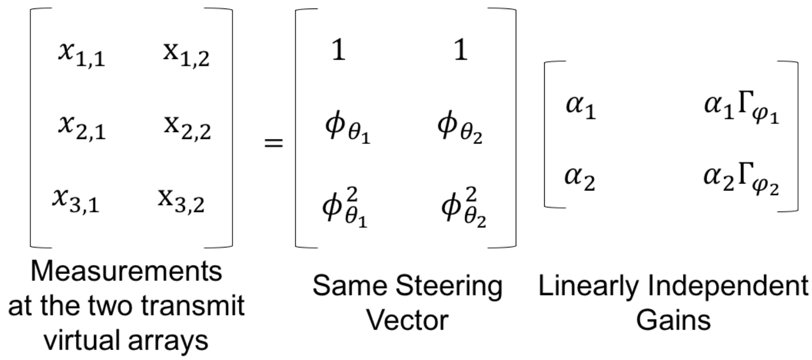

Figure 5-4: **Incoherency of Virtual Subarrays.** The transmit virtual subarrays share the same steering vector but linearly independent gains.

can jointly estimate AoA and ToF while applying MIMO smoothing. For two consecutive OFDM subcarriers, the lth path with ToF τ_l introduces a phase shift as bellow

$$\Omega(\tau_l) = e^{-j2\pi f_\delta \tau_l} \tag{5.5}$$

where f_δ is the frequency difference between two consecutive subcarriers. It should be noted that AoA and AoD do not introduce any phase shift across subcarriers because of the small frequency differences. However, we can measure the phase shifts across subcarriers based on ToF (because of the absence of speed of light factor in the denominator). Considering the sensor array as all subcarriers in all receiving antennas, the new steering vector per transmitting antenna is formed by phase shifts due to AoA and ToF as

$$\begin{aligned} a(\theta,\tau) = [1..\Omega^{K-1}(\tau), \Phi(\theta), ..., \Omega^{K-1}(\tau)\Phi(\theta), ..., \\ \Phi^{M-1}(\theta), ..., \Omega^{K-1}\Phi^{M-1}(\theta)] \end{aligned} \tag{5.6}$$

where M is the number of receiving antennas and K is the number of subcarriers. The new steering vector is of dimension $(MK) \times L$, and the measurement matrix X is of dimension $(MK) \times PN$, where P is the number of samples and N is the number of transmitting antennas. It should be noted that the MIMO smoothing could be applied for AoD-ToF estimation by defining virtual sub-arrays from receiving antennas.

Figure 5-2 illustrates the effect of a person's presence on the resolved AoA pseudo-spectrum for a sample experiment. The figure contains the variations of the power values for each angle across 1000 packets in a boxplot per angle. The comparison of the unoccupied spectrogram with others reveals that we can detect the presence of a person inside the room either with changes in the multipath components such as changes in the resolved angles in still or stationary scenarios, or with temporal changes caused by major movements in stationary or moving scenarios.

5.2.3 Feature Extraction

In addition to the multipath components extracted by Dynamic MUSIC [134] or SpotFi [30] algorithms, PeriFi uses some statistical features on relative phase values between antennas and subcarriers to capture temporal and frequential variations caused by human movements. Then, it uses a machine learning classifier to convert this high dimensional feature set into a single model to infer occupancy. In summary, we can categorize the defined features as follows:

- Temporal variations: 3 max eigenvalues of correlation matrix of successive measurements of CSI amplitude, phase, and relative phase.
- Frequential variations: 3 max eigenvalues of correlation matrix of subcarriers over multiple measurements.

Mean, max, min, median, STD, and entropy of:

- AoA, rToF, and power of 3 resolved paths by Spotfi and Dynamic MUSIC across packets.

- channel components across packets: subcarrier index and the SNR value of Deep fading, 3 abrupt change points in SNR pattern across subcarriers.

- channel variation factor for CSI amplitude, phase, and relative phase across subcarriers as

$$v = \sqrt{\frac{var(x)}{\frac{1}{M}\sum_{m=o}^{M-1}|x_m|^2}} \tag{5.7}$$

  where x is the vector of CSI measurements with length M, and $var(x)$ is the sample variance of vector x. The denominator represents the RMS value of the vector x.

- entropy of CSI amplitude, phase, and relative phase across subcarrier.

5.3 Experimental Setup

5.3.1 Implementation

To evaluate our PeriFi system, we employ two laptops equipped with Intel 5300 WiFi cards and 3 external antennas as the transmitter and receiver. The CSI tool [138] is installed on them to obtain the CSI phase and amplitude values of 30 subcarriers for each received packet per antenna resulting in a 3x3x30 CSI matrix. We conducted 6 experiments with different link conditions in a typical office building shown in Figure 5-5. The communications are operated in 5.63 GHz frequency band employing an unused 40 MHz channel.

Each experiment includes 4 different types of the occupancy states in both LOS and NLOS: (1)*empty*: when nobody is inside the room, (2)*walking*: when someone walks randomly near or far from the LOS, (3)*stationary*: when a person is in the room, but only has fine movements such as writing, (4)*still*: when the occupant is in the room, but completely still such as sleeping or sitting still. Each experiment includes multiple scenarios for each of these occupancy states, resulting in 11 different scenarios. A sample experimental setup

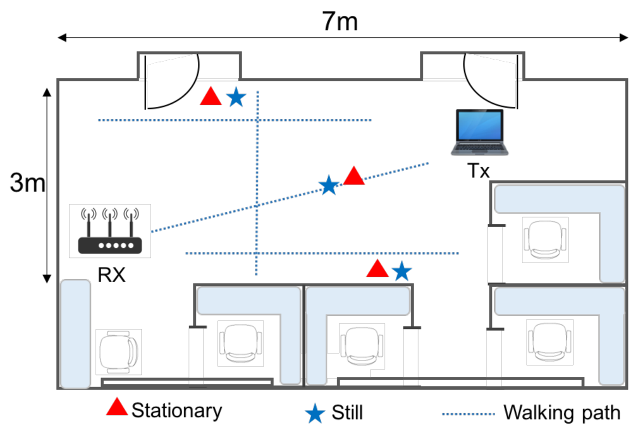

Figure 5-5: **Experimental Setup.** Floor plan and a sample experimental setup.

is shown in Figure 5-6. Each scenario is conducted for 1 minute, resulting in 96 minutes of data in total. For the collection of CSI, the transmission rate of 100 pkts/s is chosen and a sliding window mechanism with 2-second time window and 1-second sliding is used.

5.3.2 Baseline

We compare PeriFi with two recent threshold-based methods that are widely used in the literature. Both of these techniques measure the correlation of CSI values for an empty room and define a threshold line to differentiate occupied and unoccupied conditions. The temporal-base thresholding algorithms such as PADS [42] and DeMan [43] apply eigen decomposition on the CSI correlation matrices of successive measurement to extract time dimension information and characterize the temporal variations of wireless signals caused by human motions. However, they cannot detect stationary or still occupants with fine movements. On the other hand, the frequential-base thresholding algorithms [132] use the subcarrier dimension information of CSI and extract the eigenvalues of the correlation matrices of subcarriers over multiple measurements. The observations show that there is a correlation among CSI changes across subcarriers in the presence of an occupant. In both of these algorithms, the threshold value is usually obtained by employing the well-known Support Vector Machine

Method (%)	Acc	FNR	FPR	F-Score
PeriFi	96.7	7.6	0	96.1
Temporal Base	56.1	11.1	69.5	63.8
Frequential Base	76.8	23.6	22.8	74.2

Table 5.1: Detailed performance comparison of PeriFi with two baselines

(SVM) classification. To have a fair comparison, we use the same classification model to train PeriFi.

5.3.3 Evaluation Metrics

To detect home occupancy, PeriFi requires a WiFi module in every room of the home to form a wireless mesh. Therefore, the goal of PeriFi is to use all information gathered from multiple links for inferring occupancy. To address this requirement, we build one classification model for all 6 experiments to represent multiple links in home. In spite of previous works which require separate training for each link condition, PeriFi provides a generalizable and scalable solution to the size of homes. To evaluate the classification models, we use Leave-One-Scenario-Out (LOSO) to provide a calibration-free evaluation for different occupancy scenarios. In addition, we can evaluate the performance of the proposed system in detecting the occupancy of scenarios not seen in the training phase.

We measure the following metrics: (1) Detection Rate: the fraction of cases where the human presence or absence is detected correctly, (2) False Positive: where a false "human presence" is announced, (3) False Negative: where a false "human absence" is announced.

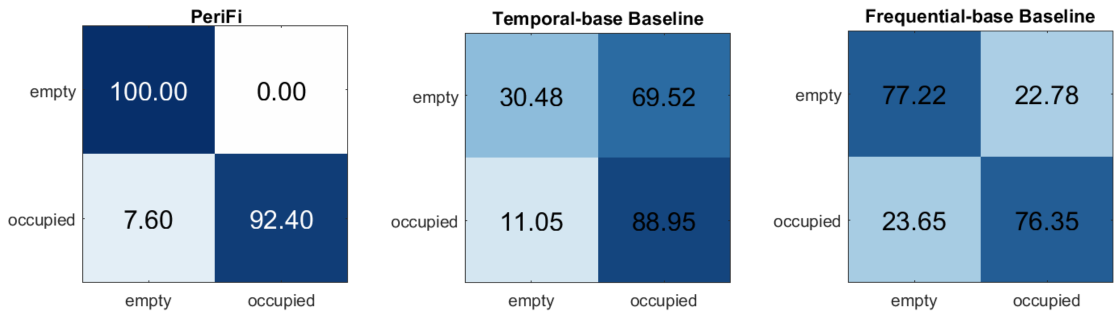

Figure 5-6: **Occupancy Detection Accuracy.** PeriFi achieves 96.7% accuracy compared with 56.1% in temporal and 76% in frequential baseline.

5.4 Evaluation

5.4.1 Detection Accuracy

Table 5.1 summarizes the performance of three methods based on accuracy, FNR, FPR, and F-Score. PeriFi performs 96.7% accurately compared with 56.1% and 76% in temporal and frequential baselines, respectively. Figure 5-6 elaborates these numbers in the form of a confusion matrices. We expect PeriFi to outperform the temporal and frequential baselines in differentiating empty states from occupied states with stationary or still targets, since it doesn't rely on temporal or frequential variations to detect occupancy. The results in Figure 5-6 show that PeriFi outperforms the baselines by 100% correctly detecting empty states, compared with 30% and 77% in the baselines. In addition, PeriFi achieves 92% accuracy in detecting occupied conditions including moving, stationary, and still scenarios, while the baselines only achieves 89% and 76%. In spite of PeriFi which performs accurately in differentiating the occupancy states, temporal baseline shifted the threshold line toward higher values, thus providing a higher accuracy in detecting occupied scenarios, while producing higher false positives. The frequential baseline could define the threshold line more balanced, however it couldn't correctly differentiate empty and occupied states in 20% of cases.

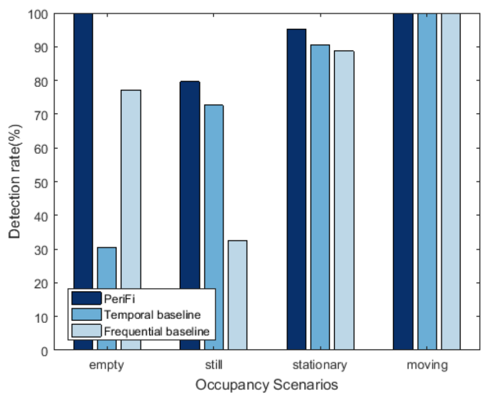

Figure 5-7: **Overall Accuracy.** PeriFi achieves 93.75% averaged detection rate in all types of occupancy states compared to 74% and 72% in the baselines.

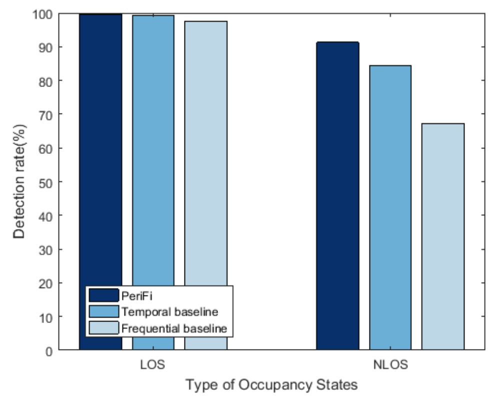

Figure 5-8: **NLoS Accuracy.** Although PeriFi outperforms the baselines in overall, it still has lower accuracy in NLOS conditions.

5.4.2 Occupancy Status Detection

To better understand the reason of false negatives in all three approaches, we provide detection rates based on the type of occupancy states in Figure 5-7. As expected, all three algorithms could detect moving states 100% because of high disturbance. Low accuracy of temporal baseline in detecting empty states and frequential baseline in detecting still states indicate that a threshold-base method is not enough to detect little-movement occupants. On the other hand, PeriFi could provide a higher accuracy in detecting all types of occupancy, but it still misses 12% of low-movement still and stationary states. These misdetections could happen in scenarios where the target is not in the Fresnel zone of LOS path or any of the main reflections.

5.4.3 NLoS Performance

Finally, we categorize the detection rates based on whether the occupant's presence happened in the LOS or NLOS. As shown in Figure 5-8, PeriFi could enhance the sensing coverage by using the multipath reflections. However, it still has lower detection rate in NLOS conditions

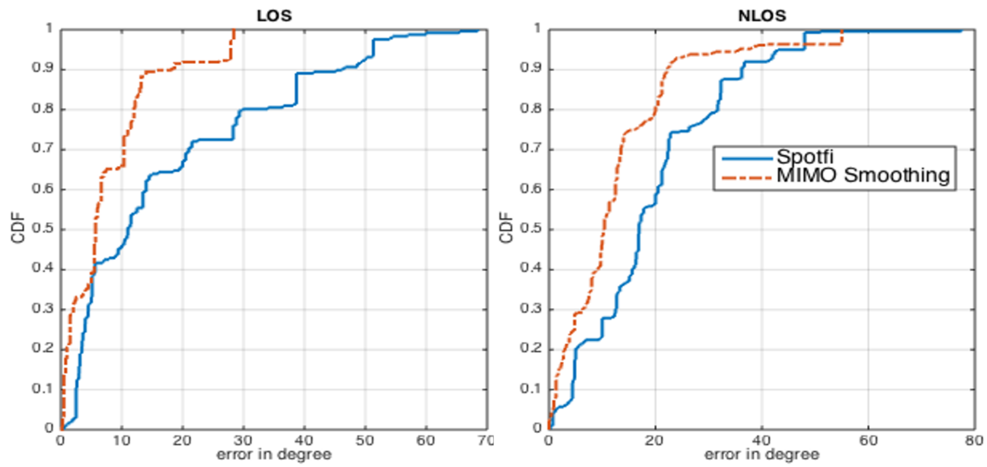

Figure 5-9: **MIMO Smoothing Performance.** It achieves an average improvement of 6.9 degree over SpotFi in AoA estimation

since the number of resolvable paths are limited by the size of antenna array. Although increasing number of antennas or links is a common solution for this problem, we believe part of this issue could be addressed by defining higher resolution features to detect chest movement in completely still occupancy states.

5.4.4 MIMO Smoothing Performance

to evaluate MIMO smoothing, we use 10 mini-PCs that are equipped with Intel 5300 cards, CSI tool [92], and 3 antennas. Each of these nodes can work in transmitting or receiving modes. We conducted a round robin experiment, where in each round one node is transmitting and the other nine nodes are receiving. Since we only have ground truth AoA for the direct path between the transmitter and receivers, we measure the accuracy of the AoA estimation as the minimum difference of the ground truth value and estimated AoAs. Figure 5-9 shows the CDFs for AoA estimation error and compare MIMO smoothing with SpotFi which introduces a 2D smoothing for AoA-ToF estimation. In line-of-sight (LoS) cases, MIMO smoothing achieves median AoA accuracy of 7.1 degrees better than that achieved by SpotFi. In non-line of sight (NLoS) scenarios, we achieve an improvement of 6.8 degree

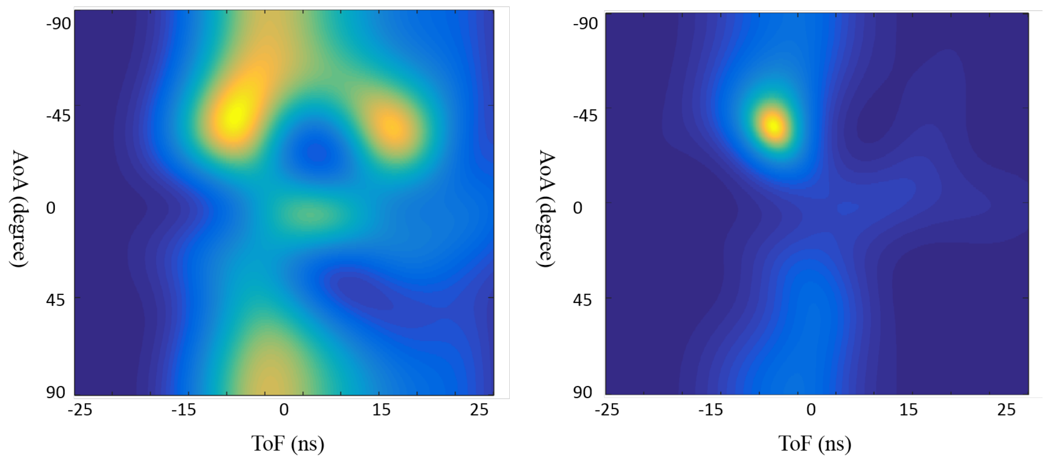

Figure 5-10: **Snapshot of MIMO Smoothing Effect.** (Left) can resolve more paths compared to SpotFi (Right)

in direct path AoA errors.

Our empirical analyses show that MIMO Smoothing can also resolve more paths as shown in Figure 5-10. The higher resolution in addition to more accurate estimations provides the opportunity of using Wireless signals and commodity WiFi devices for reliable presence sensing [2, 71] and precise localization of people/robots in the physical environment even if the reflected signals from human body is so weak.

5.5 Discussion and Future Opportunities

The analysis in this research considers empty room as a static environment. Therefore, if the links conditions change such as replacement of the transmitter or receiver, or adding new links, the system requires to be recalibrated. However, to reduce the need of recalibration, we do not rely on portable devices such as cellphones and laptops. Instead, we use plug-in WiFi modules which will be deployed in every room. In addition, we didn't study the performance of our method in the presence of a moving object such as a fan or pets. In our future work, we will differentiate these conditions based on the differences in size of disturbances and breathing rates. For example, a moving animal will create low signal disturbance but high Doppler values and will affect a changing set of paths, while a stationary person will create low signal disturbance with low Doppler values, affecting only a fixed set of paths. In addition, in this work we didn't study the effect of furniture movements. As our future work, we plan to design an automatic calibration model inspired from our previous work [139, 140] to detect empty room in offline mode and use that period to retrain the classification model.

5.6 Conclusion

In this work, we present an innovative approach for occupancy detection which converts distortions caused by multipath propagation to a useful sensing method. Our proposed approach addresses the challenge of detecting the presence of non-moving people and provides a single solution to infer home occupancy by using the concept of peripheral WiFi vision. Our analyses show that PeriFi can achieve 96.7% accuracy in occupancy detection with different occupancy scenarios including empty, moving, stationary, and still.

Chapter 6

Conclusion

This dissertation focuses on the sensing capability of pervasive wireless infrastructures and more specifically WiFi networks. The presented technologies demonstrate that a pre-existing network of commodity WiFi devices can sense the physical environment by accurately locating WiFi-enabled devices, battery-free object, or even IoT devices that don't have a WiFi transceiver. In addition, we show that the presence of a person inside the room can be detected by tracking the wireless multipath signals since a person within the effective area of the wireless network unavoidably disturb the wireless propagation. The key advantage of the WiFi-based sensing solutions provided in this thesis is that they can realize these capabilities by just leveraging the available infrastructure, which eliminates the need for new hardware. In addition, they can sense almost everywhere due to the ubiquity of wireless signals. Context information provided by these sensing systems will provide great opportunities for new public services such as security monitoring and emergency rescue, or personal services such as monitoring the user's interactions with the physical world for fall detection, well-being monitoring, or home automation. In the following sections, we provide a summary of contributions, limitations and assumptions, and potential extensions of this research in the future.

6.1 Summary of Contributions:

This thesis primarily presents multiple systems for sensing and localizing *things* in the physical environment by just relying on the pervasive wireless infrastructure. However, the contributions of this research can be framed at a higher level as follows:

- From a system perspective, this research presents a fundamentally new approach of *unilateral sensing*, in which the individual devices are empowered to unilaterally sense and localize other devices, objects, and people without relying on any coordination or synchronization with other devices, data sharing or even establishing a two-way communication.
- From the signal processing perspective, this dissertation introduces a novel 3D super-resolution algorithm that disentangles wireless multipath signals and accurately estimates the geometric parameters of each path such as their angle of arrival, angle of departure, and relative time of flight with respect to each other. We demonstrate that this information can enable new sensing and localization services.
- The contribution of this research may be also viewed in geometrics as we introduce a new triangulation method that only relies on the relative length of two sides of a triangle with respect to another side. The conventional triangulation relies on the angle-side-angle congruence theorem to find the unique triangle between 3 vertices, however, Multipath Triangulation uses what we call *angle-relative Side-angle* theorem. The fact that this geometry can be solved and that enables big practical gains in localization is one of the main contributions of this research.
- From a networking perspective, this dissertation expands the role of wireless networks to pervasive sensing infrastructure. The systems developed in this thesis can be *fully piggybacked* on top of WiFi communications without imposing additional requirements beyond the standard WiFi protocol. We called this *sensor piggybacking* and show its

capability in localizing WiFi-enabled devices and battery-free objects as well as sensing people in the physical environment.

6.2 Future Work

While this dissertation has taken major steps toward *omnipresent sensing*, the presented methods have some limitations, which are worth exploring in the future. In this section, we first review these limitations and potential solutions to extend the current designs, and then highlight some of the exciting research directions toward a holistic intelligent sensing platform.

Below are some of the assumptions and limitations of our proposed systems:

- *Mobility:* In this thesis, we evaluated the presented systems in a regular environment with multiple people moving around, demonstrating the robustness of these algorithms to environmental dynamics. However, in our current implementations, we assume that the WiFi transceivers themselves are stationary. The movement of the WiFi transceivers changes the length of multipath signals independently, which requires further consideration in the super-resolution algorithms. Future work can explore more advanced algorithms to capture not only the direction and length of multipath signals but also the Doppler shift of each path caused by mobility.

- *Form-factor:* Our proposed methods leverage the spatial diversity on the WiFi transmitter and receiver to disentangle wireless multipath signals. So, the presence of antenna arrays on the WiFi transceivers is necessary. However, this limits these solutions to devices that can fit the antenna array (6cm). Many WiFi devices including laptops, APs, robots, and smart appliances already have 3-element antenna arrays and this is becoming even more common with MIMO technology. For smaller devices, utilizing their mobility to create virtual antenna arrays is an interesting research proposal for future work.

- *3D Tracking:* The systems developed in this dissertation are focused on 2D sensing and localization, which is sufficient for many applications such as home automation or elderly monitoring. However, to extend these systems for robotic applications such as personal drones or 3D motion tracking for gesture recognition, we need to extend these systems to 3 dimensions. Future works may use 3D antenna arrangements to overcome this limitation.

- *NLoS Sensing:* Our designs rely on the existence of a direct path between the WiFi receiver and the target of interest, whether it is another WiFi device, an object, or a person. The in-situ experiments conducted throughout this thesis demonstrate that these systems work robustly in NLoS scenarios where the direct path is not the strongest signal. However, in the case of complete blockage of the LoS path, the accuracies drop significantly. Currently, all other tracking systems also have this limitation and localizing *things* without a direct path or reflection is still an open problem.

Beyond overcoming these limitations, we believe this approach to evolve wireless medium into intelligent sensing networks that sense the surrounding environment with human-scale context information. So, we envision the future of wireless sensing to be significantly driven by the ongoing paradigm shift toward smart cities, autonomous systems, and virtual reality. Below are some of the areas for future research:

- *Autonomous Vehicles:* The performance and capabilities of autonomous cars or aerial drones can be greatly enhanced through wireless coordination such as driving at high speed around blind corners by leveraging the sensing capabilities of the cars ahead through wireless communication. However, mobility has traditionally been a challenge for wireless networks due to rapid fluctuations of the wireless channel. By leveraging the sensing techniques developed in this research and characterizing multipath propagation, we can assess the wireless quality and control the trajectory of the mobile agents to guarantee wireless connectivity. This allows mobile systems to realize the performance benefits of wireless coordination while preserving the ability to provide provable safety guarantees.

- *Smart Health:* The systems we built can accurately track devices, object, and people, which provides the fundamental context for higher-level applications. The integration of these sets of information to infer semantics enables new methodologies for remote sensing of physiological and psychological signs. The body movement, emotional reactions, and cognitive performance are examples of the semantics that can be inferred with wireless sensing. This eventually converts smart homes into continuous well-being monitoring systems that can diagnose critical health situations.

- *Human as a Mobile Sensor:* With the ubiquity of personal smart wearables such as cell phones, smartwatches, or tablets, the pervasive wireless infrastructure is converting to a mobile platform, which can dynamically sense people's behavior and their interactions with each other and the physical environment. This thesis demonstrates the power of WiFi in human sensing and localization, which creates the basis for a ubiquitous sensor-fusion system. This can be achieved by transforming our proposed stand-alone sensing platform to a collaborative crowd-sourced system.

Bibliography

[1] E. Soltanaghaei, A. Kalyanaraman, and K. Whitehouse. “Multipath triangulation: Decimeter-level wifi localization and orientation with a single unaided receiver”. In: *Proceedings of the 16th Annual International Conference on Mobile Systems, Applications, and Services*. ACM. 2018, pp. 376–388.

[2] E. Soltanaghaei, A. Kalyanaraman, and K. Whitehouse. “Peripheral WiFi Vision: Exploiting Multipath Reflections for More Sensitive Human Sensing”. In: *Proceedings of the 4th International on Workshop on Physical Analytics*. 2017, pp. 13–18.

[3] C. Peng, G. Shen, Y. Zhang, Y. Li, and K. Tan. “Beepbeep: a high accuracy acoustic ranging system using cots mobile devices”. In: *Proceedings of the 5th international conference on Embedded networked sensor systems*. ACM. 2007, pp. 1–14.

[4] J. Yang, S. Sidhom, G. Chandrasekaran, T. Vu, H. Liu, N. Cecan, Y. Chen, M. Gruteser, and R. P. Martin. “Detecting driver phone use leveraging car speakers”. In: *Proceedings of the 17th annual international conference on Mobile computing and networking*. ACM. 2011, pp. 97–108.

[5] A. Harter, A. Hopper, P. Steggles, A. Ward, and P. Webster. “The anatomy of a context-aware application”. In: *Wireless Networks* 1.1 (2001).

[6] N. B. Priyantha, A. Chakraborty, and H. Balakrishnan. “The cricket location-support system”. In: *Proceedings of the 6th annual international conference on Mobile computing and networking*. ACM. 2000, pp. 32–43.

[7] Y. Chen, D. Lymberopoulos, J. Liu, and B. Priyantha. “FM-based indoor localization”. In: *Proceedings of the 10th international conference on Mobile systems, applications, and services*. ACM. 2012, pp. 169–182.

[8] R. Want, A. Hopper, V. Falcao, and J. Gibbons. “The active badge location system”. In: *ACM Transactions on Information Systems (TOIS)* 10.1 (1992), pp. 91–102.

[9] L. M. Ni, Y. Liu, Y. C. Lau, and A. P. Patil. “LANDMARC: indoor location sensing using active RFID”. In: *Proceedings of the First IEEE International Conference on Pervasive Computing and Communications, 2003.(PerCom 2003).* IEEE. 2003, pp. 407–415.

[10] Y. Zhao, Y. Liu, and L. M. N. VIRE. “Active RFID-based Localization Using Virtual Reference Elimination, Parallel Processing, 2007 [C]”. In: *Xian* 56 (2007).

[11] M. S. Bargh and R. de Groote. “Indoor localization based on response rate of bluetooth inquiries”. In: *Proceedings of the first ACM international workshop on Mobile entity localization and tracking in GPS-less environments*. ACM. 2008, pp. 49–54.

[12] V. Otsason, A. Varshavsky, A. LaMarca, and E. De Lara. “Accurate GSM indoor localization”. In: *International conference on ubiquitous computing*. Springer. 2005, pp. 141–158.

[13] E. de Lara, S. Saroiu, et al. “CILoS: a CDMA indoor localization system”. In: *Proceedings of the 10th international conference on Ubiquitous computing*. ACM. 2008, pp. 104–113.

[14] D. Zhang and L. M. Ni. “Dynamic clustering for tracking multiple transceiver-free objects”. In: *2009 IEEE International Conference on Pervasive Computing and Communications*. IEEE. 2009, pp. 1–8.

[15] J. Wilson and N. Patwari. “A fade-level skew-laplace signal strength model for device-free localization with wireless networks”. In: *IEEE Transactions on Mobile Computing* 11.6 (2012), pp. 947–958.

[16] P. Bahl, V. N. Padmanabhan, et al. “RADAR: An in-building RF-based user location and tracking system”. In: *IEEE infocom*. Vol. 2. 2000. INSTITUTE OF ELECTRICAL ENGINEERS INC (IEEE). 2000, pp. 775–784.

[17] M. Youssef and A. Agrawala. “The Horus WLAN location determination system”. In: *Proceedings of the 3rd international conference on Mobile systems, applications, and services*. ACM. 2005, pp. 205–218.

[18] M. Youssef, M. Mah, and A. Agrawala. “Challenges: device-free passive localization for wireless environments”. In: *Proceedings of the 13th annual ACM international conference on Mobile computing and networking*. ACM. 2007, pp. 222–229.

[19] R. J. Fontana. “Recent system applications of short-pulse ultra-wideband (UWB) technology”. In: *IEEE Transactions on microwave theory and techniques* 52.9 (2004), pp. 2087–2104.

[20] S. Gezici, Z. Tian, G. B. Giannakis, H. Kobayashi, A. F. Molisch, H. V. Poor, and Z. Sahinoglu. “Localization via ultra-wideband radios: a look at positioning aspects for future sensor networks”. In: *IEEE signal processing magazine* 22.4 (2005), pp. 70–84.

[21] D. Halperin, W. Hu, A. Sheth, and D. Wetherall. “Predictable 802.11 packet delivery from wireless channel measurements”. In: *ACM SIGCOMM Computer Communication Review* 41.4 (2011), pp. 159–170.

[22] J. Wilson and N. Patwari. "See-through walls: Motion tracking using variance-based radio tomography networks". In: *IEEE Transactions on Mobile Computing* 10.5 (2011), pp. 612–621.

[23] Y. Zeng, P. H. Pathak, C. Xu, and P. Mohapatra. "Your ap knows how you move: fine-grained device motion recognition through wifi". In: *Proceedings of the 1st ACM workshop on Hot topics in wireless*. ACM. 2014, pp. 49–54.

[24] M. A. A. H. Khan, R. Kukkapalli, P. Waradpande, S. Kulandaivel, N. Banerjee, N. Roy, and R. Robucci. "RAM: Radar-based activity monitor". In: *INFOCOM 2016-The 35th Annual IEEE International Conference on Computer Communications, IEEE*. IEEE. 2016, pp. 1–9.

[25] Y. Wang, K. Wu, and L. M. Ni. "Wifall: Device-free fall detection by wireless networks". In: *IEEE Transactions on Mobile Computing* 16.2 (2017), pp. 581–594.

[26] Y. Wang, J. Liu, Y. Chen, M. Gruteser, J. Yang, and H. Liu. "E-eyes: device-free location-oriented activity identification using fine-grained wifi signatures". In: *Proceedings of the 20th annual international conference on Mobile computing and networking*. ACM. 2014, pp. 617–628.

[27] X. Liu, J. Cao, S. Tang, and J. Wen. "Wi-Sleep: Contactless sleep monitoring via WiFi signals". In: *Real-Time Systems Symposium (RTSS), 2014 IEEE*. IEEE. 2014, pp. 346–355.

[28] C. Xu, B. Firner, R. S. Moore, Y. Zhang, W. Trappe, R. Howard, F. Zhang, and N. An. "SCPL: Indoor device-free multi-subject counting and localization using radio signal strength". In: *Information Processing in Sensor Networks (IPSN), 2013 ACM/IEEE International Conference on*. IEEE. 2013, pp. 79–90.

[29] J. Xiong, K. Sundaresan, and K. Jamieson. "Tonetrack: Leveraging frequency-agile radios for time-based indoor wireless localization". In: *Proceedings of the 21st Annual International Conference on Mobile Computing and Networking*. ACM. 2015, pp. 537–549.

[30] M. Kotaru, K. Joshi, D. Bharadia, and S. Katti. "Spotfi: Decimeter level localization using wifi". In: *ACM SIGCOMM Computer Communication Review*. Vol. 45. 2015, pp. 269–282.

[31] J. Xiong and K. Jamieson. "Arraytrack: A fine-grained indoor location system". In: Usenix. 2013.

[32] S. Sen, B. Radunovic, R. R. Choudhury, and T. Minka. "You are facing the Mona Lisa: spot localization using PHY layer information". In: *Proceedings of the 10th international conference on Mobile systems, applications, and services*. ACM. 2012, pp. 183–196.

[33] G. V. Zàruba, M. Huber, F. Kamangar, and I. Chlamtac. "Indoor location tracking using RSSI readings from a single Wi-Fi access point". In: *Wireless networks* 13.2 (2007), pp. 221–235.

[34] C. P. Kumar, R. Poovaiah, A. Sen, and P. Ganadas. "Single access point based indoor localization technique for augmented reality gaming for children". In: *Students' Technology Symposium (TechSym), 2014 IEEE*. IEEE. 2014, pp. 229–232.

[35] L. Sun, S. Sen, D. Koutsonikolas, and K.-H. Kim. "Widraw: Enabling hands-free drawing in the air on commodity wifi devices". In: *Proceedings of the 21st Annual International Conference on Mobile Computing and Networking*. ACM. 2015, pp. 77–89.

[36] K. Ali, A. X. Liu, W. Wang, and M. Shahzad. "Keystroke recognition using wifi signals". In: *Proceedings of the 21st Annual International Conference on Mobile Computing and Networking*. ACM. 2015, pp. 90–102.

[37] Y. Zhao, N. Patwari, J. M. Phillips, and S. Venkatasubramanian. "Radio tomographic imaging and tracking of stationary and moving people via kernel distance". In: *Proceedings of the 12th international conference on Information processing in sensor networks*. ACM. 2013, pp. 229–240.

[38] Y. Zeng, P. H. Pathak, and P. Mohapatra. "WiWho: wifi-based person identification in smart spaces". In: *Proceedings of the 15th International Conference on Information Processing in Sensor Networks*. IEEE Press. 2016, p. 4.

[39] F. Hong, X. Wang, Y. Yang, Y. Zong, Y. Zhang, and Z. Guo. "WFID: passive device-free human identification using WiFi signal". In: *Proceedings of the 13th International Conference on Mobile and Ubiquitous Systems: Computing, Networking and Services*. ACM. 2016, pp. 47–56.

[40] D. Vasisht, S. Kumar, and D. Katabi. "Decimeter-Level Localization with a Single WiFi Access Point." In: *NSDI*. 2016, pp. 165–178.

[41] Z. Zhou, Z. Yang, C. Wu, L. Shangguan, and Y. Liu. "Towards omnidirectional passive human detection". In: *INFOCOM*. IEEE. 2013.

[42] K. Qian, C. Wu, Z. Yang, Y. Liu, and Z. Zhou. "PADS: Passive detection of moving targets with dynamic speed using PHY layer information". In: *Parallel and Distributed Systems (ICPADS)*. 2014.

[43] C. Wu, Z. Yang, Z. Zhou, X. Liu, Y. Liu, and J. Cao. "Non-invasive detection of moving and stationary human with WiFi". In: *IEEE Journal on Selected Areas in Communications* (2015).

[44] K. Wu, J. Xiao, Y. Yi, M. Gao, and L. M. Ni. "Fila: Fine-grained indoor localization". In: *2012 Proceedings IEEE INFOCOM*. IEEE. 2012, pp. 2210–2218.

[45] D. Zhang, Y. Liu, X. Guo, M. Gao, and L. M. Ni. “On distinguishing the multiple radio paths in rss-based ranging”. In: *INFOCOM, 2012 Proceedings IEEE*. IEEE. 2012, pp. 2201–2209.

[46] K. Chintalapudi, A. Padmanabha Iyer, and V. N. Padmanabhan. “Indoor localization without the pain”. In: *Proceedings of the sixteenth annual international conference on Mobile computing and networking*. ACM. 2010, pp. 173–184.

[47] Y. Gwon and R. Jain. “Error characteristics and calibration-free techniques for wireless LAN-based location estimation”. In: *Proceedings of the second international workshop on Mobility management & wireless access protocols*. ACM. 2004, pp. 2–9.

[48] H. Lim, L.-C. Kung, J. C. Hou, and H. Luo. *Zero-configuration, robust indoor localization: Theory and experimentation*. Tech. rep. 2005.

[49] D. Madigan, E Einahrawy, R. P. Martin, W.-H. Ju, P. Krishnan, and A. Krishnakumar. “Bayesian indoor positioning systems”. In: *Proceedings IEEE 24th Annual Joint Conference of the IEEE Computer and Communications Societies.* Vol. 2. IEEE. 2005, pp. 1217–1227.

[50] M. Kotaru and S. Katti. “Position Tracking for Virtual Reality Using Commodity WiFi”. In: *arXiv preprint arXiv:1703.03468* (2017).

[51] X. Li, D. Zhang, Q. Lv, J. Xiong, S. Li, Y. Zhang, and H. Mei. “IndoTrack: Device-Free Indoor Human Tracking with Commodity Wi-Fi”. In: *Proceedings of the ACM on Interactive, Mobile, Wearable and Ubiquitous Technologies* 1.3 (2017), p. 72.

[52] S. Kumar, S. Gil, D. Katabi, and D. Rus. “Accurate indoor localization with zero start-up cost”. In: *Proceedings of the 20th annual international conference on Mobile computing and networking*. ACM. 2014, pp. 483–494.

[53] J. Gjengset, J. Xiong, G. McPhillips, and K. Jamieson. “Phaser: Enabling phased array signal processing on commodity WiFi access points”. In: *Proceedings of the 20th annual international conference on Mobile computing and networking*. ACM. 2014, pp. 153–164.

[54] J.-Y. Lee and R. A. Scholtz. “Ranging in a dense multipath environment using an UWB radio link”. In: *IEEE Journal on Selected Areas in Communications* 20.9 (2002), pp. 1677–1683.

[55] K. Chetty, G. E. Smith, and K. Woodbridge. “Through-the-wall sensing of personnel using passive bistatic wifi radar at standoff distances”. In: *IEEE Transactions on Geoscience and Remote Sensing* 50.4 (2012), pp. 1218–1226.

[56] J. Xiong, K. Jamieson, and K. Sundaresan. “Synchronicity: pushing the envelope of fine-grained localization with distributed mimo”. In: *Proceedings of the 1st ACM workshop on Hot topics in wireless*. ACM. 2014, pp. 43–48.

[57] J. C. Mosher and R. M. Leahy. "Source localization using recursively applied and projected (RAP) MUSIC". In: *IEEE Transactions on signal processing* 47.2 (1999), pp. 332–340.

[58] R. Schmidt. "Multiple emitter location and signal parameter estimation". In: *IEEE transactions on antennas and propagation* 34.3 (1986), pp. 276–280.

[59] Y. Xie, J. Xiong, M. Li, and K. Jamieson. "xD-track: leveraging multi-dimensional information for passive wi-fi tracking". In: *Proceedings of the 3rd Workshop on Hot Topics in Wireless*. ACM. 2016, pp. 39–43.

[60] P Misra and P Enge. "Special issue on global positioning system". In: *Proceedings of the IEEE* 87.1 (1999), pp. 3–15.

[61] V. N. Padmanabhan and L. Subramanian. "Determining the geographic location of Internet hosts". In: *SIGMETRICS/Performance*. 2001, pp. 324–325.

[62] J. Werb and C. Lanzl. "Designing a positioning system for finding things and people indoors". In: *IEEE spectrum* 35.9 (1998), pp. 71–78.

[63] M. Youssef, A. Youssef, C. Rieger, U. Shankar, and A. Agrawala. "Pinpoint: An asynchronous time-based location determination system". In: *Proceedings of the 4th international conference on Mobile systems, applications and services*. ACM. 2006, pp. 165–176.

[64] A. T. Mariakakis, S. Sen, J. Lee, and K.-H. Kim. "Sail: Single access point-based indoor localization". In: *Proceedings of the 12th annual international conference on Mobile systems, applications, and services*. ACM. 2014, pp. 315–328.

[65] S. Lanzisera, D. Zats, and K. S. Pister. "Radio frequency time-of-flight distance measurement for low-cost wireless sensor localization". In: *IEEE Sensors Journal* 11.3 (2011), pp. 837–845.

[66] J. Xu, M. Ma, and C. L. Law. "Position estimation using UWB TDOA measurements". In: *Ultra-wideband, the 2006 IEEE 2006 International Conference on*. IEEE. 2006, pp. 605–610.

[67] S. Krishnan, P. Sharma, Z. Guoping, and O. H. Woon. "A UWB based localization system for indoor robot navigation". In: *Ultra-Wideband, 2007. ICUWB 2007. IEEE International Conference on*. IEEE. 2007, pp. 77–82.

[68] C. Wang, Q. Yin, and H. Chen. "Robust Chinese remainder theorem ranging method based on dual-frequency measurements". In: *IEEE Transactions on Vehicular Technology* 60.8 (2011), pp. 4094–4099.

[69] C. Wang, Q. Yin, and W. Wang. "An efficient ranging method for wireless sensor networks". In: *Acoustics Speech and Signal Processing (ICASSP), 2010 IEEE International Conference on*. IEEE. 2010, pp. 2846–2849.

[70] M. C. Vanderveen, C. B. Papadias, and A. Paulraj. “Joint angle and delay estimation (JADE) for multipath signals arriving at an antenna array”. In: *IEEE Communications letters* 1.1 (1997), pp. 12–14.

[71] E. Soltanaghaei, A. Kalyanaraman, and K. Whitehouse. “Poster: Occupancy state detection using wifi signals”. In: *Proceedings of the 15th Annual International Conference on Mobile Systems, Applications, and Services*. ACM. 2017, pp. 161–161.

[72] J. Lin, Y. Liu, M. B. Hullin, and Q. Dai. “Fourier analysis on transient imaging with a multifrequency time-of-flight camera”. In: *Proceedings of the IEEE Conference on Computer Vision and Pattern Recognition*. 2014, pp. 3230–3237.

[73] F. Heide, M. B. Hullin, J. Gregson, and W. Heidrich. “Low-budget transient imaging using photonic mixer devices”. In: *ACM Transactions on Graphics (ToG)* 32.4 (2013), p. 45.

[74] J. P. Godbaz, M. J. Cree, and A. A. Dorrington. “Understanding and ameliorating non-linear phase and amplitude responses in amcw lidar”. In: *Remote Sensing* 4.1 (2011), pp. 21–42.

[75] F. Adib, C.-Y. Hsu, H. Mao, D. Katabi, and F. Durand. “Capturing the human figure through a wall”. In: *ACM Transactions on Graphics (TOG)* 34.6 (2015), p. 219.

[76] F. Adib, Z. Kabelac, D. Katabi, and R. C. Miller. “3D Tracking via Body Radio Reflections.” In: *NSDI*. 2014.

[77] F. Adib, Z. Kabelac, and D. Katabi. “Multi-Person Localization via RF Body Reflections.” In: *NSDI*. 2015, pp. 279–292.

[78] R. Zetik, S. Crabbe, J. Krajnak, P. Peyerl, J. Sachs, and R. Thomä. “Detection and localization of persons behind obstacles using M-sequence through-the-wall radar”. In: *Sensors, and Command, Control, Communications, and Intelligence (C3I) Technologies for Homeland Security and Homeland Defense V*. Vol. 6201. International Society for Optics and Photonics. 2006, p. 62010I.

[79] A. Kalyanaraman, D. Hong, E. Soltanaghaei, and K. Whitehouse. “Forma track: tracking people based on body shape”. In: *Proceedings of the ACM on Interactive, Mobile, Wearable and Ubiquitous Technologies* 1.3 (2017), p. 61.

[80] J. Wang, J. Xiong, H. Jiang, X. Chen, and D. Fang. “D-Watch: Embracing “Bad” Multipaths for Device-Free Localization With COTS RFID Devices”. In: *IEEE/ACM Transactions on Networking* 25.6 (2017), pp. 3559–3572.

[81] J. Wang, H. Jiang, J. Xiong, K. Jamieson, X. Chen, D. Fang, and B. Xie. “LiFS: low human-effort, device-free localization with fine-grained subcarrier information”. In: *Proceedings of the 22nd Annual International Conference on Mobile Computing and Networking*. ACM. 2016, pp. 243–256.

[82] L. Chang, X. Chen, Y. Wang, D. Fang, J. Wang, T. Xing, and Z. Tang. “FitLoc: Fine-grained and low-cost device-free localization for multiple targets over various areas”. In: *IEEE/ACM Transactions on Networking (TON)* 25.4 (2017), pp. 1994–2007.

[83] R. Elbakly and M. Youssef. “A robust zero-calibration RF-based localization system for realistic environments”. In: *Sensing, Communication, and Networking (SECON), 2016 13th Annual IEEE International Conference on*. IEEE. 2016, pp. 1–9.

[84] J. Haverinen and A. Kemppainen. “Global indoor self-localization based on the ambient magnetic field”. In: *Robotics and Autonomous Systems* 57.10 (2009), pp. 1028–1035.

[85] L. M. Ni, Y. Liu, Y. C. Lau, and A. P. Patil. “LANDMARC: indoor location sensing using active RFID”. In: *Wireless networks* 10.6 (2004), pp. 701–710.

[86] C.-C. Tsai. “A localization system of a mobile robot by fusing dead-reckoning and ultrasonic measurements”. In: *IEEE Transactions on Instrumentation and Measurement* 47.5 (1998), pp. 1399–1404.

[87] A. Kim and M. Golnaraghi. “A quaternion-based orientation estimation algorithm using an inertial measurement unit”. In: *Position Location and Navigation Symposium, 2004. PLANS 2004*. IEEE. 2004, pp. 268–272.

[88] A. R. Jimenez, F. Seco, C. Prieto, and J. Guevara. “A comparison of pedestrian dead-reckoning algorithms using a low-cost MEMS IMU”. In: *Intelligent Signal Processing, 2009. WISP 2009. IEEE International Symposium on*. IEEE. 2009, pp. 37–42.

[89] M. H. Afzal, V. Renaudin, and G. Lachapelle. “Multi-Magnetometer Based Perturbation Mitigation for Indoor Orientation Estimation”. In: *Navigation* 58.4 (2011), pp. 279–292.

[90] M. Mahfoudi, T Turletti, T. Parmentelat, F. Ferrero, L. Lizzi, R Staraj, and W Dabbous. “ORION: Orientation estimation using commodity Wi-Fi”. In: May 2017, pp. 1233–1238.

[91] A. Shahmansoori, G. E. Garcia, G. Destino, G. Seco-Granados, and H. Wymeersch. “Position and orientation estimation through millimeter wave MIMO in 5G systems”. In: *arXiv preprint arXiv:1702.01605* (2017).

[92] D. Halperin, W. Hu, A. Sheth, and D. Wetherall. “Predictable 802.11 packet delivery from wireless channel measurements”. In: *ACM SIGCOMM Computer Communication Review*. Vol. 40. 4. ACM. 2010, pp. 159–170.

[93] M. Kotaru. “Supplementary Material of Wicapture”. In: https://bitbucket.org/mkotaru/wicapturesourcecode.

[94] R. Miesen, F. Kirsch, and M. Vossiek. "Holographic localization of passive UHF RFID transponders". In: *RFID (RFID), 2011 IEEE International Conference on*. IEEE. 2011, pp. 32–37.

[95] J. Wang and D. Katabi. "Dude, where's my card?: RFID positioning that works with multipath and non-line of sight". In: *ACM SIGCOMM Computer Communication Review*. Vol. 43. 4. ACM. 2013, pp. 51–62.

[96] Y. Ma, N. Selby, and F. Adib. "Minding the billions: Ultra-wideband localization for deployed rfid tags". In: *Proceedings of the 23rd Annual International Conference on Mobile Computing and Networking*. ACM. 2017, pp. 248–260.

[97] M. Kotaru, K. Joshi, D. Bharadia, and S. Katti. "Spotfi: Decimeter level localization using wifi". In: *ACM SIGCOMM Computer Communication Review*. Vol. 45. 4. ACM. 2015, pp. 269–282.

[98] M. Bouet and A. L. Dos Santos. "RFID tags: Positioning principles and localization techniques". In: *2008 1st IFIP Wireless Days*. Ieee. 2008, pp. 1–5.

[99] K. Chawla, C. McFarland, G. Robins, and C. Shope. "Real-time RFID localization using RSS". In: *2013 International Conference on Localization and GNSS (ICL-GNSS)*. IEEE. 2013, pp. 1–6.

[100] J. Zhou and J. Shi. "RFID localization algorithms and applications—a review". In: *Journal of intelligent manufacturing* 20.6 (2009), p. 695.

[101] D. Arnitz, K. Witrisal, and U. Muehlmann. "Multifrequency continuous-wave radar approach to ranging in passive UHF RFID". In: *IEEE transactions on microwave theory and techniques* 57.5 (2009), pp. 1398–1405.

[102] X. Li, Y. Zhang, and M. G. Amin. "Multifrequency-based range estimation of RFID tags". In: *2009 IEEE International Conference on RFID*. IEEE. 2009, pp. 147–154.

[103] J. Wang, F. Adib, R. Knepper, D. Katabi, and D. Rus. "RF-compass: Robot object manipulation using RFIDs". In: *Proceedings of the 19th annual international conference on Mobile computing & networking*. ACM. 2013, pp. 3–14.

[104] L. Yang, Y. Chen, X.-Y. Li, C. Xiao, M. Li, and Y. Liu. "Tagoram: Real-time tracking of mobile RFID tags to high precision using COTS devices". In: *Proceedings of the 20th annual international conference on Mobile computing and networking*. ACM. 2014, pp. 237–248.

[105] S. Azzouzi, M. Cremer, U. Dettmar, R. Kronberger, and T. Knie. "New measurement results for the localization of uhf rfid transponders using an angle of arrival (aoa) approach". In: *2011 IEEE International Conference on RFID*. IEEE. 2011, pp. 91–97.

[106] C. Hekimian-Williams, B. Grant, X. Liu, Z. Zhang, and P. Kumar. “Accurate localization of RFID tags using phase difference”. In: *2010 IEEE International Conference on RFID (IEEE RFID 2010)*. IEEE. 2010, pp. 89–96.

[107] R. Kronberger, T. Knie, R. Leonardi, U. Dettmar, M. Cremer, and S. Azzouzi. “UHF RFID localization system based on a phased array antenna”. In: *2011 IEEE International Symposium on Antennas and Propagation (APSURSI)*. IEEE. 2011, pp. 525–528.

[108] G. Mao, B. Fidan, and B. D. Anderson. “Wireless sensor network localization techniques”. In: *Computer networks* 51.10 (2007), pp. 2529–2553.

[109] J. Zhou, H. Zhang, and L. Mo. “Two-dimension localization of passive RFID tags using AOA estimation”. In: *2011 IEEE International Instrumentation and Measurement Technology Conference*. IEEE. 2011, pp. 1–5.

[110] B. Ferris, D. Fox, and N. D. Lawrence. “WiFi-SLAM Using Gaussian Process Latent Variable Models.” In: *IJCAI*. Vol. 7. 1. 2007, pp. 2480–2485.

[111] A. Goswami, L. E. Ortiz, and S. R. Das. “WiGEM: A learning-based approach for indoor localization”. In: *Proceedings of the Seventh COnference on emerging Networking EXperiments and Technologies*. ACM. 2011, p. 3.

[112] K. Joshi, S. Hong, and S. Katti. “Pinpoint: Localizing interfering radios”. In: *Presented as part of the 10th {USENIX} Symposium on Networked Systems Design and Implementation ({NSDI} 13)*. 2013, pp. 241–253.

[113] D. Niculescu and B. Nath. “VOR base stations for indoor 802.11 positioning”. In: *Proceedings of the 10th annual international conference on Mobile computing and networking*. ACM. 2004, pp. 58–69.

[114] S. Sen, J. Lee, K.-H. Kim, and P. Congdon. “Avoiding multipath to revive inbuilding WiFi localization”. In: *Proceeding of the 11th annual international conference on Mobile systems, applications, and services*. ACM. 2013, pp. 249–262.

[115] S. A. Golden and S. S. Bateman. “Sensor measurements for Wi-Fi location with emphasis on time-of-arrival ranging”. In: *IEEE Transactions on Mobile Computing* 6.10 (2007), pp. 1185–1198.

[116] A. Marcaletti, M. Rea, D. Giustiniano, V. Lenders, and A. Fakhreddine. “Filtering noisy 802.11 time-of-flight ranging measurements”. In: *Proceedings of the 10th ACM International on Conference on emerging Networking Experiments and Technologies*. ACM. 2014, pp. 13–20.

[117] M. Kotaru, P. Zhang, and S. Katti. “Localizing low-power backscatter tags using commodity WiFi”. In: *Proceedings of the 13th International Conference on emerging Networking EXperiments and Technologies*. ACM. 2017, pp. 251–262.

[118] B. Kellogg, A. Parks, S. Gollakota, J. R. Smith, and D. Wetherall. “Wi-Fi backscatter: Internet connectivity for RF-powered devices”. In: *ACM SIGCOMM Computer Communication Review*. Vol. 44. 4. ACM. 2014, pp. 607–618.

[119] D. Bharadia, K. R. Joshi, M. Kotaru, and S. Katti. “Backfi: High throughput wifi backscatter”. In: *ACM SIGCOMM Computer Communication Review* 45.4 (2015), pp. 283–296.

[120] B. Kellogg, V. Talla, S. Gollakota, and J. R. Smith. “Passive wi-fi: Bringing low power to wi-fi transmissions”. In: *13th {USENIX} Symposium on Networked Systems Design and Implementation ({NSDI} 16)*. 2016, pp. 151–164.

[121] P. Zhang, D. Bharadia, K. Joshi, and S. Katti. “Hitchhike: Practical backscatter using commodity wifi”. In: *Proceedings of the 14th ACM Conference on Embedded Network Sensor Systems CD-ROM*. ACM. 2016, pp. 259–271.

[122] P. Zhang, C. Josephson, D. Bharadia, and S. Katti. “Freerider: Backscatter communication using commodity radios”. In: *Proceedings of the 13th International Conference on emerging Networking EXperiments and Technologies*. ACM. 2017, pp. 389–401.

[123] J. Zhao, W. Gong, and J. Liu. “Spatial Stream Backscatter Using Commodity WiFi”. In: *Proceedings of the 16th Annual International Conference on Mobile Systems, Applications, and Services*. ACM. 2018, pp. 191–203.

[124] P. Zhang, M. Rostami, P. Hu, and D. Ganesan. “Enabling practical backscatter communication for on-body sensors”. In: *Proceedings of the 2016 ACM SIGCOMM Conference*. ACM. 2016, pp. 370–383.

[125] A. N. Parks, A. P. Sample, Y. Zhao, and J. R. Smith. “A wireless sensing platform utilizing ambient RF energy”. In: *2013 IEEE Topical Conference on Biomedical Wireless Technologies, Networks, and Sensing Systems*. IEEE. 2013, pp. 154–156.

[126] H. J. Visser, A. C. Reniers, and J. A. Theeuwes. “Ambient RF energy scavenging: GSM and WLAN power density measurements”. In: *2008 38th European Microwave Conference*. IEEE. 2008, pp. 721–724.

[127] V. H. Tran, A. Misra, J. Xiong, and N. Hirunima. “Can WiFi Beamforming Support an Energy-Harvesting Wearable?” In: *Proceedings of the Fifth ACM International Workshop on Energy Harvesting and Energy-Neutral Sensing Systems*. ACM. 2017, pp. 14–20.

[128] V. Talla, B. Kellogg, B. Ransford, S. Naderiparizi, S. Gollakota, and J. R. Smith. “Powering the next billion devices with wi-fi”. In: *Proceedings of the 11th ACM Conference on Emerging Networking Experiments and Technologies*. ACM. 2015, p. 4.

[129] M. Gast. *802.11 n: a survival guide*. ” O’Reilly Media, Inc.”, 2012.

[130] R. Ayyalasomayajula, D. Vasisht, and D. Bharadia. “BLoc: CSI-based accurate localization for BLE tags”. In: *Proceedings of the 14th International Conference on emerging Networking EXperiments and Technologies*. ACM. 2018, pp. 126–138.

[131] K. Qian, C. Wu, Y. Zhang, G. Zhang, Z. Yang, and Y. Liu. “Widar2. 0: Passive human tracking with a single wi-fi link”. In: *Proceedings of the 16th Annual International Conference on Mobile Systems, Applications, and Services*. ACM. 2018, pp. 350–361.

[132] S. Palipana, P. Agrawal, and D. Pesch. “Channel State Information Based Human Presence Detection using Non-linear Techniques”. In: *the 3rd ACM Conference on BuildSys*. 2016.

[133] F. Adib, H. Mao, Z. Kabelac, D. Katabi, and R. C. Miller. “Smart homes that monitor breathing and heart rate”. In: *CHI’15, the 33rd Annual ACM Conference*. 2015.

[134] X. Li, S. Li, D. Zhang, J. Xiong, Y. Wang, and H. Mei. “Dynamic-music: accurate device-free indoor localization”. In: *Proceedings of the 2016 ACM International Joint Conference on Pervasive and Ubiquitous Computing*. ACM. 2016, pp. 196–207.

[135] E. Soltanaghaei, A. Kalyanaraman, and K. Whitehouse. “Poster: Occupancy State Detection using WiFi Signals”. In: *MobiSys*. 2017.

[136] T.-J. Shan, M. Wax, and T. Kailath. “On spatial smoothing for direction-of-arrival estimation of coherent signals”. In: *IEEE Transactions on Acoustics, Speech, and Signal Processing* 33.4 (1985), pp. 806–811.

[137] S. U. Pillai and B. H. Kwon. “Forward/backward spatial smoothing techniques for coherent signal identification”. In: *IEEE Transactions on Acoustics, Speech, and Signal Processing* 37.1 (1989), pp. 8–15.

[138] D. Halperin, W. Hu, A. Sheth, and D. Wetherall. “Predictable 802.11 packet delivery from wireless channel measurements”. In: *ACM SIGCOMM Computer Communication Review*. 2010.

[139] E. Soltanaghaei and K. Whitehouse. “WalkSense: Classifying Home Occupancy States Using Walkway Sensing”. In: *BuildSys*. ACM. 2016.

[140] A. Kalyanaraman, E. Griffiths, and K. Whitehouse. “TransTrack: Tracking Multiple Targets by Sensing Their Zone Transitions”. In: *Distributed Computing (DCOSS)*. IEEE. 2016.